الجمهورية الجزائرية الديمقراطية الشعبية
DEMOCRATIC AND POPULAR ALGERIAN REPUBLIC
وزارة التعليم العالي و البحث العلمي
MINISTRY OF HIGHER EDUCATION AND SCIENTIFIC RESEARCH
جامعة الشهيد حمه لخضر الوادي
ECHAHID HAMMA LAKHDAR UNIVERSITY OF EL-OUED
كلية العلوم الطبيعية والحياة
FACULTY OF NATURAL SCIENCES AND LIFE
قسم البيولوجيا الخلوية والجزيئية
DEPARTMENT OF CELLULAR AND MOLECULAR BIOLOGY

Master's Thesis

In order obtain a diploma of an Academic Master

In biological sciences

Specialty: Toxicology

Theme

Rational Design and Multiscale Investigation of Ferrocenyl Acetylaniline Derivatives Targeting Topoisomerase IIα: From Synthesis to Molecular Dynamics and ADMET Profiling

Presented by : BERROUBA Nardjes and BOUZIANI Assala

President	**Dr. Guemmouda Messaouda**		**El-Oued Universi**
Examiner	**Dr. Boudebia Ouafa**		**El-Oued Universi**
Supervisor	**Dr. LANEZ Elhafnaoui**	**M.C.A**	**El-Oued Universi**

2025/ 2026

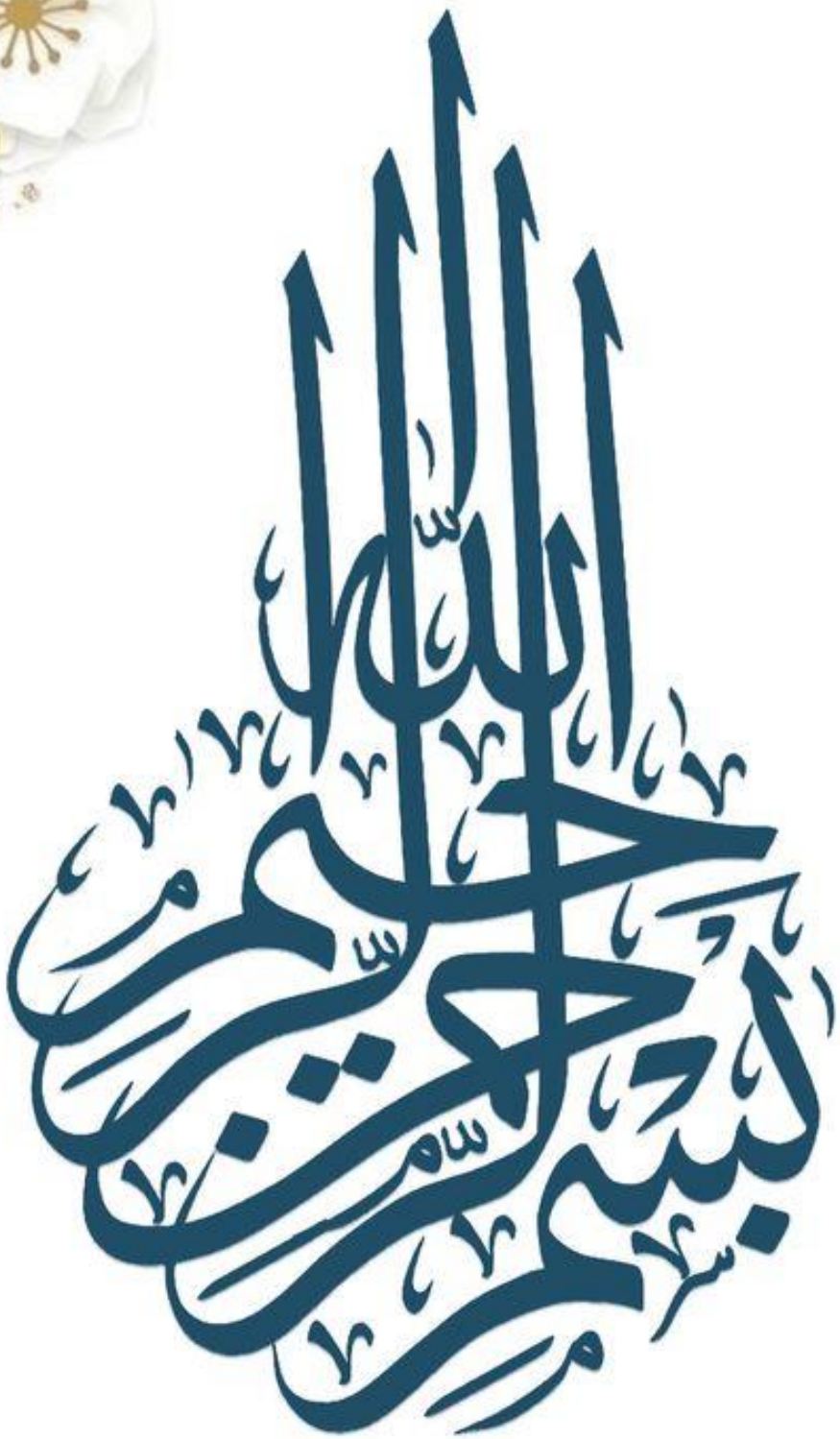
بسم الله الرحمن الرحيم

Dedication

"قُلِ اعْمَلُوا فَسَيَرَى اللَّهُ عَمَلَكُمْ وَرَسُولُهُ وَالْمُؤْمِنُونَ"

All praise is due to Allah, without whose gratitude the night finds no comfort, without whose obedience the day bears no goodness, without whose remembrance moments hold no sweetness, and without whose forgiveness the Hereafter offers no peace. To Him belongs all praise, in the beginning and in the end. Peace and blessings be upon the Prophet of mercy and the light of the worlds, our master Muhammad—may the most complete blessings and salutations be upon him.

To those whose righteousness Allah has made a path to Paradise, whose prayers have been my refuge at every step—my beloved parents —may Allah bless their lives and grant me the ability to honor them throughout my lifetime.

To those whom Allah has granted me as a source of support in this life, my sisters—may He preserve the love between us always.

To the one with whom I shared this work, my dear friend Nardjes.

To every kind soul who has crossed my path and left a lasting and beautiful impression—may Allah reward you all abundantly.

Bouziani Assala

Dedication

بسم الله الرحمن الرحيم

﴿وَقُل رَّبِّ ارْحَمْهُمَا كَمَا رَبَّيَانِي صَغِيرًا﴾

﴿رَبِّ اشْرَحْ لِي صَدْرِي * وَيَسِّرْ لِي أَمْرِي﴾

To those whose contentment Allah has made part of His own pleasure,

to those whose prayers have been my provision on this journey,

and whose light has illuminated the paths of my days,

to my father and my mother,

I ask Allah to bless your lives,

to reward you on my behalf with the best of rewards,

to place what you have done for me on the scale of your good deeds,

and to keep you as a crown upon my head and a light in my life.

To my dear siblings,

I ask Allah to protect you from all harm, to bless you,

to maintain between us sincere love and brotherhood,

to always make us a support for one another in this life,

to gather us upon goodness and joy in this world and the Hereafter,

and never to separate us, and to make our coming days filled with happiness and success.

And to my friend and companion in this journey, Assala,

I ask Allah to grant you success and to fulfill all that you wish for.

Berrouba Nardjes

Acknowledgment

قال الله تعالى:

﴿فَاذْكُرُونِي أَذْكُرْكُمْ وَاشْكُرُوا لِي وَلَا تَكْفُرُونِ﴾

وعملاً بقول النبي صلى الله عليه وسلم: "من لا يشكر الناس لا يشكر الله"

In recognition of those to whom credit is due, we extend our deepest gratitude, sincere appreciation, and heartfelt thanks to the esteemed Professor "LANEZ Elhafnaoui", who honored us by accepting to supervise this dissertation, and for his valuable support, guidance, and insightful advice. May Allah reward him abundantly and grant him the best of rewards on our behalf.

We would also like to express our gratitude to the respected professors and members of the examination committee for kindly agreeing to evaluate and discuss this dissertation.

Finally, we would like to convey our highest expressions of respect and appreciation, along with sincere thanks and affection, to those who have carried the most noble mission in life and who have paved for us the path of knowledge and learning—our teachers throughout our academic journey—and to everyone who extended a helping hand and support in completing this work.

ملخص

تتناول هذه الدراسة تصميم وتخليق وتوصيف وتقييم حاسوبي لمشتقات الفيروسينيل أسيتيل أنيلين(FcMe2Ac) ، FcMe3Ac، (FcMe4Ac، مع التركيز على خصائصها الإلكترونية وتفاعلها مع إنزيم توبويزوميرازIIα ، وهو هدف مهم في علاج السرطان. تم تحضير المركبات بتفاعل استبدال نوكليوفيلي، مع مردود متوسط إلى مرتفع (48–80%)، وتم تأكيد بنيتها باستخدام تقنيات FT-IR و UV–Visibleو.NMR

أظهرت الدراسات الكهروكيميائية سلوكًا شبه انعكاسي لنظام(Fe(II)/Fe(III ، مع اعتماد واضح على نمط الاستبدال. بينت حسابات DFT أن فجوة الطاقة (HOMO–LUMO) تتراوح بين 3.99 و4.29 إلكترون فولت، مما يدل على استقرار متوسط وتفاعلية مناسبة. كما لوحظت زيادة في العزم ثنائي القطب، مما يعكس ارتفاع القطبية الجزيئية.

أظهرت دراسات الإرساء الجزيئي ارتباطًا قويًا مع الإنزيم (6.95−) إلى (8.72−kcal/mol ، حيث سجل المركب FcMe4Acأفضل تقارب. كما أكدت محاكاة الديناميكيات الجزيئية استقرار المعقدات. وأظهرت توقعات ADMET خصائص دوائية جيدة، مثل الامتصاص المرتفع وعدم وجود سمية ملحوظة.

تشير النتائج إلى أن التعديل البنيوي يؤثر بشكل كبير على الخصائص الفيزيائية والحيوية، ويُعد المركب FcMe4Ac الأكثر وعدًا كمركب مرشح لتطوير أدوية مضادة للسرطان.

تُثبت هذه الدراسة بنجاح الإمكانات العلاجية لمشتقات **الفيروسينيل أسيتيل أنيلين** الجديدة، مع إبراز المركب **FcMe4Ac** بوصفه المركب الرائد الأكثر وعدًا. ومن خلال الدمج المتكامل بين التخليق التجريبي والدراسات الكهروكيميائية والنمذجة الحاسوبية المتقدمة، تمهد هذه النتائج الطريق لتصميم جيل جديد من مثبطات **إنزيم التوبويزوميراز IIα** المعتمدة على المركبات العضوية الفلزية، ذات فعالية محسنة ضد السرطان وخصائص أمان أفضل.

الكلمات المفتاحية :مشتقات الفيروسينيل؛ أسيتيل أنيلين؛ توبويزوميرازIIα ؛ الإرساء الجزيئي؛DFT ؛ مضادات السرطان؛.ADMET

Abstract

This thesis investigates the design, synthesis, physicochemical characterization, and in silico evaluation of ferrocenyl acetylaniline derivatives (FcMe2Ac, FcMe3Ac, and FcMe4Ac), with emphasis on their electronic properties and interactions with Topoisomerase IIα, a key anticancer target. The compounds were synthesized via nucleophilic substitution, yielding regioisomers with moderate to high yields (48–80%). Structural elucidation was confirmed using FT-IR, UV–Visible, and NMR spectroscopy, revealing characteristic signals of ferrocenyl and aromatic moieties.

Electrochemical analysis by cyclic voltammetry indicated quasi-reversible Fe(II)/Fe(III) redox behavior, with potentials ranging from 43.9 to 57.5 mV. Diffusion coefficients and electron transfer rates suggested that substitution patterns significantly influence electrochemical properties. Density Functional Theory (DFT) calculations showed HOMO energies between −5.83 and −5.68 eV and energy gaps of 3.99–4.29 eV, indicating moderate stability and reactivity. Increased dipole moments confirmed enhanced molecular polarity.

Molecular docking against Topoisomerase IIα demonstrated favorable binding affinities (−6.95 to −8.72 kcal/mol), with FcMe4Ac showing the strongest interaction. Molecular dynamics simulations (100 ns) confirmed complex stability, with low RMSD values. ADMET predictions revealed favorable pharmacokinetic profiles, including high gastrointestinal absorption, balanced lipophilicity, and absence of toxicity risks.

Overall, structural modification significantly affects electronic and biological behavior. FcMe4Ac emerged as the most promising candidate, combining strong binding, stability, and favorable drug-like properties, suggesting its potential as a lead compound for anticancer drug development.

This study successfully establishes the therapeutic potential of novel ferrocenyl acetylaniline derivatives, highlighting **FcMe4Ac** as a premier lead compound. By seamlessly bridging experimental synthesis and electrochemistry with advanced computational modeling, these findings pave the way for designing next-generation, organometallic-based Topoisomerase IIα inhibitors with optimized anticancer efficacy and safety profiles.

Keywords: Ferrocenyl derivatives; Acetylaniline; Topoisomerase IIα; Molecular docking; DFT; Anticancer agents; ADMET.

Résumé

Cette thèse porte sur la conception, la synthèse, la caractérisation physicochimique et l'évaluation in silico de dérivés ferrocenyl-acétylaniline (FcMe2Ac, FcMe3Ac et FcMe4Ac), en mettant l'accent sur leurs propriétés électroniques et leur interaction avec la topoisomérase IIα, une cible clé en oncologie. Les composés ont été synthétisés par substitution nucléophile avec des rendements modérés à élevés (48–80 %). Leur structure a été confirmée par FT-IR, UV–Visible et RMN.

L'étude électrochimique a révélé un comportement rédox quasi réversible Fe(II)/Fe(III), avec des potentiels compris entre 43,9 et 57,5 mV. Les paramètres de diffusion et de transfert électronique dépendent fortement du motif de substitution. Les calculs DFT ont montré des énergies HOMO entre −5,83 et −5,68 eV et des gaps de 3,99–4,29 eV, indiquant une stabilité modérée. L'augmentation du moment dipolaire traduit une polarité accrue.

Les études de docking moléculaire ont montré de bonnes affinités (−6,95 à −8,72 kcal/mol), avec FcMe4Ac comme meilleur ligand. Les simulations de dynamique moléculaire ont confirmé la stabilité des complexes. Les prédictions ADMET ont révélé de bonnes propriétés pharmacocinétiques et une faible toxicité.

En conclusion, FcMe4Ac apparaît comme le candidat le plus prometteur pour le développement de nouveaux agents anticancéreux.

Cette étude démontre avec succès le potentiel thérapeutique de nouveaux dérivés de **ferrocényl acétylaniline**, en mettant en évidence **FcMe4Ac** comme le composé chef de file le plus prometteur. En intégrant de manière harmonieuse la synthèse expérimentale, les études électrochimiques et la modélisation computationnelle avancée, ces résultats ouvrent la voie à la conception d'une nouvelle génération d'inhibiteurs organométalliques de la **Topoisomérase IIα**, présentant une efficacité anticancéreuse optimisée ainsi qu'un meilleur profil de sécurité.

Mots-clés : Dérivés ferrocenyl; Acétylaniline; Topoisomérase IIα; Docking moléculaire; DFT; Agents anticancéreux; ADMET.

Table of Content

Chapter 2: Computational Approaches in Molecular Modelling and Drug Design

Second part: Experimental Analysis

Chapter 01: Materials & Methods

Chapter 02: Results & Discussion

List of figures

List of tables

List of Abbreviation

- **ADMET**: Absorption, Distribution, Metabolism, Excretion, and Toxicity
- **ATP**: Adenosine Triphosphate
- **B3LYP**: Becke, 3-parameter, Lee–Yang–Parr Functional
- **Cp**: Cyclopentadienyl
- **CV**: Cyclic Voltammetry
- **DFT**: Density Functional Theory
- **DMF**: Dimethylformamide
- **DMSO**: Dimethyl Sulfoxide
- **DNA**: Deoxyribonucleic Acid
- **EAS**: Electrophilic Aromatic Substitution
- **EDC**:1-Ethyl-3(3dimethylaminopropyl) carbodiimide
- **ESP**: Electrostatic Surface Potential
- **Fc**: Ferrocene
- **FcMe2Ac**: N-[(Ferrocenyl)methyl]-2-acetylaniline
- **FcMe3Ac**: N-[(Ferrocenyl)methyl]-3-acetylaniline
- **FcMe4Ac**: N-[(Ferrocenyl)methyl]-4-acetylaniline
- **Fe**: Iron
- **FT-IR**: Fourier Transform Infrared Spectroscopy
- **GA**: Genetic Algorithm
- **HBA**: Hydrogen Bond Acceptor
- **HBD**: Hydrogen Bond Donor
- **HMBC**: Heteronuclear Multiple Bond Correlation
- **HOMO**: Highest Occupied Molecular Orbital
- **HSQC**: Heteronuclear Single Quantum Coherence
- **HUMO**: Lowest Unoccupied Molecular Orbital
- **IC50**: Half Maximal Inhibitory Concentration
- **LGA**: Lamarckian Genetic Algorithm
- **LUMO**: Lowest Unoccupied Molecular Orbital
- **MD**: Molecular Dynamics
- **MEP**: Molecular Electrostatic Potential
- **MM-PBSA**: Molecular Mechanics Poisson–Boltzmann Surface Area
- **MO**: Molecular Orbital
- **MolSA**: Molecular Surface Area
- **NBO**: Natural Bond Orbital
- **NHE**: Normal Hydrogen Electrode
- **NICS**: Nucleus-Independent Chemical Shift
- **NMR**: Nuclear Magnetic Resonance
- **NPT**: Constant Number of particles, Pressure, and Temperature
- **NVT**: Constant Number of particles, Volume, and Temperature
- **PDB**: Protein Data Bank
- **PSA**: Polar Surface Area
- **QSAR**: Quantitative Structure–Activity Relationship
- **RMSD**: Root Mean Square Deviation
- **RMSF**: Root Mean Square Fluctuation
- **ROS**: Reactive Oxygen Species
- **SAR**: Structure–Activity Relationship
- **SCF**: Self-Consistent Field
- **Topo IIα**: Topoisomerase II Alpha
- **UV–Vis**: Ultraviolet–Visible Spectroscopy

GENERAL INTRODUCTION

Cancer remains one of the most formidable healthcare challenges of the 21st century, characterized by uncontrolled cellular proliferation and high mortality rates worldwide. Despite significant advancements in oncology, conventional chemotherapeutic agents often suffer from severe limitations, including a lack of selectivity, systemic toxicity, and the rapid development of multi-drug resistance (MDR). Consequently, there is an urgent and continuous imperative in medicinal chemistry to design and develop novel, highly targeted anticancer agents that exhibit enhanced therapeutic efficacy coupled with minimized adverse effects on healthy tissues.

In the quest for specific biological targets, Type IIα Topoisomerase (Topo IIα) has emerged as a crucial enzyme in cancer cell survival and proliferation. Topo IIα plays an indispensable role in managing DNA topology by generating transient double-stranded breaks to relieve torsional strain during essential cellular processes such as DNA replication, transcription, and chromosome segregation. Because rapidly proliferating cancer cells exhibit a marked over-expression of Topo IIα compared to normal cells, inhibiting this enzyme or poisoning its DNA-cleavage complex represents a highly validated and strategic approach in targeted anticancer drug design.

Concurrently, the field of bioorganometallic chemistry has revolutionized rational drug design by bridging the gap between classical organic coordination chemistry and medicine. Among various organometallic frameworks, ferrocene ($Fe(C_5H_5)_2$) has attracted paramount attention. Ferrocene-based compounds possess a unique, highly stable sandwich-like structural geometry, chemical robustness, low intrinsic toxicity, and favorable lipophilicity, which significantly enhances cellular uptake across biological membranes. Crucially, the reversible Fe(II)/Fe(III) redox behavior of the ferrocenyl core allows these molecules to undergo intracellular redox cycling, leading to the selective generation of Reactive Oxygen Species (ROS) within the oxidative stress-susceptible tumor microenvironment.

While certain ferrocene conjugates, such as ferrocifens, have demonstrated remarkable antiproliferative activities, the exploration of ferrocenyl acetylaniline derivatives remains an open and highly promising frontier. Incorporating an acetylaniline pharmacophore into the ferrocene skeleton provides a unique scaffolding that can potentially optimize hydrogen-bonding networks and electronic interactions within the catalytic pocket of Topo IIα. However, understanding how structural modifications and spatial geometry dictate biological efficacy remains a complex task

that requires a multiscale investigative approach combining wet-lab synthesis with advanced computational modeling.

Despite the recognized therapeutic potential of ferrocene-containing complexes, a major hurdle in organometallic drug design is achieving an optimal balance between target-specific binding affinity, structural stability, and ideal pharmacokinetic profiles. In particular, the exact influence of substituent positioning on the aromatic ring of the acetylaniline moiety is not fully understood. The electronic distribution, steric hindrance, and molecular conformation of these compounds vary significantly depending on the geometric arrangement, directly impacting their pharmacological behavior.

So, How do the structural and positional modifications—specifically the ortho, meta, and para regioisomers—of newly designed ferrocenyl acetylaniline derivatives influence their physicochemical and electronic properties, and to what extent do these spatial variations govern their binding affinity, structural stability, and ADMET (Absorption, Distribution, Metabolism, Excretion, and Toxicity) profiles when targeting the Topoisomerase IIα enzyme for anticancer therapy؟

To resolve this problematic, this study adopts an integrated, multiscale methodology divided into two main trajectories:

1.Experimental Synthesis and Characterization: Synthesizing the specific regioisomers (ortho, meta, and para) of ferrocenyl acetylaniline and confirming their molecular structures using advanced spectroscopic techniques (FT-IR,UV-Vis, and NMR) alongside electrochemical investigations to evaluate their redox properties.

2.Computational (In Silico) Evaluation: Utilizing Density Functional Theory (DFT) to map the electronic structures (HOMO/LUMO gaps) and chemical reactivity descriptors; performing molecular docking to map binding orientations within Topo IIα; executing Molecular Dynamics (MD) simulations to assess the long-term stability of the enzyme-ligand complexes; and conducting predictive ADMET profiling to evaluate drug-likeness and toxicological safety.

To present the findings systematically, the dissertation is structured into two main parts, subdivided into four distinct chapters:

• PART I: BIBLIOGRAPHIC REVIEW (Theoretical Framework)

Chapter 1: Ferrocene Derivatives: Structure, Reactivity, and Applications: This chapter provides a comprehensive review of the chemical, electronic, and electrochemical features of

ferrocene, emphasizing its historical evolution and modern applications in medicinal chemistry and oncology.

Chapter 2: Computational Approaches in Molecular Modeling and Drug Design: This chapter establishes the theoretical background behind the computational toolkit employed in this research, detailing the principles of DFT calculations, molecular docking algorithms, molecular dynamics, and predictive toxicology models.

• PART II: EXPERIMENTAL AND COMPUTATIONAL INVESTIGATION (Practical Framework)

Chapter 1: Materials and Methods: This chapter outlines the practical protocols, chemical reagents, and instrumentation used for the chemical synthesis and spectroscopic analysis, as well as the specific software parameters and workflows applied during the in silico multiscale simulations.

Chapter 2: Results and Discussion: This chapter presents a detailed analysis of the experimental and computational data. It correlates the structural differences of the ortho, meta, and para regioisomers with their electronic properties, binding thermodynamics with Topo IIα, dynamic structural stability, and toxicological safety profiles.

Finally, a General Conclusion summarizes the major insights gained from this study and proposes prospective pathways for the future optimization and in vitro screening of these promising organometallic agents.

First part:

Bibliographic Study

Chapter Abstract

This theoretical component of the thesis comprises two interconnected chapters that collectively provide the foundational knowledge necessary for the rational design and multiscale investigation of ferrocenyl acetylaniline derivatives as potential topoisomerase IIα inhibitors. Chapter 1 systematically examines the structural, electronic, electrochemical, and biological properties of ferrocene and its derivatives. Beginning with the historical discovery and structural characterisation of ferrocene, the chapter elucidates how the unique sandwich geometry and the readily accessible Fe(II)/Fe(III) redox couple endow ferrocenyl compounds with properties that are exploitable in medicinal chemistry. The synthesis and functionalisation strategies enabling the preparation of biologically relevant ferrocenyl conjugates are reviewed, and the electrochemical behaviour underpinning redox-mediated cytotoxicity mechanisms is analysed. The pharmacological literature on ferrocene-based anticancer, antimalarial, and antimicrobial agents is critically synthesised, with particular emphasis on structure–activity relationships relevant to the present investigation. Chapter 2 addresses the computational toolkit employed throughout this research. Density functional theory (DFT) and its role in computing electronic descriptors are discussed critically, with evaluation of functional and basis-set selection. Molecular docking methodologies are reviewed with respect to scoring function reliability and receptor-preparation protocols for topoisomerase IIα. The principles of molecular dynamics (MD) simulation, including force-field selection, system preparation, and trajectory analysis, are expounded. Finally, the computational prediction of ADMET properties and drug-likeness assessment frameworks are examined, highlighting both the utility and the inherent limitations of in silico approaches. Together, these chapters establish the theoretical framework that guides the experimental and computational work reported in subsequent sections of this thesis.

Chapter 1:

Ferrocene Derivatives: Structure, Reactivity And Applications

1.1 Introduction

The discovery of ferrocene (dicyclopentadienyliron, Fc) in 1951 by Kealy and Pauson, followed almost simultaneously by the independent synthesis reported by Miller and colleagues, initiated a transformative era in organometallic chemistry (Kealy & Pauson, 1951; Miller et al., 1952). The compound's surprising stability and distinctive aroma prompted an immediate re-evaluation of prevailing bonding models. The definitive elucidation of the sandwich structure by Wilkinson, Rosenblum, Whiting, and Woodward in 1952, and the subsequent confirmation by X-ray crystallography performed by Dunitz and colleagues, established ferrocene as the archetypal metallocene and provided the conceptual basis for a vast family of transition-metal sandwich complexes (Wilkinson et al., 1952; Dunitz et al., 1956).

Since those foundational studies, ferrocene has occupied a singular position in both fundamental and applied chemistry. Its chemical robustness—attributable to the 18-electron configuration of iron(II) in the sandwich geometry—combined with its facile, reversible one-electron oxidation to the ferricinium cation (Fc^+), its electrophilic aromatic substitution reactivity comparable to that of aniline, and its low inherent toxicity in mammals have made it an exceptionally versatile scaffold (Long, 1998; Togni & Hayashi, 1995). The past three decades have witnessed an exponential growth in the synthesis and application of ferrocenyl derivatives across diverse fields including asymmetric catalysis, materials science, electroanalytical chemistry, and—most pertinently for the present work—medicinal chemistry and drug design (Štěpnička, 2008; Ornelas, 2011).

In the context of anticancer drug development, ferrocene derivatives have attracted sustained interest owing to their potential to generate reactive oxygen species (ROS) in the tumour microenvironment through iron-mediated redox cycling, their ability to mimic and interact with biologically relevant estrogen and nucleoside scaffolds, and the pharmacokinetic advantages conferred by the lipophilic cyclopentadienyl moiety (Jaouen et al., 2010; Biot & Chibale, 2006). The bioorganometallic chemistry of ferrocene thus represents a rich, albeit pharmacologically underexplored, dimension of rational drug design. The present chapter provides a systematic account of ferrocene's structural and electronic properties (Section 1.2), synthetic and functionalisation strategies (Section 1.3), electrochemical behaviour (Section 1.4), and biological and pharmacological relevance (Section 1.5), thereby establishing the conceptual framework for the design of the target ferrocenyl acetylaniline derivatives investigated in this thesis.

1.2 Structural and Electronic Properties of Ferrocene

1.2.1 Crystal Structure and Molecular Geometry

Ferrocene consists of an iron atom sandwiched symmetrically between two parallel cyclopentadienyl (Cp) rings, each contributing five π electrons to a total electron count of 18 at the metal centre (Wilkinson et al., 1952). In the gas phase, electron diffraction studies have established that the molecule adopts a staggered (D5d) conformation, whereas in the crystalline state the rings are nearly eclipsed (D5h symmetry), with the energy barrier between the two conformers being exceptionally small—approximately 0.9 kcal mol−1—indicating essentially free rotation about the ring-iron axis (Haaland & Nilsson, 1968; Seiler & Dunitz, 1979). The Fe–C bond lengths are uniform at approximately 2.04 Å, and the C–C distances within the Cp rings are equivalent at ~1.43 Å, consistent with aromatic delocalisation and confirming the high-symmetry, pseudo-aromatic character of the complex (Seiler & Dunitz, 1979).

The near-perfect equivalence of all ten Fe–C bonds, the planarity of the Cp rings, and the short metal–ring centroid distance (~1.66 Å) collectively reflect the dominant η5 coordination mode in which all five carbons of each ring are bound to the metal with equal strength (Long, 1998). These structural features have been reproduced with high fidelity by DFT calculations using hybrid functionals, confirming that the bonding description based on molecular orbital theory is both qualitatively and quantitatively sound (Mohajeri & Shakerin, 2004).

1.2.2 Molecular Orbital Description and Frontier Orbitals

The electronic structure of ferrocene is most rigorously described within the framework of ligand-field theory as extended to the D5h or D5d point groups. The 10 π orbitals of the two Cp rings combine to form five bonding (a1g, e1g, e2g and their ungerade partners) and five antibonding symmetry-adapted linear combinations; the iron 3d, 4s, and 4p atomic orbitals interact with these combinations according to symmetry selection rules (Shriver & Atkins, 2010). The resultant molecular orbital (MO) diagram places the highest occupied orbitals in the dz2-dominated a1g level and the degenerate (dxz, dyz)-dominated e1g levels, with the e2g (dxy, dx2–y2) and e1u* (ligand-based antibonding) orbitals lying above. The HOMO of ferrocene is predominantly metal-centred (e1g symmetry) with significant π-back-donation character, while the LUMO is a higher-lying e2g* orbital (Jørgensen, 1962; Rösch & Streitwieser, 1983).

Frontier molecular orbital analysis reveals that the HOMO–LUMO gap of ferrocene is approximately 5.2 eV (computed at the B3LYP/6-311+G(d,p) level), indicative of substantial kinetic stability and the reluctance of the molecule to engage in spontaneous chemical reaction under ambient conditions (Mohajeri & Shakerin, 2004). The relatively high-lying HOMO, however, facilitates one-electron oxidation to the 17-electron ferricinium cation Fc+. Importantly, the electronic properties of the ferrocene core are exquisitely sensitive to substituent effects on the Cp rings: electron-withdrawing groups lower the HOMO energy and oxidation potential, whereas electron-donating groups exert the opposite effect, a relationship that has been extensively exploited in the design of electrochemical sensors and redox-active drug candidates (Bildstein, 2000).

1.2.3 Aromaticity and Electrophilic Reactivity

The aromatic character of ferrocene—manifested in its susceptibility to electrophilic aromatic substitution (EAS), its characteristic 1H NMR resonance at δ ~4.2 ppm, and the negative nucleus-independent chemical shift (NICS) value at the ring centroid—has been the subject of sustained theoretical debate (Schleyer et al., 2001). Although ferrocene does not satisfy the planar 4n+2 π-electron rule that defines Hückel aromaticity, multi-dimensional aromaticity criteria (NICS, aromatic fluctuation index, electron localisation function) converge in assigning ferrocene a high degree of three-dimensional aromaticity comparable to that of benzene (Corminboeuf et al., 2006). This aromaticity underpins the EAS reactivity that makes ferrocene an exceptionally versatile synthetic building block: it undergoes acylation (Friedel–Crafts), formylation (Vilsmeier–Haack), lithiation, and aminomethylation reactions with high efficiency and, in many cases, controllable regio- and stereoselectivity (Štěpnička, 2008).

Table 1: Key structural and electronic parameters of ferrocene and selected derivatives.

Compound	Fe–C (Å)	HOMO (eV)	LUMO (eV)	E1/2 (V vs SHE)
Ferrocene (Fc)	2.046	−4.82	−0.41	+0.40
Acetylferrocene	2.049	−5.18	−0.83	+0.51
Ferrocenemethanol	2.044	−4.71	−0.35	+0.37

1,1'-Diacetylferrocene	2.053	−5.53	−1.21	+0.63
Ferroquine	2.047	−4.96	−0.62	+0.44

Note. HOMO/LUMO energies computed at B3LYP/6-311+G(d,p) level; E1/2 values in acetonitrile. Adapted from Bildstein (2000); Jaouen et al. (2010); Mohajeri & Shakerin (2004).

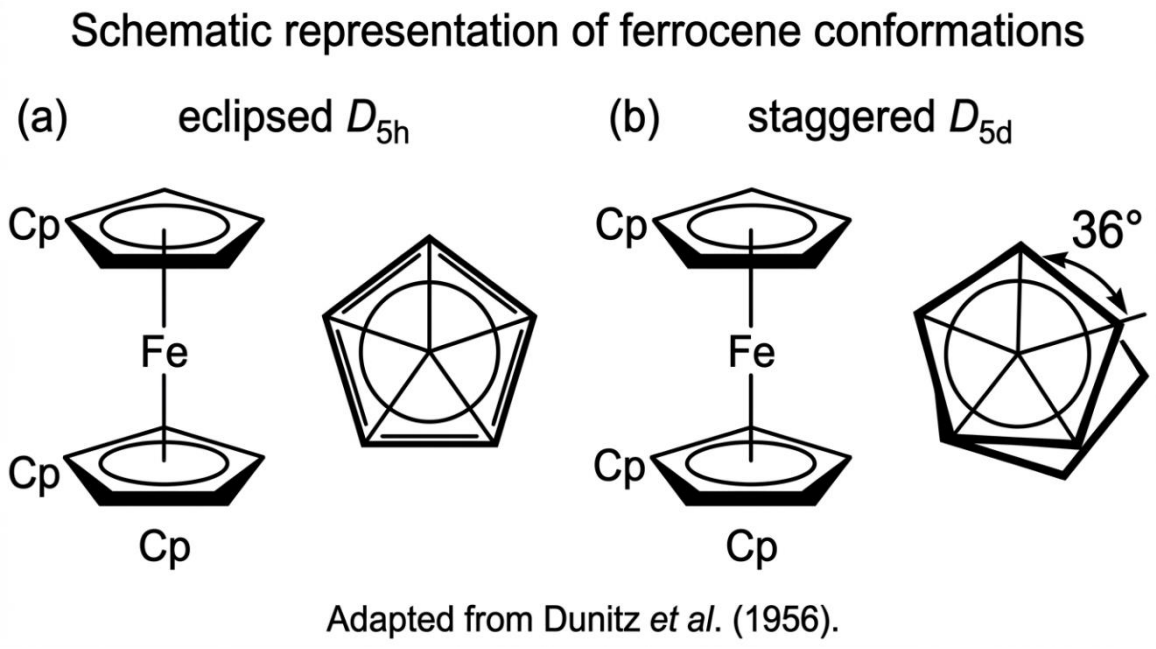

Figure 1: Schematic representation of ferrocene in (a) eclipsed D5h and (b) staggered D5d conformations, showing the parallel Cp rings and central iron atom. Adapted from Dunitz et al. (1956).

1.3 Synthesis and Functionalisation of Ferrocenyl Derivatives

1.3.1 Direct Synthesis of Ferrocene

The original synthesis of ferrocene by Kealy and Pauson employed the reaction of cyclopentadienyl magnesium bromide with ferric chloride, affording a product of initially puzzling stability (Kealy & Pauson, 1951). The more practical and now universally adopted route involves the reaction of freshly cracked cyclopentadiene with potassium hydroxide to generate the cyclopentadienyl anion, which subsequently reacts with anhydrous ferrous chloride in tetrahydrofuran under inert atmosphere (Jolly, 1976). Alternative large-scale preparations employ the direct reaction of cyclopentadiene vapour with iron powder at elevated temperatures, although this approach yields a more complex product mixture. The commercial availability of ferrocene at low cost has,

however, rendered its synthesis largely an academic exercise; functionalisation chemistry—rather than primary synthesis—constitutes the more practically significant domain.

1.3.2 Electrophilic Aromatic Substitution on Ferrocene

The high electron density of the ferrocene Cp ring renders it approximately one million-fold more reactive toward electrophilic substitution than benzene (Gottlied & Neufeld, 1965). Friedel–Crafts acylation using acyl chlorides or anhydrides in the presence of aluminium trichloride or phosphoric acid preferentially affords monoacylated products at mild temperatures; elevated temperatures and excess reagent favour symmetric 1,1'-diacylation (Knox & Pauson, 1961). This monoacylation selectivity arises from the electron-withdrawing effect of the initially introduced acyl group, which deactivates the substituted ring toward further electrophilic attack and directs a second electrophile to the unsubstituted Cp ring.

Formylation via the Vilsmeier–Haack protocol, employing phosphoryl chloride and dimethylformamide, provides ferrocenecarboxaldehyde in good yield; the aldehyde functionality serves as a versatile handle for condensation reactions, reductive amination, and Wittig olefination (Rinehart & Curby, 1957). Lithiation of ferrocene using n-butyllithium in the presence of TMEDA, or regioselective directed metalation using strong bases in combination with directing groups, provides lithioferrocene intermediates that react with a broad range of electrophiles to install carbon, nitrogen, oxygen, and halogen substituents with controlled regiochemistry (Snieckus, 1990).

1.3.3 Transition-Metal-Catalysed Cross-Coupling

The advent of palladium-catalysed cross-coupling chemistry substantially expanded the synthetic repertoire available for ferrocene functionalisation. Haloferrocenes—particularly the readily accessible iodide and bromide derivatives—participate efficiently in Suzuki–Miyaura (arylboronic acid), Sonogashira (terminal alkyne), Negishi (organozinc), and Kumada (Grignard) coupling reactions under standard Pd(0) or Pd(II) catalytic conditions (Štěpnička, 2008). The stereochemical consequences of planar chirality in 1,2-disubstituted ferrocenes are of particular relevance to asymmetric synthesis: the two faces of the monosubstituted ferrocene are diastereotopic, and direct metalation with chiral auxiliaries (Ugi's amine, Josiphos-type ligands) permits the diastereoselective preparation of enantiomerically enriched 1,2-disubstituted ferrocenes of importance in asymmetric catalysis (Togni & Hayashi, 1995; Richards et al., 2006).

1.3.4 Ferrocenyl Conjugate Synthesis for Medicinal Applications

The preparation of biologically active ferrocenyl conjugates typically involves the coupling of the ferrocene scaffold to a pharmacophore-bearing fragment. Common strategies include: (i) condensation of ferrocenecarbaldehyde with amines or hydrazides to give Schiff base derivatives; (ii) acylation of ferrocenecarboxylic acid or its activated esters (NHS, CDI) with amine-bearing pharmacophores; (iii) reductive amination of ketone-functionalised ferrocenes; and (iv) the use of ferrocene-containing linkers in prodrug design (Biot & Chibale, 2006; Jaouen et al., 2010). The synthesis of ferrocenyl acetylaniline derivatives—directly relevant to the present work—generally proceeds via the condensation of acetylferrocene with appropriate aniline derivatives under acidic conditions, or via amide-bond formation between ferrocenecarboxylic acid and substituted anilines using standard peptide-coupling reagents (Ornelas, 2011).

Table 2: Summary of major synthetic routes and functionalisation strategies for ferrocenyl derivatives.

Strategy	Key Reagents	Products	References
Friedel–Crafts Acylation	RCOCl, AlCl3 or H3PO4	Acylferrocenes	Knox & Pauson (1961)
Vilsmeier–Haack Formylation	POCl3/DMF	Ferrocenecarboxaldehyde	Rinehart & Curby (1957)
Directed Lithiation	n-BuLi, TMEDA	1,2-Disubstituted Fc	Snieckus (1990)
Suzuki–Miyaura Coupling	ArB(OH)2, Pd(PPh3)4, base	Arylferrocenes	Štěpnička (2008)
Schiff Base Condensation	FcCHO, R-NH2, acid catalyst	Ferrocenyl imines	Ornelas (2011)
Amide Bond Formation	FcCOOH, amine, EDC/NHS	Ferrocenyl amides	Biot & Chibale (2006)

Note. Fc = ferrocenyl; EDC = 1-ethyl-3-(3-dimethylaminopropyl)carbodiimide; NHS = N-hydroxysuccinimide.

1.4 Electrochemical Behaviour of Ferrocene Compounds

1.4.1 The Ferrocene/Ferricinium Redox Couple

The electrochemical behaviour of ferrocene is dominated by the highly reversible one-electron oxidation of Fe(II) to Fe(III), described by the half-reaction Fc → Fc+ + e− (Pavlishchuk & Addison, 2000). This process occurs at a formal potential of approximately +0.40 V versus the standard hydrogen electrode (SHE) in acetonitrile, or ~0.38 V vs. Ag/AgCl in aqueous systems, and is characterised by near-unity anodic-to-cathodic peak current ratio ($i_{pa}/i_{pc} \approx 1$) and peak separation approaching the Nernstian ideal of 59 mV, confirming kinetically facile, diffusion-controlled, fully reversible electron transfer at conventional scan rates in cyclic voltammetry (Gritzner & Kůta, 1984). The exceptional chemical reversibility of this couple—reflecting the structural similarity of the 18-electron Fc and 17-electron Fc+—has made ferrocene the universal electrochemical reference standard recommended by IUPAC (Pavlishchuk & Addison, 2000).

1.4.2 Substituent Effects on Redox Potential

The introduction of substituents on the Cp rings exerts a predictable, quantifiable influence on the Fc/Fc+ oxidation potential. Electron-donating groups (EDGs)—methyl, methoxy, amino—destabilise the positive charge on the ferricinium cation, raising the energy of the oxidised form relative to the reduced form and consequently lowering the oxidation potential (making oxidation thermodynamically easier). Conversely, electron-withdrawing groups (EWGs)—acyl, nitro, cyano—stabilise the ferricinium charge through inductive or mesomeric withdrawal, increasing the oxidation potential (Bildstein, 2000). Linear free-energy relationships analogous to Hammett correlations have been demonstrated for ferrocene derivatives, confirming that substituent effects on oxidation potential are additive and transmittable through the Cp ring system (Kuwana et al., 1960).

This tunability is of direct pharmacological relevance: the oxidation potential determines the accessibility of the Fc/Fc+ couple under physiological redox conditions (intracellular glutathione potential: ~−240 mV vs. NHE; mitochondrial membrane potential: ~−180 mV), and hence governs whether a given ferrocenyl compound will undergo intracellular oxidation to the potentially cytotoxic Fc+ state and engage in ROS generation via Fenton-type chemistry (Hillard et al., 2007).

Table 3: Electrochemical data for representative ferrocene compounds in organic and aqueous media.

Compound	E1/2 (V vs Fc)	ΔEp (mV)	Solvent	Reference
Ferrocene	0.00 (reference)	60	MeCN	Gritzner & Kůta (1984)
Acetylferrocene	+0.11	62	MeCN	Bildstein (2000)
Decamethylferrocene	−0.48	59	MeCN	Pavlishchuk & Addison (2000)
Ferroquine	+0.04	65	MeCN/H2O	Biot & Chibale (2006)
Ferrocifen	+0.02	61	DCM	Hillard et al. (2007)

Note. E1/2 reported vs. internal ferrocene standard. ΔEp = anodic–cathodic peak separation at 100 mV s−1.

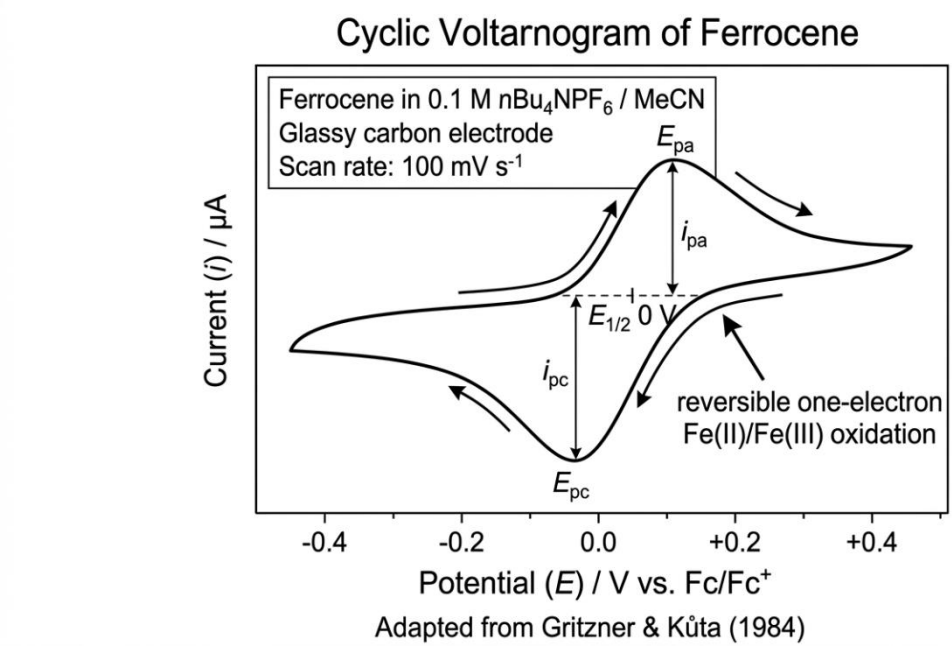

Figure 2: Cyclic voltammogram of ferrocene in 0.1 M nBu4NPF6/MeCN at a glassy carbon electrode (scan rate 100 mV s−1), showing the reversible one-electron Fe(II)/Fe(III) oxidation. Adapted from Gritzner & Kůta (1984).

1.4.3 Electrochemical Applications in Sensing and Catalysis

Beyond its role as a reference standard, the redox activity of ferrocene has been extensively exploited in electroanalytical chemistry. Ferrocene-modified electrodes and ferrocene-labelled biomolecules serve as signal transducers in amperometric biosensors; the most notable example is the use of ferrocene derivatives as mediators in electrochemical glucose sensors, where they shuttle electrons between the enzyme (glucose oxidase) and the electrode surface (Degani & Heller, 1987). The structural versatility of the ferrocene scaffold permits fine-tuning of solubility, membrane permeability, and redox potential to optimise mediator performance. In the context of cancer biology, the electrochemical accessibility of the Fc/Fc+ couple under conditions representative of the tumour microenvironment—which is characterised by elevated ROS, reduced oxygen tension, and altered redox homeostasis—provides a mechanistic rationale for the selective cytotoxicity observed for many ferrocenyl anticancer agents (Hillard et al., 2007).

1.5 Biological and Pharmacological Relevance of Ferrocene Derivatives

1.5.1 Overview of Bioorganometallic Chemistry

The field of bioorganometallic chemistry, which encompasses the design and study of metal-containing compounds intended for biological applications, has grown substantially since the demonstration of the antitumour activity of cisplatin by Rosenberg and colleagues in 1969 (Rosenberg et al., 1969). Ferrocene occupies a distinctive niche in this field: unlike platinum or ruthenium complexes whose biological activity is primarily attributable to covalent interactions with DNA or protein targets, the biological effects of ferrocene derivatives appear to involve a more complex interplay of redox activity, lipophilicity, steric effects, and target-specific non-covalent interactions (Jaouen et al., 2010). Ferrocene itself exhibits low acute toxicity in rodents (oral LD50 ~1320 mg kg−1 in rats) and is metabolised primarily to hydroxylated products by cytochrome P450 enzymes, suggesting an acceptable safety profile for medicinal use (Köpf-Maier & Köpf, 1987).

1.5.2 Anticancer Ferrocenyl Compounds

The most extensively characterised ferrocenyl anticancer agents are the ferrocifens—ferrocene-tamoxifen conjugates developed by Jaouen and co-workers—which demonstrate nanomolar cytotoxicity against hormone-receptor-positive and -negative breast cancer cell lines (Top et al., 1994; Jaouen et al., 2010). The ferrocifen series illustrates a key design principle:

conjugation of the ferrocene unit to an existing pharmacophore can confer activity in cell lines resistant to the parent drug, and the enhanced potency relative to tamoxifen appears to involve, inter alia, Fc/Fc+ cycling with concomitant generation of superoxide, hydrogen peroxide, and hydroxyl radicals in the mitochondrial environment (Hillard et al., 2007). Structure–activity relationship (SAR) studies within the ferrocifen series have demonstrated that: (i) the presence of the phenol group on the side chain is essential for activity in estrogen receptor-negative lines; (ii) the oxidation potential of the ferrocene moiety correlates with cytotoxicity; and (iii) the geometric configuration of the double bond influences receptor binding affinity (Hillard et al., 2007; Jaouen et al., 2010).

Beyond the ferrocifens, a substantial body of literature documents the cytotoxic activity of ferrocenyl Schiff bases, ferrocene-platinum conjugates, ferrocenyl nucleoside analogues, and—most relevant to the present investigation—ferrocenyl amide and acetamide derivatives (Ornelas, 2011; van Staveren & Metzler-Nolte, 2004). Several ferrocenyl compounds have been demonstrated to inhibit topoisomerase II activity, induce apoptosis, and intercalate into DNA, suggesting multiple potential mechanisms of anticancer action (Desbois et al., 2008). The precise mechanism of action of any given ferrocene derivative, however, remains incompletely characterised, and the relative contributions of target-specific interactions versus ROS-mediated cytotoxicity may vary substantially with structural context.

1.5.3 Antimalarial Activity: Ferroquine

Ferroquine (SR97193), prepared by Biot and co-workers through the attachment of a ferrocene unit to the 4-aminoquinoline pharmacophore of chloroquine, represents the most clinically advanced ferrocene-based drug candidate to date (Biot & Chibale, 2006; Dive & Biot, 2008). Ferroquine exhibits potent in vitro activity against both chloroquine-sensitive and -resistant strains of Plasmodium falciparum (IC50 values in the 10–40 nM range), surpassing chloroquine by one to two orders of magnitude in resistant strains (Biot et al., 1997). The enhanced antimalarial efficacy of ferroquine relative to chloroquine has been attributed to its ability to generate hydrogen peroxide within the acidic food vacuole of the parasite through Fc/Fc+ cycling, thereby overwhelming the parasite's haem detoxification pathway and supplementing the classical chloroquine mechanism of haemozoin crystallisation inhibition (Dive & Biot, 2008). Ferroquine has successfully completed Phase IIa clinical trials, establishing proof-of-concept for the clinical utility of the bioorganometallic approach to antiparasitic drug design (Biot et al., 2012).

1.5.4 Other Biological Activities

In addition to anticancer and antimalarial activities, ferrocene derivatives have been reported to exhibit antibacterial, antifungal, antiviral, and enzyme inhibitory properties (Ornelas, 2011; van Staveren & Metzler-Nolte, 2004). Ferrocenyl amino acid derivatives and ferrocenyl peptide conjugates have attracted interest as potential enzyme inhibitors and as probes of metalloenzyme active sites (van Staveren & Metzler-Nolte, 2004). Ferrocenyl triazoles and ferrocenyl quinolones have shown promising antibacterial activity against both Gram-positive and Gram-negative organisms, with inhibition of bacterial DNA gyrase—a type II topoisomerase—proposed as a plausible mechanism of action in some studies (Fouda et al., 2015). The structural analogy between bacterial gyrase and human topoisomerase IIα, both of which belong to the type II topoisomerase family, lends particular relevance to this observation in the context of the present thesis.

Table 4: Selected biological activities of ferrocenyl-based compounds reported in the literature.

Compound Class	Target/Disease	Activity (IC50)	Mechanism	Reference
Ferrocifens	Breast cancer (MCF-7, MDA-MB-231)	0.1–0.5 μM	ROS generation, ER modulation	Jaouen et al. (2010)
Ferroquine	P. falciparum (CQ-resistant)	15–40 nM	Haemozoin inhibition, ROS	Biot et al. (1997)
Fc-Nucleoside Analogues	HIV-1 reverse transcriptase	0.5–10 μM	Chain termination	van Staveren & Metzler-Nolte (2004)
Fc-Schiff Bases	Various cancer lines	1–50 μM	Apoptosis, DNA damage	Ornelas (2011)
Fc-Quinolones	E. coli, S. aureus	2–20 μg/mL	DNA gyrase inhibition	Fouda et al. (2015)

Note. CQ = chloroquine; ER = estrogen receptor; ROS = reactive oxygen species; FC = ferrocenyl.

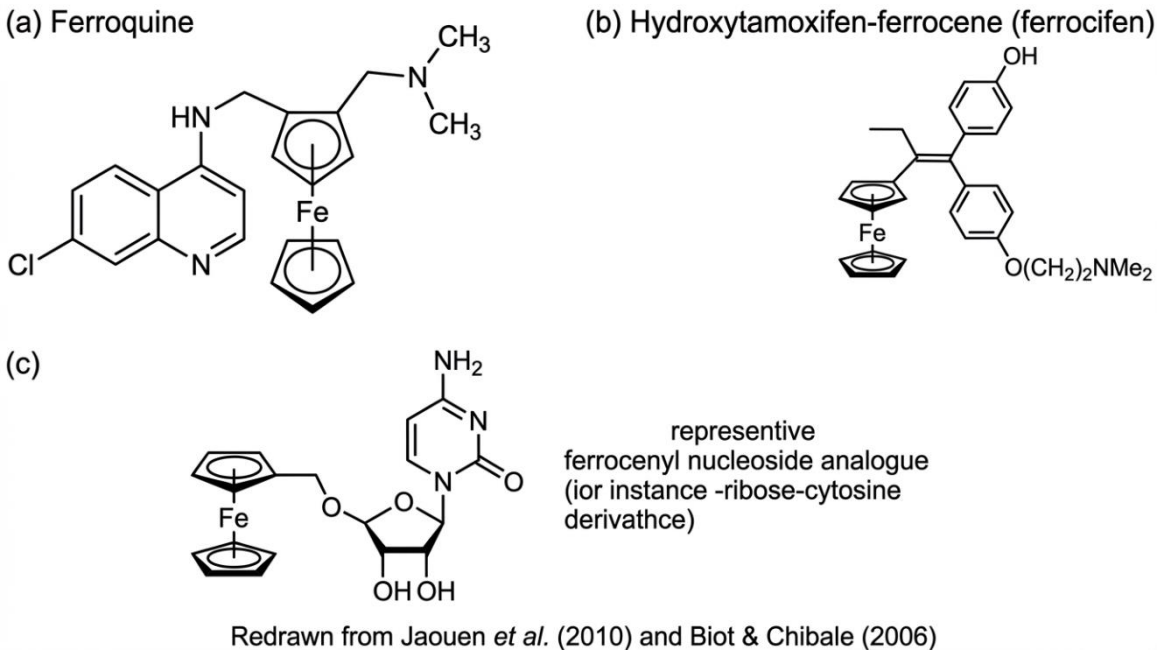

Figure 3: Structures of representative bioactive ferrocenyl compounds: (a) ferroquine, (b) hydroxytamoxifen-ferrocene (ferrocifen), and (c) a ferrocenyl nucleoside analogue. Redrawn from Jaouen et al. (2010) and Biot & Chibale (2006).

1.6 Conclusion

This chapter has provided a comprehensive account of the structural, electronic, electrochemical, and biological dimensions of ferrocene chemistry that underpin the design of the ferrocenyl acetylaniline derivatives investigated in this thesis. The unique sandwich architecture of ferrocene, which confers both structural robustness and aromatic reactivity, enables the preparation of a diverse array of functionalised derivatives through well-established electrophilic substitution, directed metalation, and cross-coupling strategies. The accessible, reversible Fc/Fc+ redox couple—whose potential is exquisitely sensitive to Cp-ring substitution—provides a mechanism by which ferrocenyl compounds can engage in intracellular redox cycling, potentially generating cytotoxic ROS selectively within the tumour microenvironment.

The pharmacological literature reviewed herein demonstrates that ferrocenyl conjugates represent a productive strategy for the development of anticancer, antimalarial, and antibacterial agents, with the clinical progression of ferroquine to Phase IIa trials providing compelling proof-of-concept. Structure–activity relationships within the ferrocifen series, and the emerging evidence for topoisomerase inhibition by ferrocenyl quinolone derivatives, motivate the hypothesis—pursued in subsequent chapters—that ferrocenyl acetylaniline derivatives may interact

productively with topoisomerase IIα, a validated cancer target. The theoretical and computational tools required to evaluate this hypothesis are examined in Chapter 2.

Chapter 2:

Computational Approaches in Molecular Modelling and Drug Design

2.1 Introduction

The past three decades have witnessed a paradigm shift in drug discovery, from predominantly empirical, phenotypic screening approaches toward rational, structure-based design underpinned by computational methods (Anderson, 2003). Computational chemistry, molecular modelling, and bioinformatics now constitute indispensable components of the modern drug discovery pipeline, enabling the rapid prioritisation of candidate molecules, the elucidation of binding modes, the prediction of pharmacokinetic and toxicological profiles, and the rationalisation of experimentally observed structure–activity relationships (Jorgensen, 2004; Leach & Gillet, 2007). For organometallic compounds such as the ferrocenyl derivatives investigated in this thesis, where the presence of a transition metal centre introduces challenges for both experimental and computational characterisation, the judicious integration of complementary in silico methods is particularly valuable (Diedrich & Grimme, 2003).

This chapter provides a critical account of the four principal computational methodologies employed in this investigation. Density functional theory (DFT) is discussed with respect to its theoretical foundations, the selection of exchange-correlation functionals and basis sets appropriate for iron-containing organometallics, and the electronic descriptors that it furnishes for QSAR and reactivity prediction (Section 2.2). Molecular docking—the in silico evaluation of ligand–receptor complementarity—is reviewed with emphasis on the specific challenges posed by topoisomerase IIα as a docking target and the reliability of the scoring functions employed (Section 2.3). Molecular dynamics (MD) simulation is examined as a method for probing the dynamic behaviour of ligand–receptor complexes, with attention to force-field selection, system preparation, and trajectory analysis metrics (Section 2.4). Finally, the computational prediction of ADMET properties and drug-likeness assessment are discussed, including the theoretical bases of the major prediction models and their limitations (Section 2.5). A critical perspective is maintained throughout: whilst acknowledging the predictive power of each methodology, we highlight the inherent approximations and known failure modes that must be borne in mind when interpreting computational results.

2.2 Density Functional Theory (DFT) and Electronic Descriptors

2.2.1 Theoretical Foundations of DFT

Density functional theory is a quantum mechanical approach to the electronic structure problem that, in contrast to wave-function-based methods, takes the electron density ρ(r) as the fundamental variable rather than the many-electron wavefunction Ψ (Hohenberg & Kohn, 1964). The theoretical foundation of modern DFT rests on the two Hohenberg–Kohn theorems: (i) the external potential v(r)—and hence all ground-state properties—is uniquely determined by the ground-state electron density; and (ii) the exact ground-state energy is the global minimum of the energy functional E[ρ], minimised over all N-representable densities (Hohenberg & Kohn, 1964). These theorems, while formally exact, do not prescribe the functional form of the exchange-correlation energy Exc[ρ], which must be approximated in practical calculations.

The Kohn–Sham (KS) formulation, introduced in 1965, renders the DFT problem computationally tractable by mapping the interacting electron system onto a fictitious non-interacting system with the same density, described by a set of one-electron Kohn–Sham orbitals {φi(r)} (Kohn & Sham, 1965). The KS equations resemble the Hartree–Fock equations but incorporate the exchange-correlation potential vxc(r) = δExc[ρ]/δρ(r), which encapsulates all many-body effects beyond the classical Hartree (Coulomb) repulsion. The self-consistent field (SCF) procedure iterates the KS equations to convergence, yielding the electron density, total energy, and orbital energies.

The accuracy of a KS-DFT calculation is determined principally by the choice of exchange-correlation functional, which approximates the unknown Exc[ρ]. The 'Jacob's Ladder' classification organises functionals in order of increasing sophistication: the local density approximation (LDA) employs only ρ(r); generalised gradient approximation (GGA) functionals additionally incorporate ∇ρ(r); meta-GGA functionals add the kinetic energy density τ(r); hybrid functionals (e.g., B3LYP, PBE0) mix a fraction of exact Hartree–Fock exchange; and double-hybrid functionals add a perturbative correlation correction (Perdew et al., 2005).

2.2.2 Functional and Basis-Set Selection for Ferrocene

The reliable treatment of organometallic systems containing iron poses well-known challenges for DFT. The B3LYP functional, which incorporates 20% exact exchange and the LYP correlation functional, has become the de facto standard for organic molecules and has been widely applied to

ferrocene and its derivatives; however, it is known to systematically underestimate the s→d excitation energies of first-row transition metals and to perform inconsistently for systems with high 3d-electron density (Furche & Perdew, 2006; Koch & Holthausen, 2001). For ferrocene specifically, B3LYP reproduces the geometry with good fidelity (Fe–C errors < 0.02 Å) but overestimates the HOMO–LUMO gap by approximately 0.3 eV relative to experiment (Mohajeri & Shakerin, 2004). Functionals incorporating greater amounts of exact exchange, such as M06-2X or PBE0, may improve the description of charge-transfer states but introduce other systematic errors.

The basis set must be sufficiently flexible to describe both the contracted core orbitals of iron and the diffuse, polarisation-rich π system of the Cp rings. The Pople-type 6-31G(d) basis set is commonly employed for geometry optimisation of ferrocene derivatives; the larger 6-311+G(d,p) is preferred for single-point energy and property calculations (Clark et al., 1983). For iron, effective core potentials (ECPs) such as the Stuttgart–Dresden (SDD) potential are frequently employed to account for relativistic effects on the core electrons while retaining a reasonable computational cost (Dolg et al., 1987). The combination B3LYP/6-31G(d) (organic atoms) with SDD (iron) represents a pragmatic and well-validated approach for the calculation of ferrocene geometries, vibrational frequencies, and frontier orbital energies, and is widely adopted in the literature (Mohajeri & Shakerin, 2004; Diedrich & Grimme, 2003).

Table 5: Comparison of DFT functionals and basis sets used in ferrocene-related computational studies.

Functional	Basis Set (Fe / C,H,N,O)	Application	Fe–C Error (Å)	Reference
B3LYP	SDD / 6-31G(d)	Geometry, vibrational analysis	+0.018	Mohajeri & Shakerin (2004)
B3LYP	SDD / 6-311+G(d,p)	NBO, ESP charges, HOMO/LUMO	+0.015	Diedrich & Grimme (2003)

PBE0	def2-TZVP	Excitation energies, UV-Vis	+0.011	Furche & Perdew (2006)
M06-L	6-311G(d) / 6-31G(d)	Thermochemistry, barriers	+0.020	Zhao & Truhlar (2008)
BP86	TZP (all atoms)	Bond orders, NMR shifts	+0.009	Koch & Holthausen (2001)

Note. Fe–C error = computed minus experimental Fe–C bond length. SDD = Stuttgart–Dresden ECP; TZP = triple-zeta polarisation.

2.2.3 Electronic Descriptors Derived from DFT

DFT calculations furnish a range of electronic descriptors that are widely used in QSAR modelling and the rationalisation of reactivity. The energies of the highest occupied molecular orbital (HOMO, εHOMO) and the lowest unoccupied molecular orbital (LUMO, εLUMO) are related to the vertical ionisation potential and electron affinity, respectively, through Koopmans' theorem (strictly valid only for Hartree–Fock orbitals, but conventionally applied to KS eigenvalues) (Koopmans, 1934). From these, chemical hardness $\eta = (\varepsilon LUMO - \varepsilon HOMO)/2$, chemical softness $S = 1/(2\eta)$, global electrophilicity index $\omega = \mu^2/(2\eta)$ (where the electronic chemical potential $\mu = (\varepsilon HOMO + \varepsilon LUMO)/2$), and Fukui functions for local reactivity are derived within the conceptual DFT framework (Parr & Yang, 1989; Gázquez et al., 2007).

For ferrocenyl drug candidates, the HOMO energy correlates with the ease of one-electron oxidation (redox potential), while the LUMO energy is related to the ability of the compound to accept electrons from biological nucleophiles. The HOMO–LUMO gap ($\Delta E = \varepsilon LUMO - \varepsilon HOMO$) serves as a measure of kinetic stability and polarisability: molecules with small gaps are more reactive and more easily polarised by the biological environment (Fleming, 1976). The electrostatic surface potential (ESP) map, derived from the molecular electron density and nuclear charges, visualises the electrophilic and nucleophilic regions of the molecule and guides the prediction of non-covalent interactions with receptor residues (Murray & Politzer, 1998). Natural bond orbital (NBO) analysis provides atom-centred charges and bond orders that are less basis-set-dependent

than Mulliken charges and are widely used to parametrise electrostatic interaction terms in docking scoring functions (Reed et al., 1988).

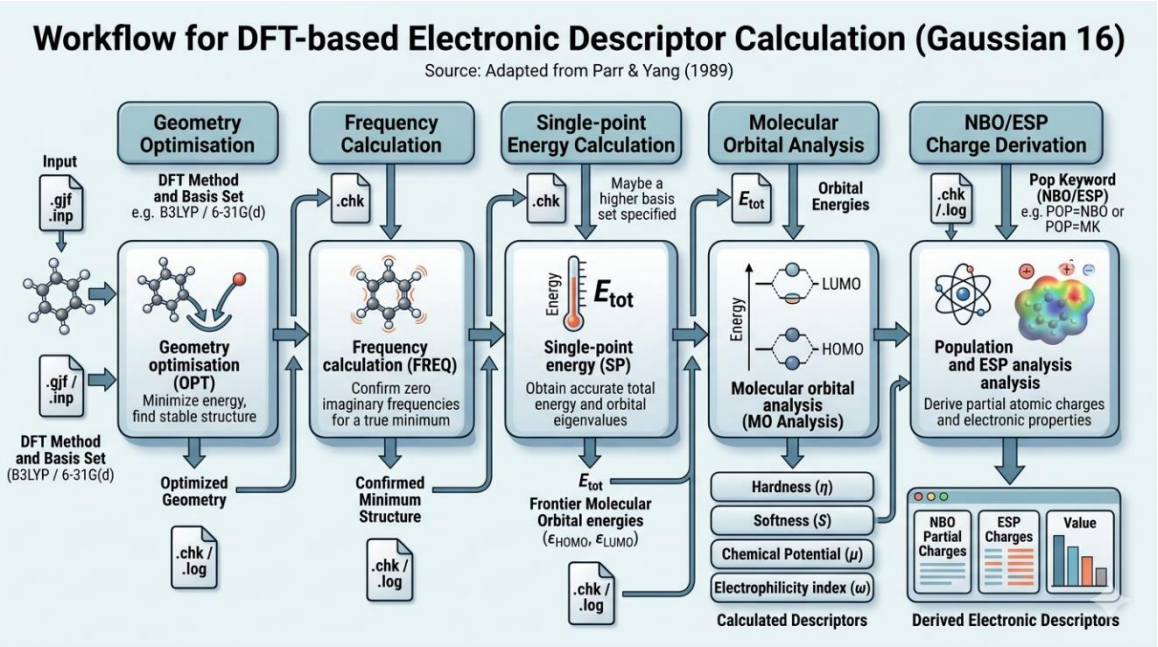

Figure 4: Workflow for DFT-based electronic descriptor calculation: geometry optimisation → frequency calculation (confirm minimum) → single-point energy calculation → molecular orbital analysis → NBO/ESP charge derivation. Software: Gaussian 16. Adapted from Par

2.3 Molecular Docking and Ligand–Protein Interactions

2.3.1 Principles of Molecular Docking

Molecular docking is a computational method that predicts the preferred binding orientation (pose) of a small molecule (ligand) within the binding site of a macromolecular receptor, and estimates the free energy of binding through a scoring function (Morris & Lim-Wilby, 2008). The docking procedure consists of two conceptually distinct but computationally interlinked components: a search algorithm that explores the conformational and configurational space of the ligand within the receptor binding site, and a scoring function that evaluates the quality (thermodynamic favourability) of each sampled pose (Lengauer & Rarey, 1996). The accuracy of the docked pose and the predicted binding affinity depend critically on both components, and the limitations of current docking methods—particularly the approximate treatment of receptor flexibility and the empirical nature of most scoring functions—must be carefully considered when interpreting results (Huang et al., 2010).

2.3.2 Search Algorithms

Three principal classes of search algorithm are employed in molecular docking software: systematic search methods, random/stochastic methods, and deterministic methods. Systematic search algorithms exhaustively sample all rotatable bonds and translational/rotational degrees of freedom of the ligand; while theoretically complete, they become computationally intractable for flexible ligands with many rotatable bonds (Leach, 2001). Stochastic methods—including Monte Carlo (MC), simulated annealing, and genetic algorithms (GA)—explore conformational space probabilistically, accepting or rejecting moves according to energy criteria; the genetic algorithm implemented in AutoDock and its derivatives represents the most widely used approach (Morris et al., 1998). The Lamarckian Genetic Algorithm (LGA) employed in AutoDock 4 combines global search by GA with local gradient-based optimisation, achieving a good balance between conformational sampling completeness and computational efficiency (Morris et al., 1998). More recent implementations such as AutoDock Vina employ an iterated local search algorithm with a gradient-based optimisation step, offering substantially improved speed without compromising pose prediction accuracy for most ligand–receptor systems (Trott & Olson, 2010).

2.3.3 Scoring Functions

Scoring functions estimate the binding free energy ΔGbind from structural descriptors of the docked complex. Three families of scoring functions may be distinguished: force-field-based functions, which sum pairwise Lennard-Jones and electrostatic interaction energies between ligand and protein atoms with empirical corrections for desolvation; empirical functions, which fit a parameterised sum of interaction terms (van der Waals, hydrogen bond, desolvation, torsional entropy) to a training set of experimental binding affinities; and knowledge-based (statistical potential) functions, which derive atom-pair interaction potentials from the statistical analysis of known protein–ligand crystal structures (Huang et al., 2010). The empirical scoring function of AutoDock Vina incorporates steric, hydrophobic, and hydrogen-bonding terms and has been benchmarked extensively against crystallographic binding modes; for established drug targets, pose prediction accuracy (percentage of poses within 2 Å RMSD of the crystal structure) exceeds 70% for typical drug-like molecules (Trott & Olson, 2010).

For organometallic ligands such as ferrocenyl derivatives, standard scoring functions present limitations because the iron centre may coordinate to protein residues (histidine, cysteine, glutamate) in a manner that is not captured by the non-bonded van der Waals and electrostatic

terms alone (Diedrich & Grimme, 2003). In practice, coordinatively saturated 18-electron ferrocene is unlikely to form coordinate bonds with protein residues under physiological conditions; however, the overall accuracy of the predicted binding affinity may be diminished by the inadequate parametrisation of the Fe atom in standard force fields. A common approach to address this limitation is to derive custom van der Waals parameters for Fe from quantum chemical calculations and to validate the docking protocol against available crystal structures or experimental IC50 data (Ortega-Arizmendi et al., 2014).

Table 6: Representative docking scoring functions and their mathematical formulations

Software	Function Type	Key Terms	Reference
AutoDock 4	Force-field + empirical	vdW, electrostatics, H-bond, desolvation, torsion	Morris et al. (1998)
AutoDock Vina	Empirical (Gaussian)	Steric, H-bond, hydrophobic, torsion penalty	Trott & Olson (2010)
Glide (Schrödinger)	Empirical (GlideScore)	vdW, Coulomb, H-bond, lipophilic, penalty terms	Friesner et al. (2004)
GOLD	Force-field (ChemScore)	H-bond, metal, lipophilic contact, torsion	Jones et al. (1997)
MOE Dock	Knowledge-based	PMF, ASE, GBVI/WSA terms	Corbeil et al. (2012)

Note. vdW = van der Waals; H-bond = hydrogen bond; PMF = potential of mean force; GBVI = GB volume integral.

2.3.4 Topoisomerase IIα as a Docking Target

Human topoisomerase IIα (Topo IIα; EC 5.99.1.3) is a homodimeric type II topoisomerase that modulates DNA topology by catalysing the ATP-dependent passage of one double-stranded DNA segment through a transient double-strand break in a second segment (Wang, 2002). The enzyme is essential for chromosome segregation during mitosis and for the relief of torsional stress generated during replication and transcription; its elevated expression in proliferating tumour cells makes it a validated cancer target for drugs including doxorubicin, etoposide, and amsacrine

(Nitiss, 2009). Topo IIα inhibitors may operate as 'poisons'—stabilising the cleavable complex to produce irreversible DSBs—or as catalytic inhibitors that block ATP hydrolysis, DNA binding, or enzyme dimerisation without trapping the cleavage complex (Nitiss, 2009).

The crystal structure of the human Topo IIα ATPase domain (PDB: 1ZXM) and the DNA-binding/cleavage core domain (PDB: 4FM9) provide structural bases for structure-based virtual screening and docking (Wei et al., 2005; Wu et al., 2011). The ATP-binding site—occupied by AMPPNP in 1ZXM—contains a deep hydrophobic pocket lined by residues Lys168, Asn150, Ile141, and Ala167, and a hydrogen bond network involving Asn91, Asp94, and Glu87 that contacts the adenine and ribose moieties of the nucleotide (Wei et al., 2005). For docking of ferrocenyl candidates targeting the ATP binding site, the grid box should encompass the AMPPNP binding cleft; receptor preparation requires removal of water molecules outside the binding site, assignment of protonation states at physiological pH (pH 7.4), and energy minimisation of the hydrogen-atom positions (Morris & Lim-Wilby, 2008).

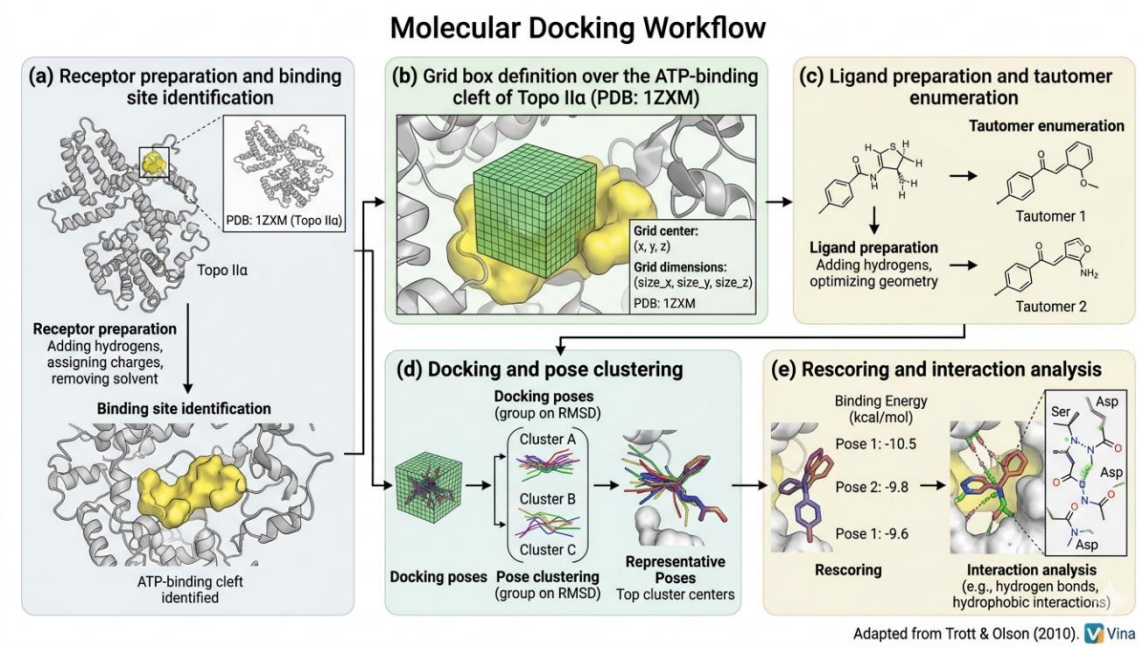

Figure 5: Schematic of the molecular docking workflow: (a) receptor preparation and binding site identification, (b) grid box definition over the ATP-binding cleft of Topo IIα (PDB: 1ZXM), (c) ligand preparation and tautomer enumeration, (d) docking and pose clus

2.4 Molecular Dynamics Simulation

2.4.1 Theoretical Foundations

Molecular dynamics simulation is a computational technique that generates the time evolution of an atomic system by numerically integrating Newton's equations of motion for each atom, using classical mechanics (Allen & Tildesley, 1987). For a system of N atoms with masses {mi} at positions {ri}, Newton's second law gives $F_i = m_i(d^2r_i/dt^2)$, where the force on atom i is derived from the total potential energy function $U(r_1,...,r_N)$ by $F_i = -\partial U/\partial r_i$. The potential energy function—the force field—describes inter- and intra-molecular interactions through analytical terms for bond stretching, angle bending, torsional rotation, and non-bonded (van der Waals and electrostatic) interactions (Case et al., 2005). The equations of motion are integrated numerically using the Verlet, leapfrog, or velocity Verlet algorithm with timesteps typically in the range 1–2 femtoseconds.

MD simulation provides access to thermodynamic and kinetic quantities that are not readily obtainable from static computational methods (docking, DFT): free energy differences between states, conformational entropy, diffusion coefficients, protein–ligand residence times, and the dynamic character of binding interactions. For drug design, MD is particularly valuable for assessing the stability of docked poses over nanosecond to microsecond timescales, identifying protein residues that maintain persistent contact with the ligand, and evaluating the conformational changes induced in the receptor upon ligand binding (Durrant & McCammon, 2011).

2.4.2 Force Fields for Biomolecular Simulation

The quality of an MD simulation depends fundamentally on the accuracy of the force field. Several well-validated force fields are available for the simulation of proteins and nucleic acids: AMBER (ff14SB, ff19SB), CHARMM (CGenFF, CHARMM36m), GROMOS (54a7), and OPLS-AA are the most widely employed (Case et al., 2005; MacKerell et al., 1998; Schmid et al., 2011; Jorgensen et al., 1996). For the organic ligand component of a drug–protein system, the General AMBER Force Field (GAFF) and CHARMM General Force Field (CGenFF) provide parameters for most drug-like molecules; partial charges are typically assigned by the RESP (restrained electrostatic potential) fitting procedure to charges derived from HF/6-31G(d) electrostatic potential calculations (Wang et al., 2004).

For ferrocene-containing compounds, the parametrisation of the Fe atom and the Cp ring system within an MM force field is non-trivial and has been addressed in a limited number of studies. The AMBER-compatible parameters for ferrocene developed by Pavlov and co-workers, based on MP2 and DFT calculations, reproduce the Fe–C bond distances, vibrational frequencies, and rotational barriers with satisfactory accuracy (Pavlov et al., 2001). The key challenge is the correct representation of the Fe–Cp interaction, which is inherently quantum mechanical in character: pure bond stretching terms underperform relative to more sophisticated angular-restraint approaches. In the absence of established parameters, it is common practice to treat ferrocene as a rigid body—constraining the Fe–Cp geometry to its QM-optimised structure—during MD simulation, an approximation that may be acceptable when the primary interest is the dynamics of the ligand–protein interface rather than the internal coordinate fluctuations of the ferrocene unit itself (Diedrich & Grimme, 2003).

Table 7: Common force fields employed in molecular dynamics simulations of biomolecular systems.

Force Field	Applicable Systems	Charge Method	Software	Reference
AMBER ff19SB	Proteins	RESP (HF/6-31G*)	AMBER 20	Case et al. (2005)
GAFF2	Small organic molecules	RESP/AM1-BCC	AMBER 20	Wang et al. (2004)
CHARMM36m	Proteins, lipids, nucleic acids	CHARMM force matching	NAMD, GROMACS	MacKerell et al. (1998)
OPLS-AA/M	Proteins, organic molecules	CM1A/RESP	GROMACS, Maestro	Jorgensen et al. (1996)
GROMOS 54a7	Proteins, lipids	Partial equalisation	GROMOS, GROMACS	Schmid et al. (2011)

Note. RESP = restrained electrostatic potential; AM1-BCC = AM1 bond charge correction.

2.4.3 System Preparation and Simulation Protocol

Standard system preparation for MD simulation of a protein–ligand complex involves: (i) retrieval and preparation of the receptor structure from the Protein Data Bank (PDB), including addition of missing loops, removal of crystallographic water and cofactors not relevant to the binding site, assignment of protonation states using empirical pKa prediction (e.g., H++, PropKa) at pH 7.4, and capping of terminal residues; (ii) docking or manual placement of the ligand in the binding site; (iii) solvation in an explicit water box (TIP3P or SPC/E water model) with approximately 10 Å of solvent in each direction from the protein surface; (iv) addition of counter-ions (Na^+ and Cl^-) to neutralise the system and reach physiological ionic strength (~0.15 M); and (v) energy minimisation to remove steric clashes (Allen & Tildesley, 1987; Case et al., 2005).

The equilibration phase typically proceeds in stages: NVT (constant volume and temperature) equilibration with positional restraints on the protein heavy atoms, followed by NPT (constant pressure and temperature) equilibration with progressively reduced restraints to allow the system to relax to the correct density (~1.0 g cm^{-3}). Periodic boundary conditions (PBC) with the particle mesh Ewald (PME) method for long-range electrostatics, LINCS or SHAKE constraints on hydrogen-containing bonds (permitting a 2 fs timestep), and Nosé–Hoover or V-rescale thermostat and Parrinello–Rahman or Berendsen barostat are standard choices for the production simulation (Darden et al., 1993). Production runs of 50–200 ns are typically employed for the investigation of protein–ligand binding dynamics, although the convergence of binding free energies may require longer simulations or enhanced sampling techniques.

2.4.4 Trajectory Analysis: RMSD, RMSF, and Binding Free Energy

The stability and dynamics of the simulated complex are assessed through several trajectory analysis metrics. The root mean square deviation (RMSD) of the protein Cα atoms from the minimised initial structure, computed as a function of simulation time, provides a measure of overall structural drift and convergence; RMSD values below 2–3 Å for stable protein–ligand complexes indicate that the simulation has reached equilibrium (Durrant & McCammon, 2011). The root mean square fluctuation (RMSF) per residue identifies structurally labile regions of the protein and quantifies the dynamic response of the binding site to ligand occupancy; residues with high RMSF values in the ligand-bound state relative to the apo protein suggest induced-fit binding effects.

Binding free energy estimation through the MM-PBSA (molecular mechanics–Poisson-Boltzmann surface area) or MM-GBSA (GB implicit solvation) methods provides a computationally affordable means to rank ligand binding affinities from MD trajectories (Kollman et al., 2000). In these methods, $\Delta G_{bind} \approx \Delta E_{mm} + \Delta G_{PB/GB} - T\Delta S_{mm}$, where ΔE_{mm} is the molecular mechanics interaction energy (van der Waals + electrostatics), $\Delta G_{PB/GB}$ is the polar solvation free energy computed by solving the Poisson-Boltzmann or generalised Born equation, and $T\Delta S_{mm}$ is the conformational entropy change estimated from normal mode analysis. The MM-PBSA approach is known to exhibit systematic errors of 2–5 kcal mol−1 in absolute binding free energies, but relative rankings within a congeneric series are generally reliable, making it a valuable tool for lead optimisation (Hou et al., 2011).

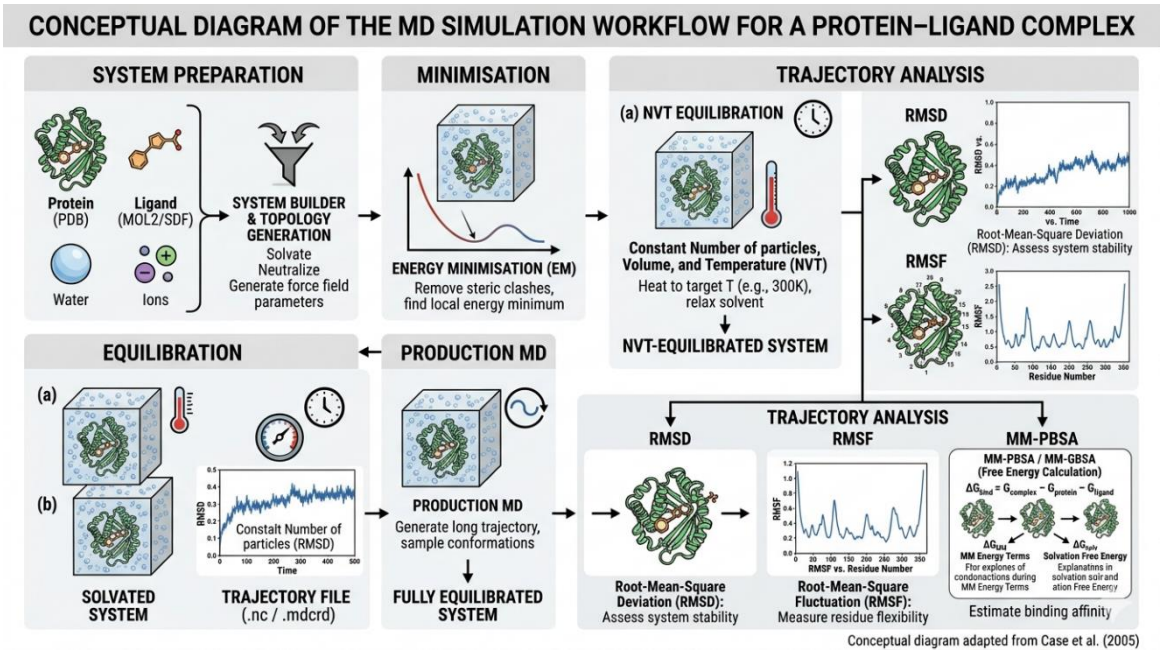

Figure 6: Conceptual diagram of the MD simulation workflow for a protein–ligand complex: system preparation → minimisation → NVT equilibration → NPT equilibration → production MD → trajectory analysis (RMSD, RMSF, MM-PBSA). Adapted from Case et al. (2005).

2.5 ADMET Prediction and Drug-Likeness Evaluation

2.5.1 Rationale and Overview

The attrition of drug candidates in late-stage clinical development—attributed in significant measure to suboptimal pharmacokinetic profiles and unanticipated toxicity—has driven the incorporation of in silico ADMET (absorption, distribution, metabolism, excretion, and toxicity) prediction early in the drug discovery process (Kola & Landis, 2004; van de Waterbeemd &

Gifford, 2003). In silico ADMET tools offer several advantages over experimental assays in the early hit-to-lead phase: high throughput, low cost, and the ability to predict properties for virtual compounds before synthesis. Their limitations are equally significant: predictive models are trained on historical pharmaceutical data biased toward organic small molecules, and their transferability to novel chemotypes—including organometallics such as ferrocenyl derivatives—is inherently uncertain (Daina et al., 2017).

2.5.2 Absorption and Oral Bioavailability

The oral absorption of a drug candidate depends on its aqueous solubility, intestinal permeability, and susceptibility to first-pass metabolism and efflux transporters. Lipinski's rule of five (RO5) identifies four physicochemical filters that correlate empirically with poor oral absorption in the absence of active transport: MW > 500 Da, cLogP > 5, HBD > 5, HBA > 10 (Lipinski et al., 1997). While the RO5 remains the most widely cited oral drug-likeness filter, its limitations have been documented: it was derived from orally absorbed drugs up to the Phase II clinical stage and has reduced predictive power for compounds targeting intracellular organelles, natural product-derived scaffolds, or beyond-rule-of-five (bRo5) chemical space (Doak et al., 2014). For ferrocenyl compounds, the hydrophobic Cp rings typically increase calculated logP values, potentially approaching or exceeding the Ro5 boundary; however, measured logP values may differ from calculated estimates by 0.5–1.5 log units owing to the unusual electronic structure of the ferrocene moiety.

The Caco-2 cell permeability assay provides the experimental reference for intestinal permeability predictions; in silico models based on QSAR, neural networks, or random forest algorithms trained on Caco-2 data are implemented in tools such as SwissADME, pkCSM, and ADMETlab (Daina et al., 2017; Pires et al., 2015; Xiong et al., 2021). Passive transcellular permeability is governed primarily by molecular weight, polar surface area (PSA), number of rotatable bonds, and HBD count; compounds with PSA < 90 $Å^2$ and MW < 400 Da typically exhibit high passive permeability (Veber et al., 2002).

2.5.3 Distribution and Blood–Brain Barrier Penetration

The volume of distribution (Vd) reflects the partitioning of a drug between plasma and tissue compartments; drugs with high Vd (> 0.7 L/kg) suggest extensive tissue distribution and long half-lives. Plasma protein binding—predominantly to human serum albumin (HSA) and alpha-1 acid glycoprotein—is predicted from logP, polar surface area, and aromatic ring count; highly lipophilic

compounds tend to exhibit high protein binding (>90%), which reduces the free drug concentration available for target engagement (van de Waterbeemd & Gifford, 2003). Blood–brain barrier (BBB) penetration is predicted from the BBB score (a composite of PSA, MW, HBD, and logP) or from dedicated QSAR models; while CNS penetration is not a therapeutic objective for most anticancer agents, unintended BBB penetration may raise neurotoxicity concerns (Daina et al., 2017).

2.5.4 Metabolism and CYP450 Inhibition

Cytochrome P450 enzymes (CYP1A2, CYP2C9, CYP2C19, CYP2D6, CYP3A4) are responsible for the oxidative metabolism of approximately 75% of marketed drugs; CYP inhibition can cause drug–drug interactions through the competitive displacement of co-administered substrates, potentially leading to drug accumulation and toxicity (Guengerich, 2008). In silico prediction of CYP inhibition is performed using pharmacophore models, machine-learning classifiers (random forest, SVM), or structure-based models of the CYP active site (Daina et al., 2017). For ferrocene derivatives, CYP-mediated hydroxylation of the Cp ring has been documented both in vitro and in vivo; ferrocene itself is primarily hydroxylated by CYP2B1 in rats to yield hydroxyferrocene, which undergoes further conjugation (Köpf-Maier & Köpf, 1987). The relevance of this metabolic pathway to the pharmacokinetics of the target compounds should be evaluated through dedicated metabolic stability assays.

2.5.5 Toxicity Prediction

Computational toxicity prediction encompasses a broad spectrum of endpoints, including mutagenicity (Ames test prediction), hERG channel inhibition (cardiotoxicity), hepatotoxicity, skin sensitisation, and acute oral toxicity (LD50). The hERG potassium channel mediates cardiac repolarisation, and its inhibition by drug candidates is a major cause of drug withdrawal; in silico hERG inhibition models identify structural alerts (basic nitrogen, hydrophobic aromatic groups) associated with channel blockade (Daina et al., 2017). AMES mutagenicity is predicted using the Derek Nexus or QSAR-based LAZAR tools, which flag reactive functional groups (nitro, aromatic amines, epoxides) that are precursors to DNA-reactive electrophiles (Pires et al., 2015). For ferrocenyl compounds, the potential for ROS generation—while desirable in the tumour context—raises concerns about off-target oxidative DNA damage and genotoxicity; this dual-edged character of ferrocene redox activity must be carefully considered in the toxicological profile.

Table 8: Key ADMET parameters and their accepted thresholds for oral drug candidates.

Parameter	Optimal Range	Prediction Tool	Reference
Molecular Weight (MW)	150–500 Da	SwissADME, Molinspiration	Lipinski et al. (1997)
cLogP	−0.5 to 5.0	SwissADME, ALOGPS	Lipinski et al. (1997)
Polar Surface Area (PSA)	< 90 Å²	SwissADME, pkCSM	Veber et al. (2002)
HBD	≤ 5	SwissADME, DataWarrior	Lipinski et al. (1997)
HBA	≤ 10	SwissADME, DataWarrior	Lipinski et al. (1997)
Caco-2 Permeability	> 0.90 × 10^{-6} cm/s	pkCSM, ADMETlab 2.0	Pires et al. (2015)
Plasma Protein Binding	< 90%	pkCSM, SwissADME	van de Waterbeemd & Gifford (2003)
hERG Inhibition (IC50)	> 30 μM (low risk)	pkCSM, ADMETlab 2.0	Daina et al. (2017)
AMES Mutagenicity	Negative	ProTox-II, pkCSM	Pires et al. (2015)

Note. HBD = hydrogen bond donor; HBA = hydrogen bond acceptor. Thresholds are based on consensus values from multiple sources.

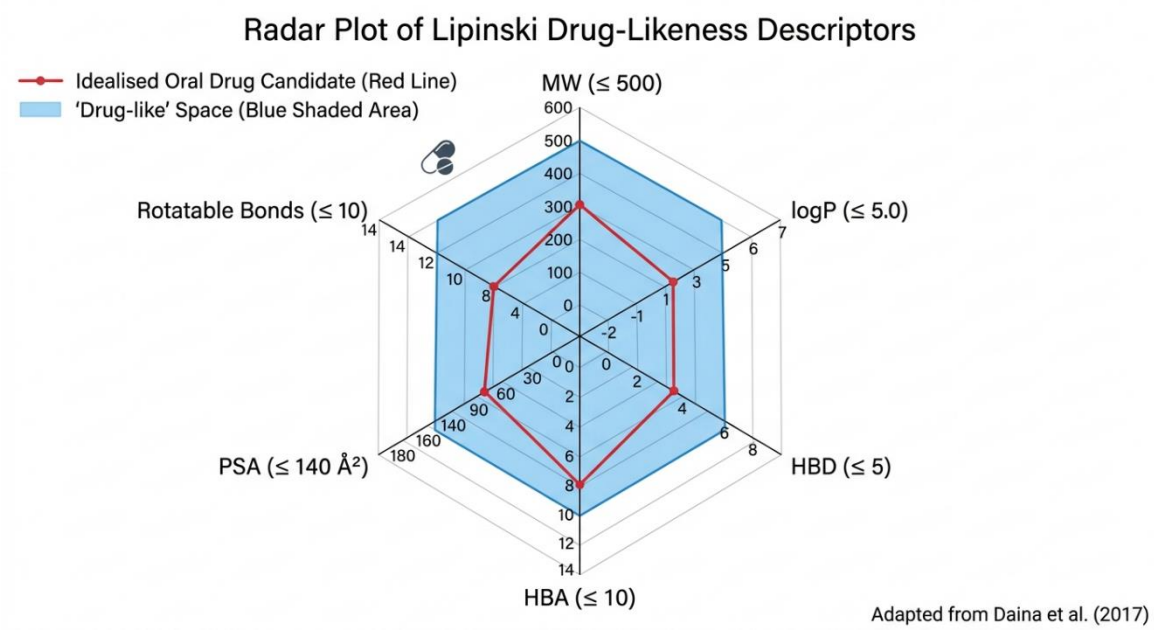

Figure 7: Radar plot of Lipinski drug-likeness descriptors (MW, logP, HBD, HBA, PSA, rotatable bonds) for an idealised oral drug candidate, with the acceptable 'drug-like' space shaded in blue. Adapted from Daina et al. (2017).

2.5.6 Limitations of In Silico ADMET Prediction

The inherent limitations of in silico ADMET prediction must be acknowledged when interpreting computational results for novel compound classes. First, current prediction models are predominantly trained on datasets of organic small molecules with drug-like physicochemical properties; the applicability domain of these models to organometallic compounds, which occupy a distinct region of chemical space, is uncertain (Daina et al., 2017). Second, the accuracy of individual property predictions varies considerably: solubility and logP predictions are typically within 0.5–1.0 log units of experimental values, while metabolic stability and toxicity predictions exhibit larger errors and higher false-positive rates (van de Waterbeemd & Gifford, 2003). Third, in vitro ADMET assays themselves exhibit interlaboratory variability, meaning that even 'experimental' reference values used to train prediction models carry measurement uncertainty.

Notwithstanding these limitations, in silico ADMET screening provides valuable guidance at the hit-identification stage by rapidly identifying compounds with obvious liabilities (e.g., excessive MW, multiple structural alerts) before costly synthesis and experimental evaluation. For the ferrocenyl acetylaniline derivatives investigated in this thesis, computational ADMET profiling serves as a flag-raising tool rather than a definitive pharmacokinetic assessment; experimental validation of key parameters—solubility, metabolic stability, CYP inhibition—is ultimately necessary and is addressed in subsequent experimental chapters.

2.6 Conclusion

This chapter has critically reviewed the four computational methodologies that constitute the in silico investigation strategy of this thesis. Density functional theory, when applied with appropriate functional and basis-set combinations, furnishes reliable geometries, electronic descriptors, and molecular orbital information for ferrocenyl compounds, with the B3LYP/6-31G(d)–SDD combination representing a validated and pragmatic choice. Molecular docking, employing the AutoDock Vina scoring function, provides a computationally efficient means of predicting binding poses and relative affinities at the Topo IIα ATP-binding cleft, subject to the acknowledged limitations of empirical scoring functions and the need for validated parametrisation of the Fe centre.

Molecular dynamics simulation extends the static docking picture to a dynamic, solution-phase description of the ligand–receptor complex, with RMSD, RMSF, and MM-PBSA analyses

providing a multidimensional characterisation of binding stability, selectivity, and free energy. Finally, in silico ADMET screening using validated web-based tools (SwissADME, pkCSM, ADMETlab 2.0) identifies potential pharmacokinetic and toxicological liabilities in the ferrocenyl series, guiding synthetic prioritisation, though the applicability domain of these models to organometallic scaffolds necessitates cautious interpretation. Together, these methodologies constitute a coherent, multiscale computational framework whose application to the target ferrocenyl acetylaniline derivatives is described in the subsequent chapters of this thesis.

Second part:

Experimental Analysis

Chapter 01:

Materials & Methods

1. General Introduction

This chapter outlines the experimental protocols and computational strategies adopted for the synthesis, structural elucidation and *in silico* investigation of ferrocenyl acetylaniline derivatives. The overall methodology combines synthetic organometallic chemistry with advanced spectroscopic, electrochemical and molecular modelling techniques in order to establish a comprehensive correlation between molecular structure, electronic properties and interaction behaviour towards anticancer targets.

The synthesis of the target compounds was carried out at the Laboratory of Valorisation and Technology of Saharian Resources (VTRS), Faculty of Technology, University of El Oued, under controlled laboratory conditions. The same research facility was used to perform all computational investigations, including density functional theory (DFT) calculations, molecular docking, molecular dynamics simulations and MM-PBSA analyses, ensuring methodological consistency between experimental and theoretical results.

Spectroscopic characterisation was conducted in collaboration with the Centre de Recherche Scientifique et Technique en Analyses Physico-Chimiques (CRAPC), University of Ouargla. A combination of FT-IR, UV–Visible spectroscopy and one- and two-dimensional NMR techniques was employed to confirm the molecular structures of the synthesised derivatives. In addition, cyclic voltammetry was used to explore the redox properties of the ferrocenyl core, which are directly related to its electronic behaviour.

Particular emphasis was placed on the evaluation of the interaction potential of these compounds with Topoisomerase IIα, a key enzyme involved in DNA replication and a well-established target in anticancer therapy. To this end, molecular docking and molecular dynamics simulations were employed to investigate binding affinity, interaction mechanisms and structural stability of the ligand–enzyme complexes.

Furthermore, *in silico* ADMET predictions were performed to assess pharmacokinetic properties, drug-likeness and potential toxicity, providing an initial evaluation of their suitability as anticancer candidates.

Overall, this integrated approach ensures the robustness and reliability of the obtained data and provides a solid framework for understanding the physicochemical behaviour and biological relevance of ferrocenyl derivatives in the context of anticancer applications.

2. Chemicals and Reagents

All reagents and solvents employed in this study were of analytical grade and used without further purification unless otherwise specified. The choice of chemicals was guided by their suitability for organometallic synthesis and compatibility with subsequent spectroscopic and electrochemical analyses.

Ferrocene (Fc, 99%) and orthophosphoric acid (85%) were supplied by Alfa Aesar. The o-, m-, and p-aminoacetophenone isomers (99%), along with tetrabutylammonium tetrafluoroborate (Bu_4NBF_4, electrochemical grade, 99%) used as supporting electrolyte, were obtained from Sigma-Aldrich. Iodomethane and anhydrous magnesium sulfate (97%) were purchased from Acros Organics, while acetic acid (99–100%) and ethanol (95%) were provided by Biochem Chemopharma.

The ferrocenylmethyl quaternary ammonium intermediate was synthesised according to previously reported procedures and used directly without additional purification (Khand et al., 1989). All aqueous solutions were prepared using double-distilled water, and solvents used for analytical measurements were of appropriate purity to ensure reproducibility.

Stock solutions were freshly prepared when required and handled under standard laboratory conditions to minimise degradation and contamination.

3. Instrumentation and Experimental Conditions

3.1. Spectroscopic Analysis

3.1.1. FT-IR Spectroscopy

Fourier-transform infrared (FT-IR) spectra were recorded using a Shimadzu 8000S spectrophotometer over the range 4000–400 cm^{-1}. Solid samples were prepared as KBr pellets.

This technique enabled identification of key functional groups, including N–H stretching, carbonyl (C=O) vibrations and aromatic C–H bonds, thereby confirming the formation of the ferrocenyl acetylaniline framework (Lanez et al., 2020a).

3.1.2. UV–Visible Spectroscopy

Electronic absorption spectra were obtained using a Shimadzu UV-1800 spectrophotometer in the range 200–900 nm. Measurements were carried out in dimethyl sulfoxide (DMSO) using quartz cuvettes (1 cm path length).

The analysis provided information on electronic transitions within the molecules, including π–π*, n–π* and metal-centred transitions, reflecting the conjugation between the ferrocenyl unit and the aromatic system (Lanez et al., 2020b)

3.2. Nuclear Magnetic Resonance (NMR)

3.2.1. ^{1}H NMR Analysis

^{1}H NMR spectra were recorded on a Bruker ARX-500 spectrometer (400 MHz) using DMSO-d_6 as solvent. Chemical shifts (δ) were referenced to tetramethylsilane (TMS).

The spectra allowed clear identification of proton environments associated with the ferrocenyl rings, aromatic moiety, methylene bridge and acetyl group, confirming the expected molecular structures (Lanez et al., 2023a)

3.2.2. ^{13}C NMR Analysis

^{13}C NMR spectra were obtained under similar experimental conditions. The analysis provided detailed assignment of carbon atoms, including carbonyl carbons, aromatic carbons, cyclopentadienyl rings and methylene carbons.

These data confirmed the successful functionalisation of the ferrocenyl scaffold 5. (Benamara et al., 2020)

3.2.3. Two-Dimensional NMR (HSQC/HMBC)

Two-dimensional NMR experiments (HSQC and HMBC) were performed to establish proton–carbon correlations.

HSQC enabled direct one-bond correlations, while HMBC provided long-range connectivity, allowing unambiguous structural assignment and confirmation of substitution patterns on the aromatic ring (Lanez et al., 2019a)

3.3. Electrochemical Measurements (Cyclic Voltammetry)

Electrochemical measurements were carried out using a PGZ301 potentiostat/galvanostat (Radiometer Analytical, France) in dimethyl sulfoxide (DMSO) under nitrogen atmosphere at 298 K.

A conventional three-electrode system was employed, consisting of a glassy carbon working electrode (0.013 cm²), a platinum counter electrode (0.05 cm²) and a saturated Hg/Hg_2Cl_2 reference electrode. Tetrabutylammonium tetrafluoroborate (0.1 M) was used as supporting electrolyte.

Prior to each experiment, the solution was purged with nitrogen to eliminate dissolved oxygen and ensure stable electrochemical conditions.

Cyclic voltammetry measurements were performed within a defined potential window to investigate the Fe(II)/Fe(III) redox behaviour of the ferrocenyl derivatives. The obtained electrochemical parameters provided insight into electron-transfer processes and the intrinsic electronic properties of the compounds (Lanez et al., 2020c)

4. Synthesis of Ferrocenyl Acetylaniline Derivatives

This section outlines the synthetic route adopted for the preparation of the ferrocenyl acetylaniline derivatives. The methodology is based on a nucleophilic substitution strategy involving a ferrocenylmethyl quaternary ammonium intermediate, allowing efficient formation of the C–N bond under relatively mild reaction conditions. This approach ensures good selectivity, operational simplicity and reproducibility in obtaining the three regioisomeric derivatives.

The overall synthetic pathway is illustrated in Figure 8, which depicts the generation of the ferrocenylmethyl intermediate followed by its coupling with the corresponding aminoacetophenone isomers.

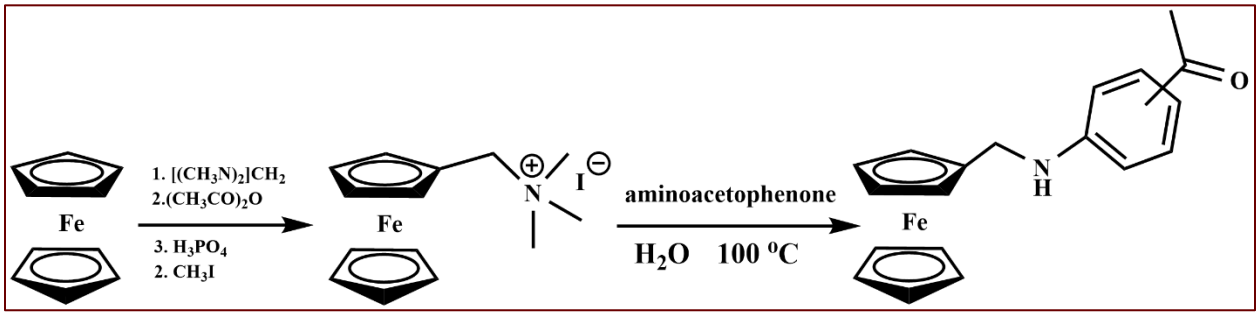

Figure 8: Synthetic route for the preparation of N-[(ferrocenyl)methyl]acetylaniline derivatives (FcMe2Ac, FcMe3Ac and FcMe4Ac).

The target compounds were synthesised via nucleophilic substitution between trimethylferrocenylmethylammonium iodide and the corresponding aminoacetophenone isomers (ortho, meta and para), as shown in Figure 8.

In a typical experiment, the selected aminoacetophenone (3.84 mmol) was progressively introduced into a stirred aqueous solution of trimethylferrocenylmethylammonium iodide (2.56 mmol) dissolved in distilled water (60 mL). The reaction mixture was maintained under reflux for 4 hours to ensure complete conversion.

After completion, the mixture was cooled to ambient temperature, resulting in the formation of a yellow precipitate. The crude product was recovered by vacuum filtration and washed thoroughly with distilled water to eliminate residual salts and unreacted reagents.

Purification was achieved by recrystallisation from a 90% ethanol/water mixture. For the meta-substituted derivative, an additional purification step using column chromatography (chloroform/methanol, 99:1 v/v) was required to obtain a higher purity product.

This synthetic protocol offers several advantages, including the use of an aqueous medium, straightforward experimental handling and avoidance of harsh conditions, making it well-suited for the reproducible synthesis of ferrocenyl derivatives (Lanez et al., 2019b)

4.1. Synthesis of Individual Compounds

4.1.1. N-[(ferrocenyl)methyl]-2-acetylaniline (FcMe2Ac)

Yield: 650 mg (77%).

Appearance: Yellow crystalline solid.

Melting point: 148–150 °C.

^{1}H NMR (500 MHz, DMSO-d_6): δ 2.60 (3H, m, CH_3), 3.40 (2H, t, α-C_5H_4), 4.05 (2H, t, β-C_5H_4), 4.15 (5H, s, C_5H_5), 4.30 (2H, d, CH_2N), 6.62 (1H, m, Ar-H), 6.84 (1H, d, Ar-H), 7.40 (1H, m, Ar-H), 7.85 (1H, d, Ar-H), 9.01 (1H, s, NH).

^{13}C NMR (500 MHz, DMSO-d_6): δ 29 (CH_3), 42 (CH_2N), 67, 68 (C_5H_4), 69 (C_5H_5), 87 (ipso-C), 112, 116, 118, 134, 138, 150 (aromatic carbons), 210 (C=O).

FT-IR (KBr, ν, cm^{-1}): 3426, 3291 (N–H), 3082 (Ar–C–H), 1647 (C=O), 1566, 1516 (C=C), 1454, 1416, 1146, 1003, 617.

UV–Vis (DMSO): λmax = 259 nm (π–π*), 380 nm (d–d).

Cyclic voltammetry (DMSO, Fc^{+}/Fc): Ipa = 29.13 μA, Ipc = −28.52 μA, Epa = 2.17 mV, Epc = −85.60 mV, ΔE = 87.8 mV, E° = 43.9 mV, Ipa/Ipc = 1.02.

4.1.2. N-[(ferrocenyl)methyl]-3-acetylaniline (FcMe3Ac)

Yield: 480 mg (48%).

Appearance: Yellow–orange crystalline solid.

Melting point: 138–140 °C.

^{1}H NMR (500 MHz, DMSO-d_6): δ 2.45 (3H, s, CH_3), 3.42 (2H, t, α-C_5H_4), 4.08 (2H, t, β-C_5H_4), 4.18 (5H, s, C_5H_5), 4.32 (2H, d, CH_2N), 6.70–7.20 (3H, m, Ar-H), 7.65 (1H, d, Ar-H), 8.95 (1H, s, NH).

^{13}C NMR (500 MHz, DMSO-d_6): δ 28 (CH_3), 43 (CH_2N), 66, 68 (C_5H_4), 69 (C_5H_5), 86 (ipso-C), 114, 118, 125, 131, 136, 152 (aromatic carbons), 205 (C=O).

FT-IR (KBr, ν, cm^{-1}): 3432, 3338 (N–H), 2925, 1650 (C=O), 1582, 1510, 1450, 1365, 1170, 820.

UV–Vis (DMSO): λmax = 268 nm, 402 nm.

Cyclic voltammetry (DMSO, Fc^+/Fc): Ipa = 52.4 μA, Ipc = −51.9 μA, Epa = 10 mV, Epc = −92 mV, ΔE = 102 mV, E° = 51.0 mV, Ipa/Ipc = 1.01.

4.1.3. N-[(ferrocenyl)methyl]-4-acetylaniline (FcMe4Ac)

Yield: 690 mg (80%).

Appearance: Deep yellow crystalline solid.

Melting point: 162–164 °C.

^{1}H NMR (500 MHz, DMSO-d_6): δ 2.35 (3H, m, CH_3), 3.41 (2H, t, α-C_5H_4), 4.10 (2H, t, β-C_5H_4), 4.20 (5H, s, C_5H_5), 4.31 (2H, d, CH_2N), 6.65 (2H, d, Ar-H), 6.78 (1H, t, NH), 7.76 (2H, d, Ar-H).

^{13}C NMR (500 MHz, DMSO-d_6): δ 28 (CH_3), 43 (CH_2N), 66 (C_5H_4), 68 (C_5H_5), 87 (ipso-C), 112, 125, 132, 154 (aromatic carbons), 194 (C=O).

FT-IR (KBr, ν, cm^{-1}): 3445, 3345 (N–H), 2932, 1651 (C=O), 1589, 1562, 1369, 1281, 1173, 822.

UV–Vis (DMSO): λmax = 432 nm.

Cyclic voltammetry (DMSO, Fc^+/Fc): Ipa = 71.07 μA, Ipc = −71.66 μA, Epa = 16 mV, Epc = −99 mV, ΔE = 115 mV, E° = 57.5 mV, Ipa/Ipc = 0.99.

5. Computational Methodology

Computational analyses were undertaken to elucidate the electronic characteristics and interaction potential of the synthesised ferrocenyl acetylaniline derivatives in relation to their activity against anticancer targets. The adopted *in silico* framework integrates density functional theory (DFT), molecular docking, molecular dynamics (MD) simulations and MM-PBSA free energy calculations, complemented by ADMET prediction tools.

This integrated methodology allows the establishment of correlations between molecular structure, electronic distribution and binding behaviour towards Topoisomerase IIα, a key enzyme involved in DNA topology regulation and a validated target in anticancer therapy.

5.1. Electronic Structure Calculations (DFT)

Quantum chemical calculations were performed using Gaussian 16 9. (Frisch et al., 2009) to investigate the electronic properties of FcMe2Ac, FcMe3Ac and FcMe4Ac.

Geometry optimisation was carried out at the B3LYP level using the 6-311++G(d,p) basis set for light atoms (C, H, N, O), while the Stuttgart–Dresden (SDD) effective core potential was applied to the iron centre (Andersson & Uvdal, 2005). Vibrational frequency calculations confirmed that all optimised structures correspond to true minima.

The optimised geometries were used to evaluate frontier molecular orbitals (HOMO and LUMO), energy gaps and global reactivity descriptors, including electronegativity, hardness, softness and electrophilicity index. These parameters provide insight into the reactivity profile and potential interaction capability of the molecules with biological targets.

In addition, molecular electrostatic potential (MEP), electron localisation function (ELF), localised orbital locator (LOL) and reduced density gradient (RDG) analyses were performed to characterise charge distribution and weak intramolecular interactions. Visualisation was carried out using GaussView and Multiwfn (Lu & Chen, 2012)

5.2. Molecular Docking Simulations

Molecular docking studies were conducted to evaluate the binding affinity and interaction mechanisms of the ferrocenyl derivatives with Topoisomerase IIα, using the crystallographic structures PDB ID: 1ZXM (Topoisomerase IIα–DNA–ligand complex) and PDB ID: 4FM9 (catalytic domain).

5.2.1. Receptor Preparation

The three-dimensional structures of the selected targets are illustrated in Figure 9, highlighting the organisation of the Topoisomerase IIα enzyme and its interaction with DNA.

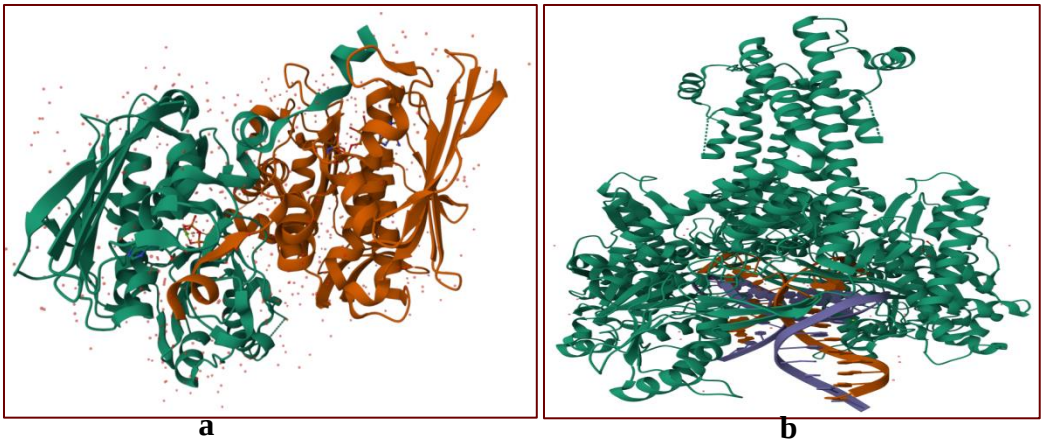

a b

Figure 9: Three-dimensional structures of Topoisomerase IIα targets used in docking studies: (a) 1ZXM complex and (b) 4FM9 catalytic domain.

The structures were retrieved from the Protein Data Bank (https://www.rcsb.org/) (Rose et al., 2017), and prepared using AutoDock Tools (ADT 1.5.7) (Morris et al., 2010). Water molecules, co-crystallised ligands and irrelevant heteroatoms were removed, while polar hydrogen atoms and Kollman charges were added. The prepared receptors were converted into PDBQT format.

5.2.2. Ligand Preparation

The optimised geometries of FcMe2Ac, FcMe3Ac and FcMe4Ac were used as input structures (Figure 10).

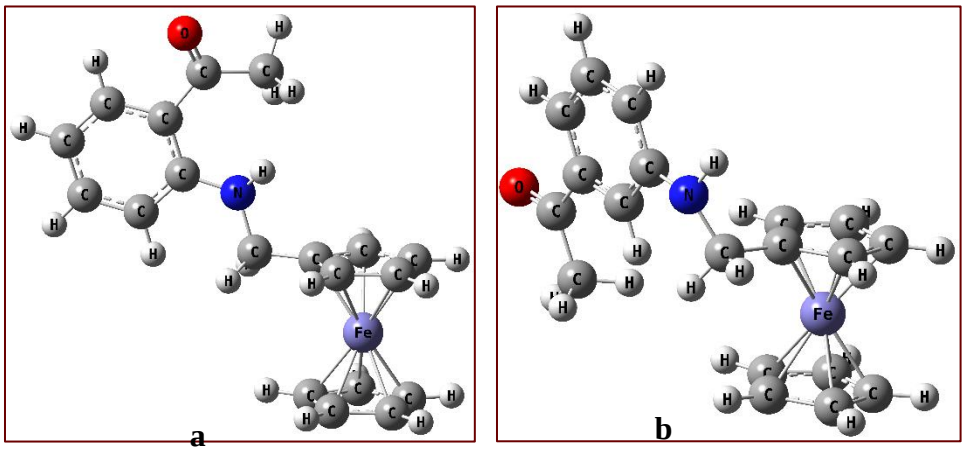

a b

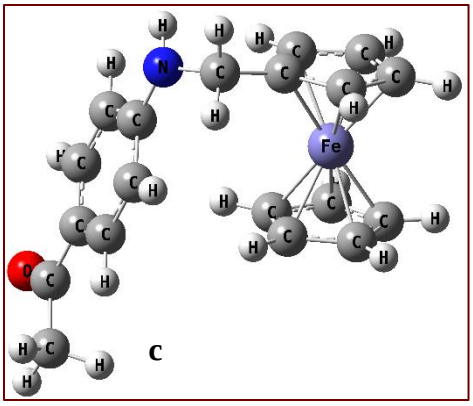

Figure 10: Optimised molecular structures of ferrocenyl derivatives used as ligands: FcMe2Ac (a), FcMe3Ac (b) and FcMe4Ac (c).

Ligands were prepared using AutoDock Tools by assigning Gasteiger charges and defining rotatable bonds, followed by conversion into PDBQT format.

5.2.3. Docking Protocol and Validation

The docking workflow is presented in Figure 11, summarising receptor preparation, ligand preparation, grid generation and docking analysis.

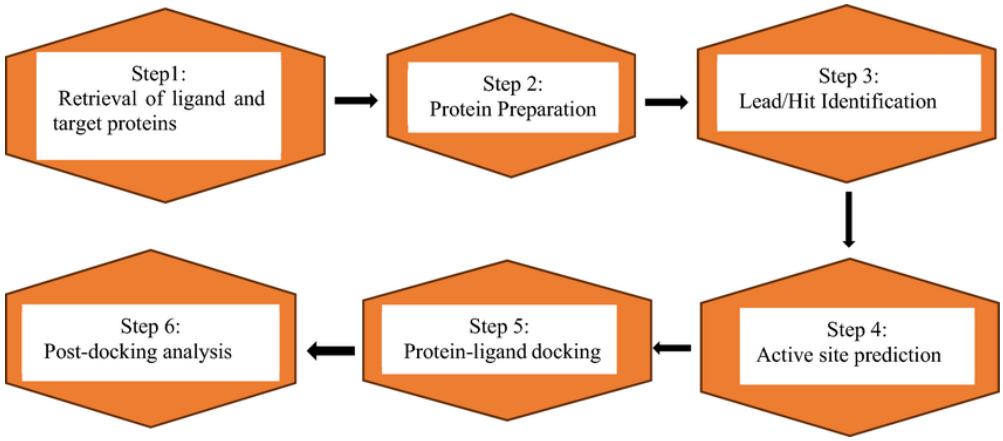

Figure 11: Molecular docking workflow illustrating protein and ligand preparation, grid generation, docking execution and interaction analysis

Docking simulations were performed using AutoDock 4.2 with the Lamarckian genetic algorithm. A grid box of 60 × 60 × 60 Å (spacing 0.375 Å) was centred on the active site region, particularly the DNA cleavage site in the 1ZXM structure.

A total of 100 independent docking runs were performed for each ligand–target system. The best binding pose was selected based on binding energy and cluster population.

Validation of the docking protocol was achieved by redocking the co-crystallised ligand and evaluating the RMSD between experimental and predicted conformations, ensuring reliability of the docking setup (Lanez et al., 2024a)

5.3. Molecular Dynamics (MD) Simulations

MD simulations were carried out to assess the stability and dynamic behaviour of the selected ligand–Topoisomerase IIα complexes using GROMACS (Lanez et al., 2023b)

5.3.1. System Setup and Solvation

The solvated system is illustrated in Figure 12, showing the protein–DNA–ligand complex embedded in an explicit water box.

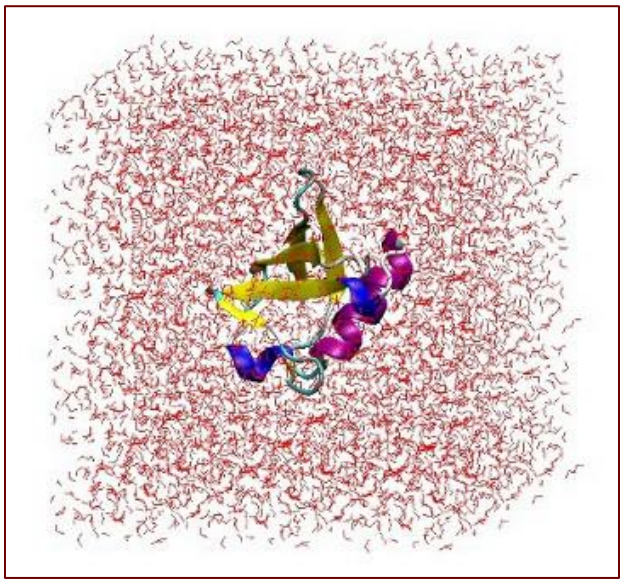

Figure 12. Solvated protein–ligand complex showing the explicit water box used for molecular dynamics simulations.

The CHARMM36 force field was used for protein and DNA parameterization (Huang & MacKerell, 2013), while ligand parameters were generated using the CGenFF protocol (Vanommeslaeghe & MacKerell, 2012). The system was placed in a cubic box with a minimum 10 Å margin and solvated using the TIP3P water model. Counter ions were added to ensure electroneutrality.

5.3.2. Energy Minimisation and Equilibration

The general molecular dynamics simulation protocol, including minimisation, equilibration and production stages, is summarised in Figure 13.

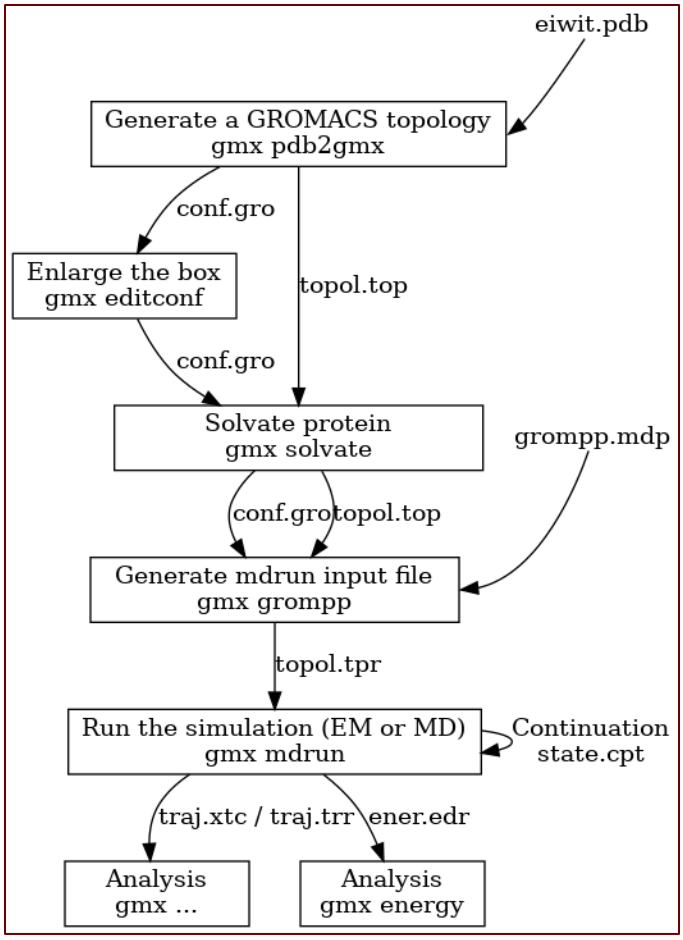

Figure 13. Molecular dynamics simulation workflow including system preparation, energy minimisation, equilibration and production phases.

Energy minimisation was performed using the steepest descent algorithm. The system was then equilibrated under NVT conditions (300 K, 500 ps) followed by NPT conditions (1 atm, 500 ps) using the V-rescale thermostat and Parrinello–Rahman barostat.

5.3.3. Production Run Parameters

Production simulations were conducted for 100 ns with a time step of 2 fs. Periodic boundary conditions were applied in all directions, and long-range electrostatic interactions were treated using the Particle Mesh Ewald (PME) method. Covalent bonds involving hydrogen atoms were constrained using the LINCS algorithm.

Trajectory analyses were carried out using GROMACS built-in tools, including RMSD, RMSF, radius of gyration (Rg), and solvent surface accessibility area (SASA).

5.4. MM-PBSA Binding Free Energy Calculations

Binding free energy calculations were performed using the g_mmpbsa tool 18. (Kumari et al., 2014). Snapshots extracted from the last 20 ns of equilibrated trajectories were used.

The total binding free energy (ΔG_bind) was estimated as the sum of van der Waals, electrostatic, polar solvation and non-polar solvation contributions.

5.5. ADMET Prediction

Pharmacokinetic and toxicity properties were predicted using ADMETlab 2.0 (Dong et al., 2018) and ProTox-II (Banerjee et al., 2018).

Key parameters included gastrointestinal absorption, blood–brain barrier permeability, cytochrome P450 interactions, plasma protein binding and toxicity indicators (hepatotoxicity, mutagenicity and LD_{50}), providing an initial assessment of the suitability of the compounds as anticancer candidates.

Chapter 02:

Results & Discussion

1. General Introduction

This chapter presents a comprehensive analysis of the experimental and computational results obtained for the synthesised ferrocenyl acetylaniline derivatives. The objective is to establish clear correlations between molecular structure, electronic properties and their interaction behaviour towards Topoisomerase IIα, a key enzymatic target in anticancer therapy.

The discussion begins with an evaluation of the synthetic outcomes, including reaction efficiency and substituent effects, followed by an in-depth structural characterisation using FT-IR, UV–visible spectroscopy, nuclear magnetic resonance (^{1}H, ^{13}C and 2D NMR) and cyclic voltammetry. These complementary techniques provide robust confirmation of molecular structures and valuable insight into the electronic properties of the ferrocenyl core.

Subsequently, computational investigations are presented to extend the experimental findings. Density functional theory calculations are employed to analyse electronic descriptors and charge distribution, while molecular docking and molecular dynamics simulations are used to explore the interaction of the synthesised compounds with Topoisomerase IIα. Finally, MM-PBSA and ADMET analyses are discussed to evaluate binding stability and pharmacokinetic suitability in the context of anticancer drug development.

2. Synthesis of Ferrocenyl Acetylaniline Derivatives

The ferrocenyl acetylaniline derivatives (FcMe2Ac, FcMe3Ac and FcMe4Ac) were successfully obtained through a nucleophilic substitution strategy involving a ferrocenylmethyl quaternary ammonium intermediate and the corresponding aminoacetophenone isomers. The adopted synthetic route demonstrated high reliability and reproducibility, affording the desired products as yellow to orange crystalline solids under relatively mild experimental conditions.

The reaction pathway is depicted in Figure 14, which outlines the key mechanistic steps leading to the formation of the C–N bond at the ferrocenylmethyl position.

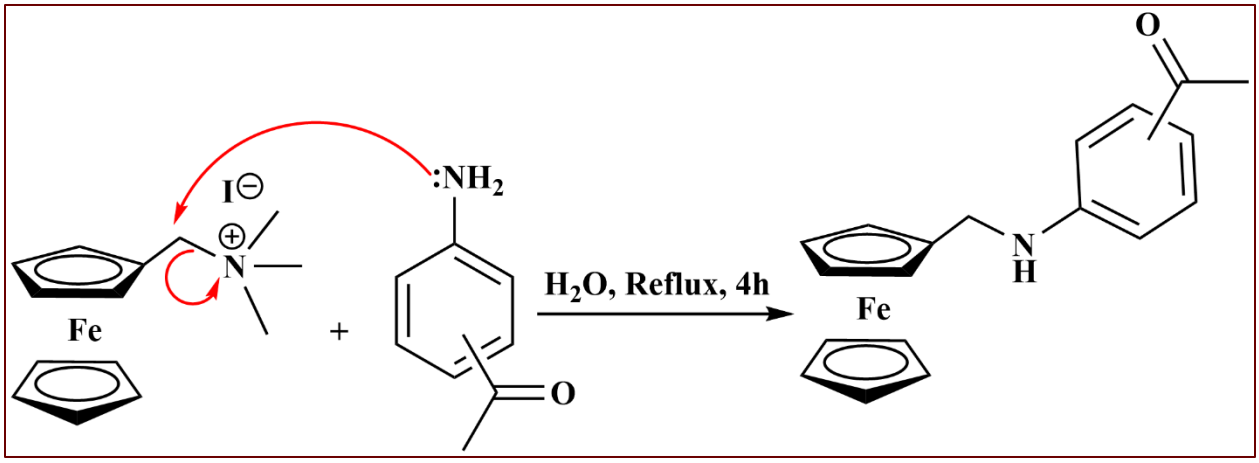

Figure 14. Proposed reaction mechanism for the formation of N-[(ferrocenyl)methyl]acetylaniline derivatives via nucleophilic substitution.

As illustrated in Figure 14, the transformation proceeds via a bimolecular nucleophilic substitution (SN2) mechanism, where the lone pair of the amino group attacks the electrophilic methylene carbon bonded to the quaternary ammonium centre. This process results in the displacement of trimethylamine as a leaving group and the formation of the ferrocenylmethylamine linkage. (Ouennoughi et al., 2017)

The efficiency of this reaction can be rationalised by both electronic and structural factors. The ferrocenyl moiety exhibits electron-donating properties, which facilitate stabilisation of the transition state and enhance the reactivity of the methylene carbon (Chebbah et al., n.d.). In parallel, the quaternary ammonium group acts as an excellent leaving group, enabling smooth bond cleavage under aqueous conditions. Such behaviour is consistent with previously reported reactivity patterns of ferrocenylmethyl derivatives, where favourable electronic delocalisation and structural flexibility promote nucleophilic substitution processes (Hanane et al., 2023) (Adaika et al., 2025a)

The chemical structures of the obtained compounds are presented in Figure 15, highlighting the positional variation of the acetyl substituent on the aromatic ring.

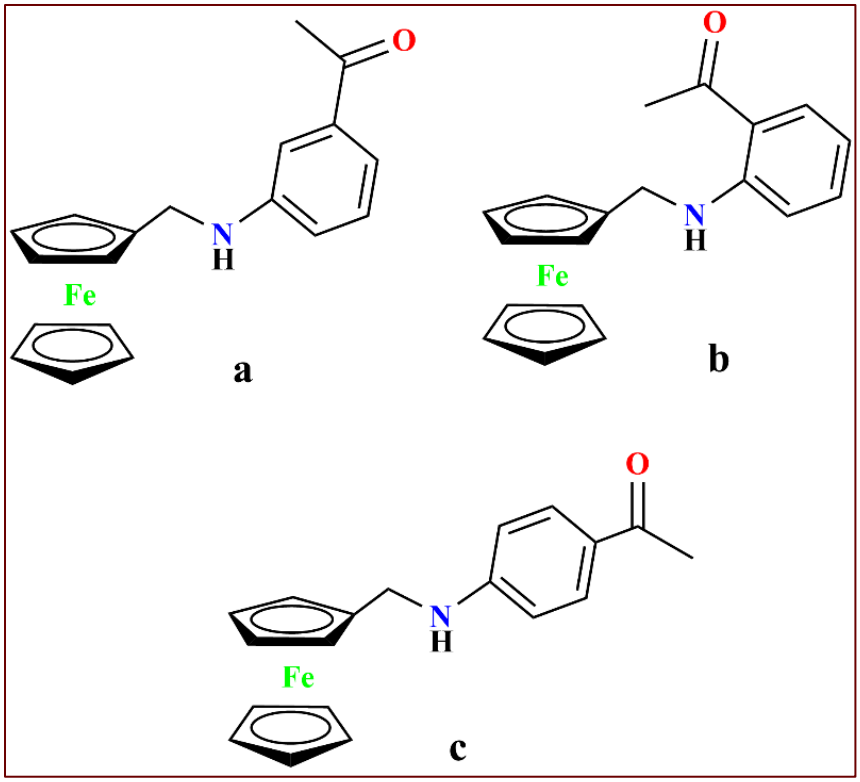

Figure 15. Chemical structures of the synthesised ferrocenyl acetylaniline derivatives: (a) FcMe2Ac (ortho), (b) FcMe3Ac (meta), and (c) FcMe4Ac (para).

As shown in Figure 15, the three derivatives differ solely by the position of the acetyl group, which significantly influences steric accessibility and electronic distribution within the molecule. These factors are known to play a critical role in modulating the nucleophilicity of the amino group and, consequently, the efficiency of the substitution reaction (Lanez et al., 2025a).

To further evaluate the synthetic performance, the yields and physical characteristics of the obtained compounds are summarised in Table 9.

Table 9. Yields and physical properties of the synthesised ferrocenyl acetylaniline derivatives.

Compound	Substituent Position	Yield (%)	Appearance	Melting Point (°C)
FcMe2Ac	Ortho	77	Yellow crystalline solid	148–150
FcMe3Ac	Meta	48	Yellow–orange solid	138–140
FcMe4Ac	Para	80	Deep yellow solid	162–164

As shown in **Table 9**, the reaction yields follow the order: FcMe4Ac > FcMe2Ac > FcMe3Ac

This trend can be rationalised by considering both steric and electronic effects, which are known to govern nucleophilic substitution reactions in aromatic amines. The para-substituted derivative (FcMe4Ac) exhibited the highest yield (80%), reflecting minimal steric hindrance and favourable resonance interaction between the acetyl group and the amino functionality. This electronic delocalisation enhances the nucleophilicity of the amine, thereby facilitating the substitution process (Lanez et al., 2025b)

In contrast, the meta derivative (FcMe3Ac) showed a significantly lower yield (48%), which can be attributed to the absence of resonance interaction between the substituents. In the meta position, the acetyl group exerts mainly an inductive electron-withdrawing effect, reducing the electron density on the amino group and consequently its nucleophilicity.

The ortho derivative (FcMe2Ac) presented intermediate behaviour (77%), where steric hindrance between adjacent substituents partially limits the accessibility of the nucleophilic site, despite favourable electronic effects.

These observations are in good agreement with previously reported studies on substituted aniline derivatives, where both steric congestion and electronic factors significantly influence reactivity. Furthermore, the results confirm that the adopted synthetic strategy is robust and well adapted for the preparation of ferrocenyl derivatives with controlled structural variation. (Benine et al., 2025)

3. FT-IR Spectral Analysis

The structural features of the synthesised ferrocenyl acetylaniline derivatives were initially investigated by Fourier-transform infrared (FT-IR) spectroscopy. The recorded spectra for FcMe2Ac, FcMe3Ac and FcMe4Ac are presented in Figure 16, while the principal absorption bands and their corresponding assignments are summarised in Table 10.

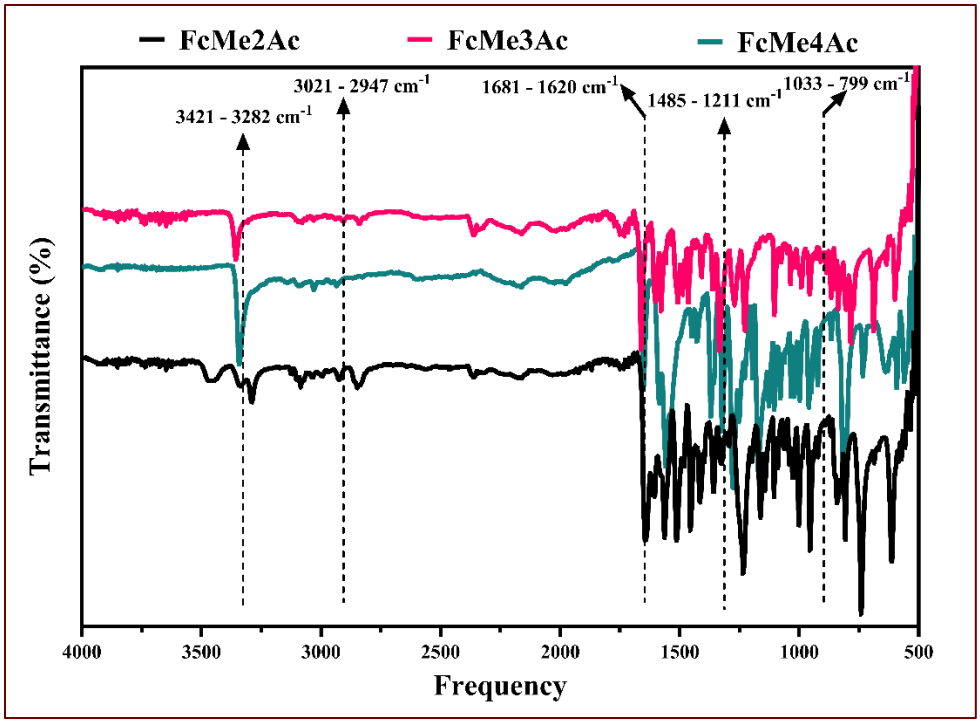

Figure 16. FT-IR spectra of the synthesised ferrocenyl acetylaniline derivatives.

Table 10. Characteristic FT-IR absorption bands (cm^{-1}) and their assignments for the synthesised compounds.

Assignment	FcMe2Ac (cm^{-1})	FcMe3Ac (cm^{-1})	FcMe4Ac (cm^{-1})	Description
N–H stretching	3426, 3291	3432, 3338	3445, 3345	Secondary amine vibration
Ar–C–H stretching	3082	—	—	Aromatic C–H
C=O stretching	1647	1650	1651	Acetyl carbonyl group
C=C (aromatic)	1566, 1516	1582, 1510	1589, 1562	Aromatic ring vibrations
C–N stretching	1146	1170	1173	Amine linkage
C–H bending	1454, 1416	1450, 1365	1369	Methyl/aromatic bending
Out-of-plane C–H	1003, 617	820	822	Aromatic substitution pattern

As shown in Figure 16, all compounds display closely related spectral profiles, confirming the preservation of the ferrocenyl acetylaniline framework across the series. Minor variations in band positions and intensities are observed and can be attributed to the different substitution patterns on the aromatic ring (Tlili et al., 2024)

Broad absorption bands in the region 3445–3291 cm^{-1} are assigned to N–H stretching vibrations, confirming the presence of secondary amine functionality formed during the nucleophilic substitution reaction. The slight shifts observed between the derivatives reflect variations in hydrogen bonding interactions and local electronic environments (Tlili et al., 2025)

The strong and well-defined bands located at 1651–1647 cm^{-1} correspond to the stretching vibration of the carbonyl (C=O) group of the acetyl substituent. The consistency of this band across all compounds confirms that the carbonyl functionality remains intact during synthesis.

Aromatic C=C stretching vibrations are observed in the region 1589–1510 cm^{-1}, providing clear evidence for the presence of the substituted benzene ring. Additionally, the bands detected between 1173–1146 cm^{-1} are attributed to C–N stretching vibrations, confirming the successful formation of the ferrocenylmethyl–aniline linkage.

Particularly informative are the out-of-plane C–H bending vibrations observed between 820 and 617 cm^{-1}, which are highly sensitive to substitution patterns. The differences in these bands among the ortho, meta and para derivatives provide strong evidence for the positional variation of the acetyl group on the aromatic ring.

Overall, the FT-IR data provide clear confirmation of the successful synthesis of the target compounds. The observed spectral features are fully consistent with the proposed structures and align well with reported data for related ferrocenyl and substituted aniline systems. (Khamouli et al., 2022)

4. UV–Visible Spectral Analysis

The electronic absorption properties of the synthesised ferrocenyl acetylaniline derivatives were investigated using UV–visible spectroscopy in DMSO. The corresponding spectra are presented in Figure 17, and the absorption maxima are summarised in Table 11.

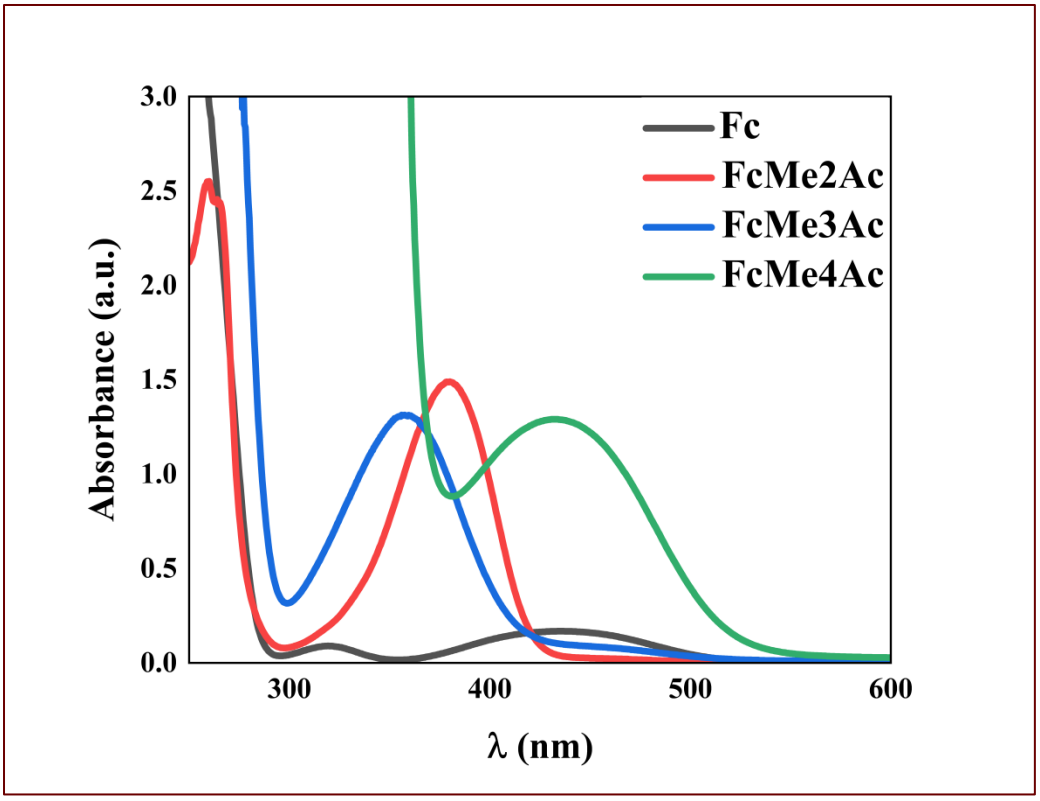

Figure 17. UV–visible absorption spectra of the synthesised ferrocenyl acetylaniline derivatives.

Table 11. UV–visible absorption maxima (λmax) of the synthesised ferrocenyl acetylaniline derivatives.

Compound	λmax (nm)	Assignment
FcMe2Ac	259	π → π* (aromatic system)
	380	d–d (Fe^{2+} centre)
FcMe3Ac	268	π → π*
	402	d–d transition
FcMe4Ac	432	d–d / charge transfer

As illustrated in Figure 17, all compounds exhibit characteristic absorption bands associated with both the aromatic system and the ferrocenyl moiety. Intense bands in the ultraviolet region (**259–268 nm**) are attributed to π → π* transitions within the conjugated aromatic system, corresponding to electronic excitation within the benzene ring (Zouaghi et al., 2025)

In the visible region, absorption bands between **380 and 432 nm** are observed, corresponding to transitions involving the ferrocenyl iron centre. These transitions can be assigned to metal-

centred d–d transitions and, in some cases, ligand-to-metal charge transfer (LMCT), reflecting the interaction between the iron centre and the surrounding π-electron system (Zegheb et al., 2021)

A pronounced bathochromic shift is observed from FcMe2Ac (380 nm) to FcMe4Ac (432 nm), indicating an increase in electronic delocalisation in the para-substituted derivative. This behaviour arises from enhanced conjugation between the acetyl substituent and the aromatic system, which lowers the energy gap between molecular orbitals and facilitates lower-energy electronic transitions.

The meta derivative (FcMe3Ac) exhibits intermediate behaviour due to the absence of effective resonance interaction between substituents, limiting electron delocalisation. In contrast, the ortho derivative (FcMe2Ac), although capable of resonance interaction, may experience steric effects that slightly distort molecular planarity and reduce conjugation efficiency.

These observations highlight the significant influence of substituent position on the electronic structure of ferrocenyl derivatives. Such variations in electronic distribution are expected to play a key role in modulating molecular recognition and interaction behaviour with biological targets (Ben Amor et al., 2025a)

5. NMR Spectral Analysis

The structural elucidation of the synthesised ferrocenyl acetylaniline derivatives was comprehensively achieved using one-dimensional (^{1}H and ^{13}C) and two-dimensional (HSQC and HMBC) NMR techniques. These complementary analyses enabled precise assignment of all proton and carbon environments and provided unambiguous confirmation of the molecular structures. To facilitate interpretation, the spectra are presented individually for each compound, allowing direct correlation between spectral features and structural elements.

5.1. ^{1}H NMR Analysis

The ^{1}H NMR spectra of FcMe2Ac, FcMe3Ac and FcMe4Ac are presented in Figure 18.

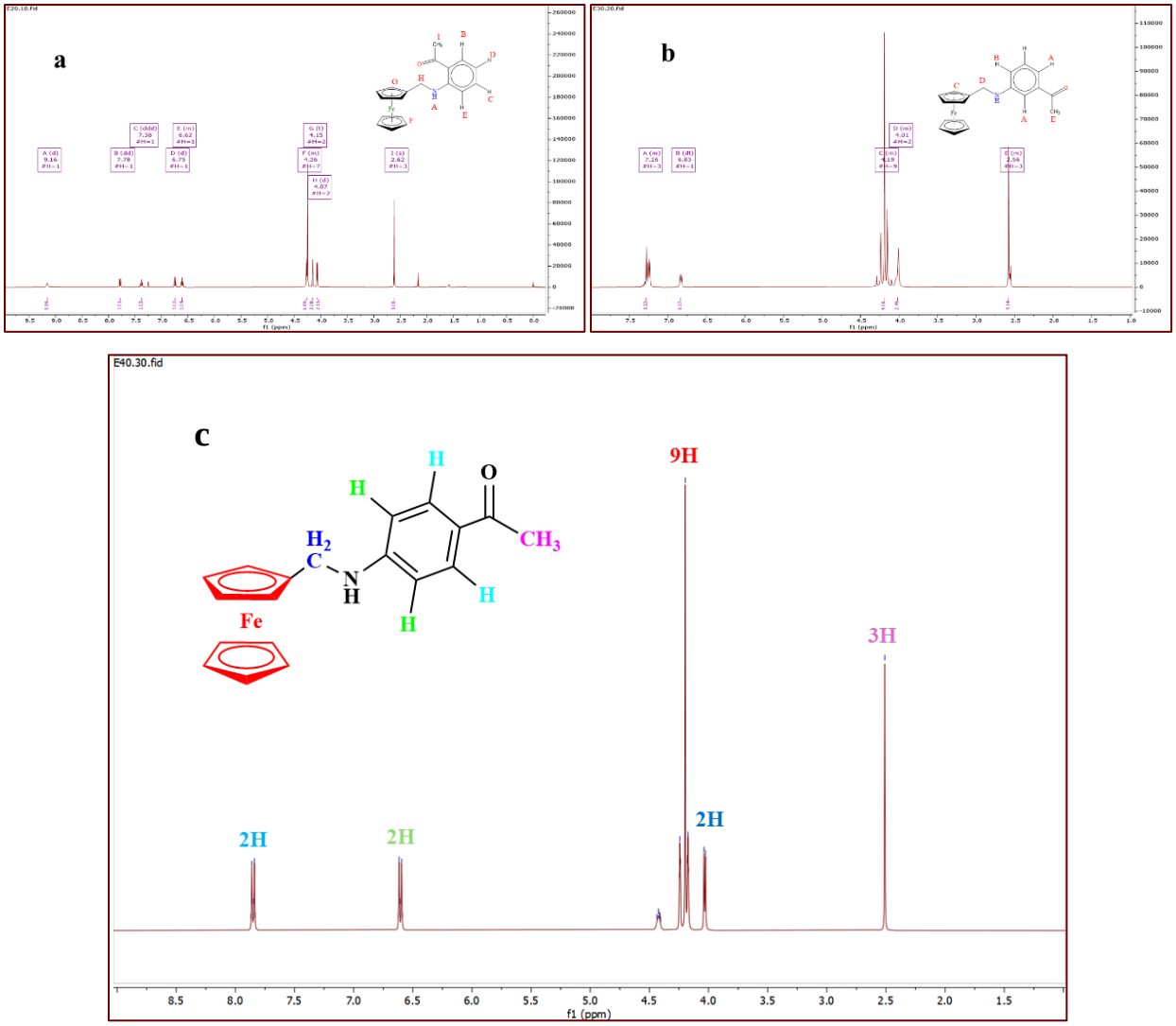

Figure 18. ^{1}H NMR spectra of the synthesised ferrocenyl acetylaniline derivatives: (a) FcMe2Ac, (b) FcMe3Ac, and (c) FcMe4Ac.

As illustrated in Figure 18, all compounds exhibit well-resolved signals consistent with the proposed molecular structures.

The methyl group of the acetyl functionality (–$COCH_3$) appears as a singlet in the region **2.35–2.60 ppm**, confirming its isolated chemical environment. The methylene bridge (–CH_2–N–), linking the ferrocenyl unit to the aromatic ring, is observed as a doublet at approximately **4.30 ppm**, providing clear evidence for the formation of the C–N bond (Rebiai et al., 2014)

The ferrocenyl moiety displays its characteristic spectral features. The unsubstituted cyclopentadienyl ring (C_5H_5) appears as a sharp singlet around **4.15–4.20 ppm**, reflecting its high symmetry. In contrast, the substituted cyclopentadienyl ring (C_5H_4) gives rise to multiplet signals

in the region **3.40–4.10 ppm**, indicative of reduced symmetry upon substitution. This splitting pattern is a well-established signature of monosubstituted ferrocenyl systems.

Aromatic protons are detected between **6.6 and 7.8 ppm**, exhibiting distinct splitting patterns depending on the substitution position. The ortho, meta and para isomers can be clearly differentiated based on their coupling patterns and signal multiplicity, reflecting differences in electronic distribution and proton–proton interactions within the aromatic ring.

The NH proton appears as a downfield singlet around **8.9–9.0 ppm** for FcMe2Ac and FcMe3Ac, suggesting involvement in intermolecular or intramolecular hydrogen bonding. In FcMe4Ac, a slight upfield shift is observed, which may be attributed to enhanced electronic delocalisation in the para-substituted system, reducing deshielding effects (Ben Amor et al., 2025b)

5.2. ^{13}C NMR Analysis

The ^{13}C NMR spectra of the synthesised compounds are shown in Figure 19.

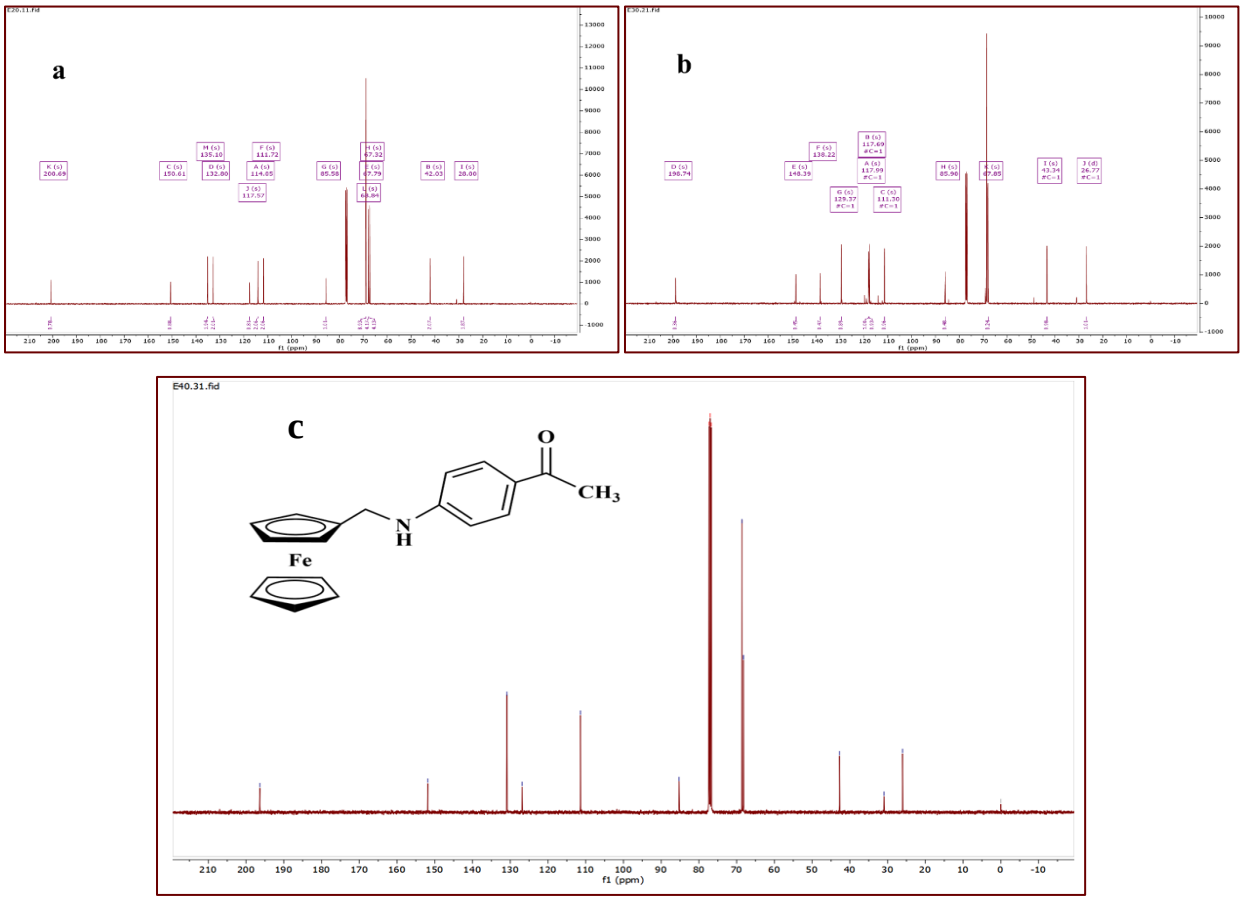

Figure 19. ^{13}C NMR spectra of the synthesised ferrocenyl acetylaniline derivatives: (a) FcMe2Ac, (b) FcMe3Ac, and (c) FcMe4Ac.

As illustrated in Figure 19, the spectra provide clear evidence for the carbon framework of the compounds.

The carbonyl carbon (C=O) is observed in the downfield region between 194 and 210 ppm, confirming the presence of the acetyl group. The variation in chemical shift among the three derivatives reflects differences in electronic environment due to substituent position.

The methylene carbon (CH_2–N) appears consistently around 42–43 ppm, confirming the linkage between the ferrocenyl moiety and the aromatic system.

The ferrocenyl carbons are detected in the range 66–69 ppm, corresponding to the cyclopentadienyl rings. The ipso carbon bonded to the substituent appears slightly downfield due to its distinct electronic environment.

Aromatic carbons are distributed between 112 and 154 ppm, with slight variations depending on substitution pattern, which is consistent with substituted benzene derivatives. (Khamouli et al., 2019)

5.3. Two-Dimensional NMR Analysis (HSQC and HMBC)

Two-dimensional NMR spectroscopy was employed to achieve unambiguous structural assignment and to confirm the connectivity within the synthesised ferrocenyl acetylaniline derivatives. The HSQC and HMBC spectra are presented separately to allow a clear interpretation of both direct and long-range correlations.

The HSQC spectra of FcMe2Ac, FcMe3Ac and FcMe4Ac are shown in Figure 20, while the corresponding HMBC spectra are presented in Figure 21.

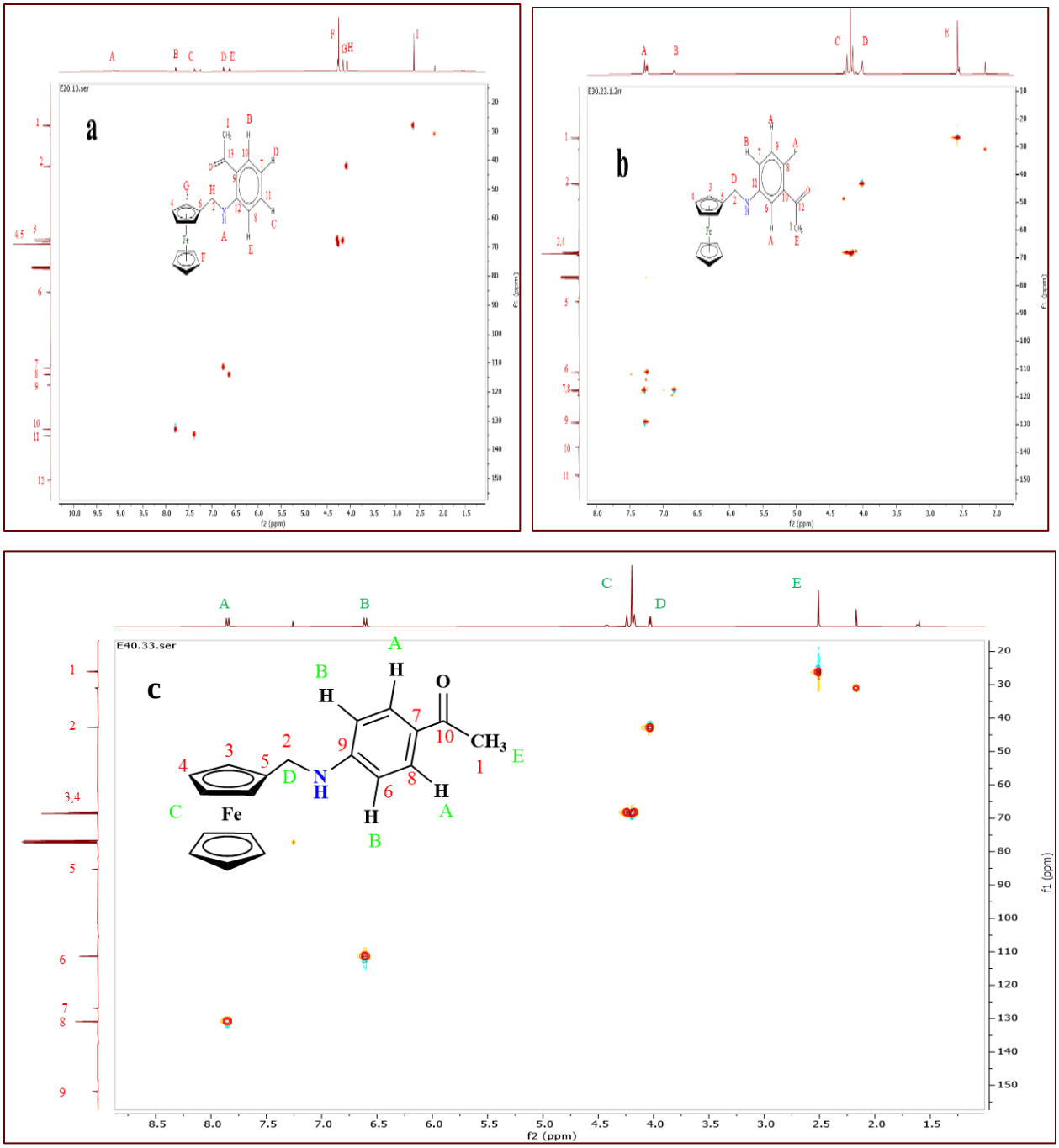

Figure 20. HSQC spectra of the synthesised ferrocenyl acetylaniline derivatives: (a) FcMe2Ac, (b) FcMe3Ac, and (c) FcMe4Ac.

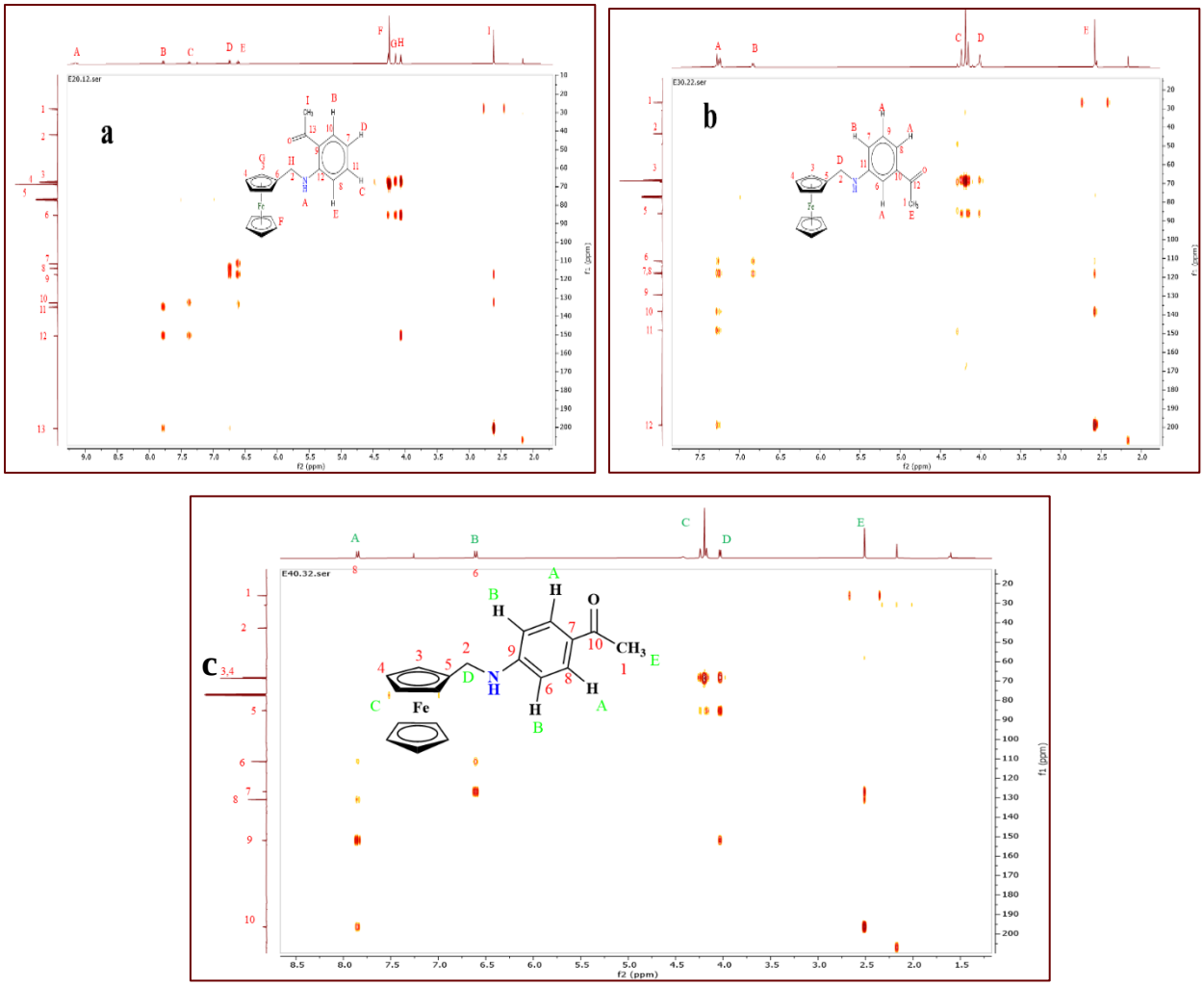

Figure 21. HMBC spectra of the synthesised ferrocenyl acetylaniline derivatives: (a) FcMe2Ac, (b) FcMe3Ac, and (c) FcMe4Ac.

As illustrated in Figure 20, the HSQC spectra provide direct one-bond correlations between proton and carbon nuclei (^{1}JCH), allowing precise assignment of all protonated carbon atoms. The methylene protons (–CH$_2$–N–), observed around 4.30 ppm in the ^{1}H NMR spectra, show clear cross-peaks with their corresponding carbon signals at approximately 42–43 ppm, confirming the presence of the ferrocenylmethyl linkage.

Similarly, the signals corresponding to the cyclopentadienyl rings exhibit well-defined correlations. The unsubstituted Cp ring (C$_5$H$_5$) shows a single correlation pattern consistent with its symmetry, whereas the substituted Cp ring (C$_5$H$_4$) displays multiple correlations reflecting the loss of equivalence upon substitution. These observations are characteristic of monosubstituted ferrocenyl systems and further confirm the structural integrity of the organometallic core.

The aromatic proton signals also show distinct HSQC correlations with their corresponding carbon atoms in the region 112–140 ppm, enabling clear assignment of the benzene ring protons. The differences observed between the ortho, meta and para derivatives further support the positional variation of the acetyl substituent (Mouada et al., 2024) (Lanez et al., 2015)

In contrast, the HMBC spectra (Figure 21) provide long-range correlations (^{2}JCH and ^{3}JCH), which are essential for confirming the connectivity between different fragments of the molecule. In particular, strong correlations are observed between the methylene protons (–CH_2–N–) and the aromatic carbons, confirming the formation of the C–N bond linking the ferrocenyl unit to the aniline moiety.

Additional long-range correlations between aromatic protons and the carbonyl carbon (C=O) are observed, allowing precise localisation of the acetyl group on the aromatic ring. These correlations are especially important for distinguishing between the regioisomers, as the HMBC patterns differ significantly depending on the substitution position (ortho, meta or para).

Furthermore, correlations involving the ferrocenyl carbons provide additional confirmation of the substitution pattern on the cyclopentadienyl ring. The combined HSQC and HMBC data therefore establish a complete mapping of proton–carbon connectivity within the molecules. (Bekkar et al., 2025a) (Bekkar et al., 2025b)

Overall, the two- NMR analysis provides definitive structural confirmation of the synthesised ferrocenyl acetylaniline derivatives. The observed correlation patterns are fully consistent with the proposed structures and are in excellent agreement with literature reports on related ferrocenyl compounds, where HSQC and HMBC techniques are commonly used to validate substitution patterns and molecular connectivity.

6. Cyclic Voltammetry Characterization

6.1. Redox Properties and Voltammetric Response

The electrochemical properties of FcMe2Ac, FcMe3Ac and FcMe4Ac were investigated by cyclic voltammetry in DMSO (1 mM) containing 0.1 M Bu_4NBF_4 as supporting electrolyte, using Hg/Hg_2Cl_2 as reference electrode. Measurements were performed within a potential window of −0.60 to +0.60 V at a scan rate of 100 $mV \cdot s^{-1}$, with the Fc/Fc^{+} redox couple used as an internal reference.

The corresponding voltammograms are presented in Figure 22, where the responses of the substituted derivatives are compared with that of ferrocene.

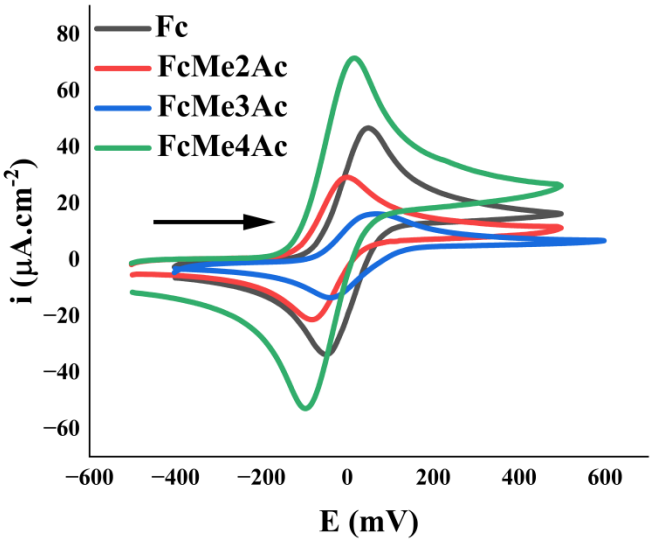

Figure 22. Cyclic voltammograms of Fc, FcMe2Ac, FcMe3Ac and FcMe4Ac recorded in DMSO containing 0.1 M Bu_4NBF_4 at a scan rate of 100 $mV \cdot s^{-1}$ (referenced to Fc^+/Fc).

As shown in Figure 22, all derivatives exhibit a single well-defined redox couple corresponding to the Fe(II)/Fe(III) transition, confirming that the ferrocenyl unit retains its electroactivity after functionalization .(Lanez et al., n.d.)

A systematic anodic shift in formal potential is observed following the order: **FcMe2Ac (43.9 mV) < FcMe3Ac (51.0 mV) < FcMe4Ac (57.5 mV)**

This trend reflects the influence of the acetylaniline substituent on the electronic environment of the ferrocenyl centre. The positive shift indicates a decrease in electron density at the iron centre, suggesting that oxidation becomes progressively less favourable. This behaviour can be attributed to the electron-withdrawing nature of the acetyl group, which modulates the electron-donating ability of the ferrocenyl moiety through inductive and resonance effects. (Nacer & Lanez, 2013)

The anodic-to-cathodic peak current ratios (Ipa/Ipc ≈ 1) indicate that the redox process is chemically reversible. However, the observed peak-to-peak separation (ΔEp = 87.8–115 mV) exceeds the theoretical value expected for an ideal reversible one-electron process (59 mV), indicating a **quasi-reversible electron transfer.** (Laraoui et al., 2023)

This deviation suggests the presence of kinetic limitations, which may arise from:

- finite heterogeneous electron-transfer rates
- uncompensated ohmic resistance in the non-aqueous medium
- structural reorganisation accompanying oxidation of the ferrocenyl unit

6.2. Scan Rate Dependence and Mass Transport Regime

The influence of scan rate on the electrochemical response was examined in the range 100–500 mV·s⁻¹. The resulting voltammograms are shown in Figure 23, while the dependence of anodic peak current on the square root of scan rate is presented in Figure 24.

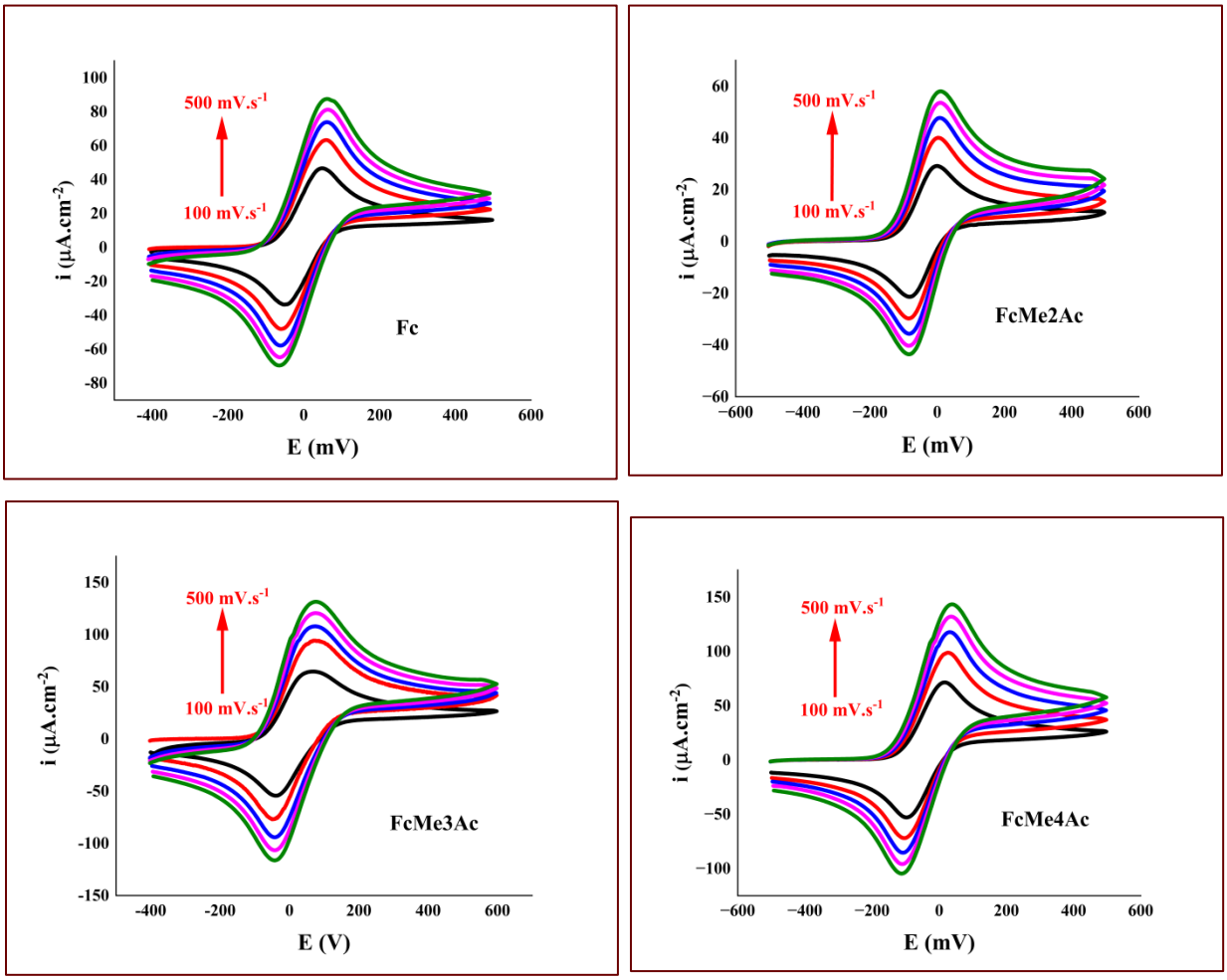

Figure 23. Cyclic voltammograms of Fc, FcMe2Ac, FcMe3Ac and FcMe4Ac at different scan rates (100–500 mV·s⁻¹).

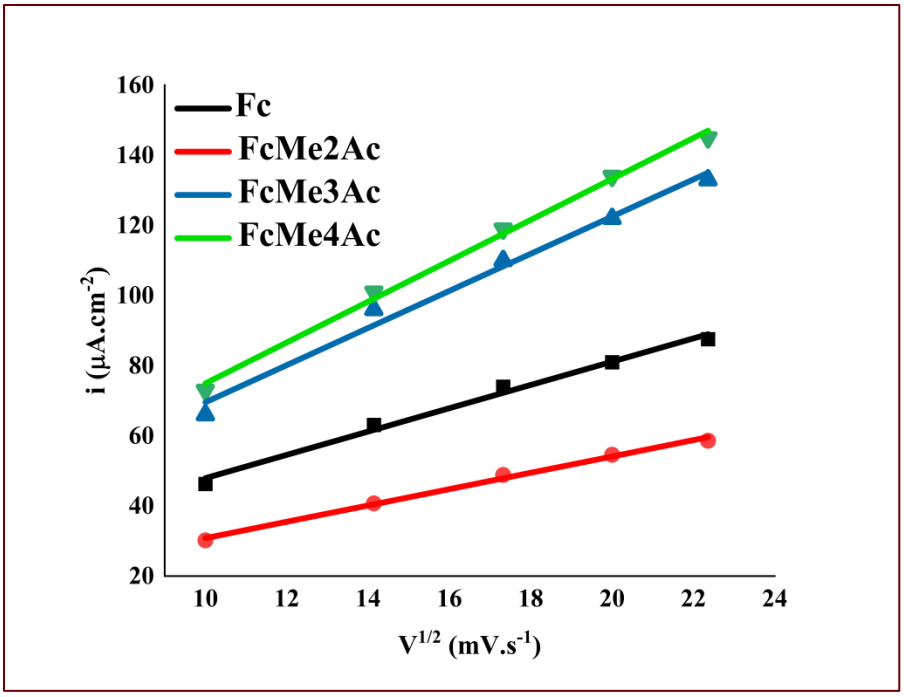

Figure 24. Linear variation of anodic peak current (i_{pa}) as a function of the square root of scan rate ($\nu^{1/2}$).

As illustrated in Figure 23, increasing the scan rate results in a proportional increase in both anodic and cathodic peak currents, without significant distortion of peak shape. This behaviour indicates that the redox process is not governed by adsorption phenomena (Lanez & Henni, 2025)

A linear relationship between anodic peak current (i_{pa}) and $\nu^{1/2}$ is clearly observed in Figure 24 for all compounds. The corresponding linear regression equations (Table 12) exhibit high correlation coefficients ($R^2 = 0.980–0.994$), confirming excellent linearity. (Khelef & Lanez, 2015)

The high R^2 values demonstrate that the experimental data closely follow the Randles–Ševčík model, thereby confirming that the electron transfer process is diffusion-controlled. Slight deviations from ideal linearity, particularly for FcMe3Ac (R^2 = 0.980), may reflect minor contributions from kinetic limitations or increased solution resistance (Zaiz & Lanez, 2015)

6.3. Diffusion Coefficients and Transport Properties

The diffusion coefficients of the electroactive species were determined using the Randles–Ševčík Equation 1 for a reversible system, which relates the peak current to the square root of the scan rate:

$$ip_a = 2.69\times10^5\left(\sqrt{n}\right)^3 SC\sqrt{D}\sqrt{v}$$ **Equation 1**

where i_p is the peak current (A), $n$is the number of electrons transferred, A is the electrode surface area (cm^2), C is the concentration of the electroactive species ($mol.cm^{-3}$), D is the diffusion coefficient ($cm^2 \cdot s^{-1}$), and v is the scan rate ($V \cdot s^{-1}$).

The diffusion coefficients (D) were calculated using the Randles–Ševčík equation, and the results are presented in Table 12.

Table 12. Diffusion coefficients and linear regression parameters obtained from Randles–Ševčík analysis.

Compound	Equation	R^2	$D \times 10^{-7}$ ($cm^2 \cdot s^{-1}$)
Fc	y = 3.321x + 14.727	0.987	6.952
FcMe2Ac	y = 2.328x + 7.539	0.993	1.108
FcMe3Ac	y = 5.298x + 16.578	0.980	5.738
FcMe4Ac	y = 5.831x + 16.638	0.994	2.255

As shown in Table 12, the diffusion coefficients of the substituted derivatives are significantly lower than that of ferrocene. This decrease can be attributed to several physicochemical factors:

- Increased molecular volume, leading to reduced translational mobility
- Enhanced solute–solvent interactions in polar DMSO medium
- Greater structural complexity and conformational flexibility

FcMe2Ac exhibits the lowest diffusion coefficient (1.11×10^{-7} $cm^2 \cdot s^{-1}$), suggesting stronger intermolecular interactions and possibly a more hindered diffusion pathway. In contrast, FcMe3Ac retains a relatively higher diffusion coefficient, which may be associated with a more favourable molecular geometry and reduced steric constraints (Lanez & Hemmami, 2016) (Benyza et al., 2022)

6.4. Electron Transfer Kinetics

The heterogeneous electron-transfer rate constants were estimated using Nicholson's method, which relates the peak-to-peak separation to the kinetic parameter Ψ and the standard rate constant as described in Equation 2:

$$\psi = \frac{K_s}{\sqrt{\pi D \frac{nFv}{RT}}}$$ **Equation 2**

where k_s is the standard heterogeneous electron-transfer rate constant (cm.s^{-1}), D is the diffusion coefficient (cm^2.s^{-1}), n is the number of electrons transferred, F is the Faraday constant (96,500 C.mol^{-1}), v is the scan rate (V.s^{-1}), R is the gas constant (8.314 J.mol^{-1}.K^{-1}), and T is the absolute temperature (K).

The heterogeneous electron-transfer rate constants (k_s) were estimated using Nicholson's method, and the results are summarised in Table 13.

Table 13. Nicholson kinetic parameters (Ψ, ΔEp) and heterogeneous electron-transfer rate constants (k_s).

Compound	Ψ	ΔEp (mV)	$k_s \times 10^3$ (cm·s^{-1})
Fc	1.51	73	2.88
FcMe2Ac	0.323	124	0.62
FcMe3Ac	0.074	263	0.14
FcMe4Ac	0.100	223	0.19

The obtained kinetic parameters clearly indicate a decrease in electron-transfer rates upon substitution. The order: Fc > FcMe2Ac > FcMe4Ac > FcMe3Ac, reflects the increasing complexity of the molecular structure and its impact on electron-transfer dynamics (Lanez et al., 2024b)

The relatively high k_s value for ferrocene confirms its well-known fast and reversible electron-transfer behaviour. In contrast, the substituted derivatives exhibit slower kinetics, which can be explained by:

- Increased **steric hindrance**, limiting effective interaction with the electrode surface
- Higher **reorganisation energy** associated with structural changes during oxidation
- Reduced **electronic coupling** between the ferrocenyl centre and the electrode

The particularly low k_s value for FcMe3Ac suggests that the meta substitution pattern is least favourable for efficient electron transfer, likely due to suboptimal electronic communication within the molecule. (Filote et al., 2022)

7. Density Functional Theory (DFT) Analysis

Density functional theory (DFT) calculations were performed to gain detailed insight into the electronic structure, reactivity and physicochemical properties of the synthesised ferrocenyl acetylaniline derivatives. These theoretical investigations provide a molecular-level interpretation of electronic distribution and complement the experimental findings, allowing a more comprehensive understanding of structure–property relationships (Boutarfaia et al., 2019).

7.1. Frontier Molecular Orbitals and Electronic Structure

The frontier molecular orbitals (HOMO and LUMO) are key descriptors governing the reactivity of molecular systems, as they define electron-donating and electron-accepting capacities. The calculated orbital energies are summarised in Table 14, while their spatial distributions are presented in Figure 25.

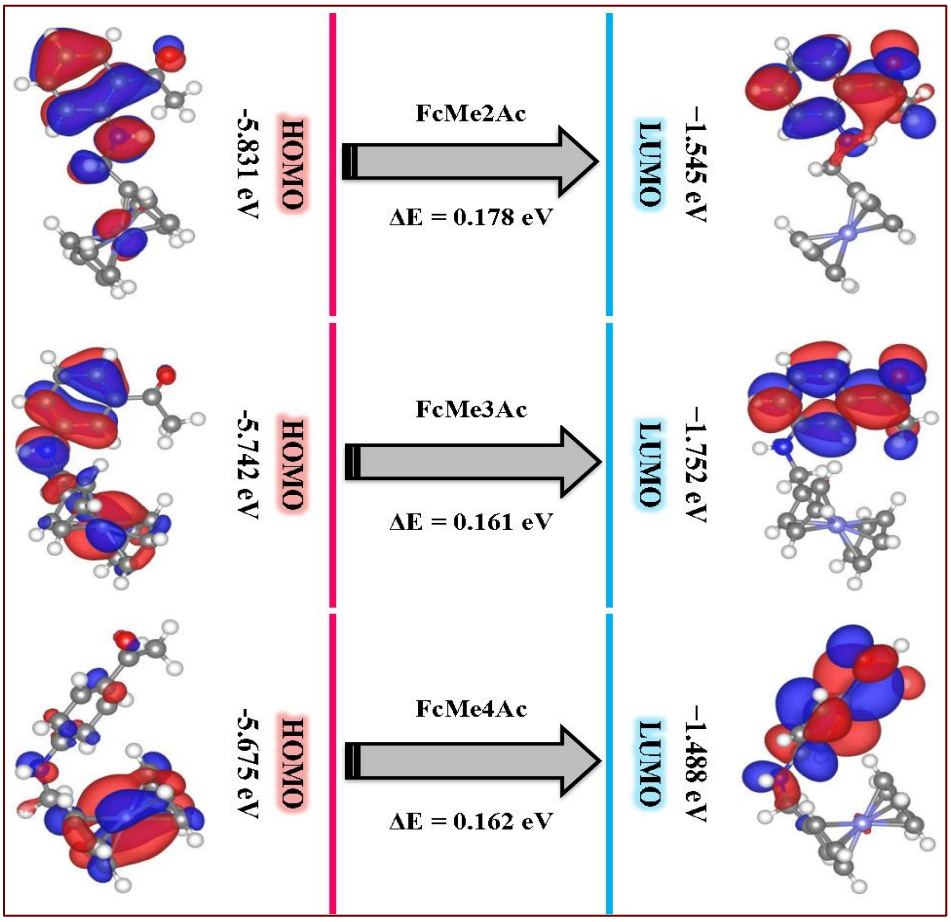

Figure 25. Frontier molecular orbitals of ferrocenyl acetylaniline derivatives: HOMO and LUMO surfaces.

Table 14. Frontier molecular orbital energies (eV) of the synthesised compounds.

Compound	EHOMO (eV)	ELUMO (eV)	ΔE (eV)
FcMe2Ac	−5.8306	−1.5453	4.285
FcMe3Ac	−5.7421	−1.7521	3.990
FcMe4Ac	−5.6752	−1.4882	4.187

The results reveal a gradual increase in HOMO energy from FcMe2Ac (−5.8306 eV) to FcMe4Ac (−5.6752 eV), indicating an enhancement of electron-donating character across the series. This trend reflects the influence of the substitution pattern on the electronic density of the ferrocenyl core, where improved conjugation promotes electron delocalisation.

The HOMO–LUMO energy gap (ΔE) ranges between **3.990 and 4.285 eV**, suggesting that all compounds possess moderate chemical stability combined with sufficient electronic flexibility. Among the derivatives, FcMe3Ac exhibits the lowest energy gap (3.990 eV), indicating increased softness and higher reactivity, whereas FcMe2Ac displays the highest gap, reflecting comparatively greater stability (Yahiaoui et al., 2023).

The orbital distribution (Figure 25) shows a clear donor–acceptor separation within the molecular framework. The HOMO is predominantly localised over the ferrocenyl moiety and partially extends towards the amine bridge, identifying this region as the principal electron donor. In contrast, the LUMO is mainly distributed over the aromatic ring and the carbonyl group, designating these sites as electron-accepting regions.

This spatial separation suggests an **intramolecular charge-transfer character**, whereby electron density is transferred from the ferrocenyl unit towards the aromatic substituent. Such donor–acceptor behaviour is particularly relevant for molecular recognition processes, as it facilitates electronic adaptation upon interaction with biological macromolecules (Kedadra et al., 2022).

7.2. Global Reactivity Descriptors and Thermodynamic Parameters

To further quantify molecular reactivity, global descriptors derived from frontier orbital energies were calculated and are summarised in Table 15.

Table 15. Global reactivity descriptors and thermodynamic parameters of the synthesised derivatives at 298.15 K.

Parameter	FcMe2Ac	FcMe3Ac	FcMe4Ac
Hardness, η (eV)	2.143	1.995	2.094
Electronegativity, χ (eV)	3.688	3.747	3.582
Chemical potential, μ (eV)	−3.688	−3.747	−3.582
Softness, S (eV^{-1})	0.233	0.251	0.239
Electrophilicity, ω (eV)	3.174	3.519	3.064
Nucleophilicity, N	2.829	2.918	2.985
Dipole moment (D)	3.82	4.46	5.12
Polarizability ($Å^3$)	38.5	42.7	47.3
Enthalpy ($kJ·mol^{-1}$)	−1245.6	−1388.2	−1531.4
Entropy ($J·mol^{-1}·K^{-1}$)	412.5	448.9	486.7
Heat capacity ($J·mol^{-1}·K^{-1}$)	236.4	258.7	281.3

The hardness (η) values confirm that all compounds exhibit moderate stability, consistent with their HOMO–LUMO gaps. FcMe3Ac presents the lowest hardness (1.995 eV) and highest softness (0.251 eV^{-1}), reinforcing its greater electronic flexibility and reactivity.

The electrophilicity index (ω) follows the order: **FcMe3Ac > FcMe2Ac > FcMe4Ac**, indicating that FcMe3Ac has the strongest electron-accepting capability. In contrast, FcMe4Ac exhibits the highest nucleophilicity index, suggesting enhanced electron-donating potential. This duality reflects the delicate balance between donor and acceptor characteristics within the series.

The negative values of chemical potential (μ) for all compounds indicate thermodynamic stability and a natural tendency towards charge redistribution. Additionally, a progressive increase in dipole moment from FcMe2Ac to FcMe4Ac is observed, reflecting enhanced molecular polarity and asymmetry (Khennoufa et al., 2021).

Similarly, polarizability increases across the series, indicating that the electronic cloud becomes more easily deformable. This property is particularly important for intermolecular interactions, as it enhances the ability of the molecule to adapt to external electrostatic environments.

Thermodynamic parameters, including entropy and heat capacity, also show an increasing trend, suggesting greater molecular flexibility and a higher number of accessible vibrational states.

This behaviour is consistent with increasing structural complexity and conformational freedom in the substituted derivatives (Meraghni et al., 2023).

7.3. Molecular Electrostatic Potential (MEP) Analysis

The molecular electrostatic potential maps provide valuable insight into charge distribution and reactive sites. The calculated MEP surfaces are presented in Figure 26.

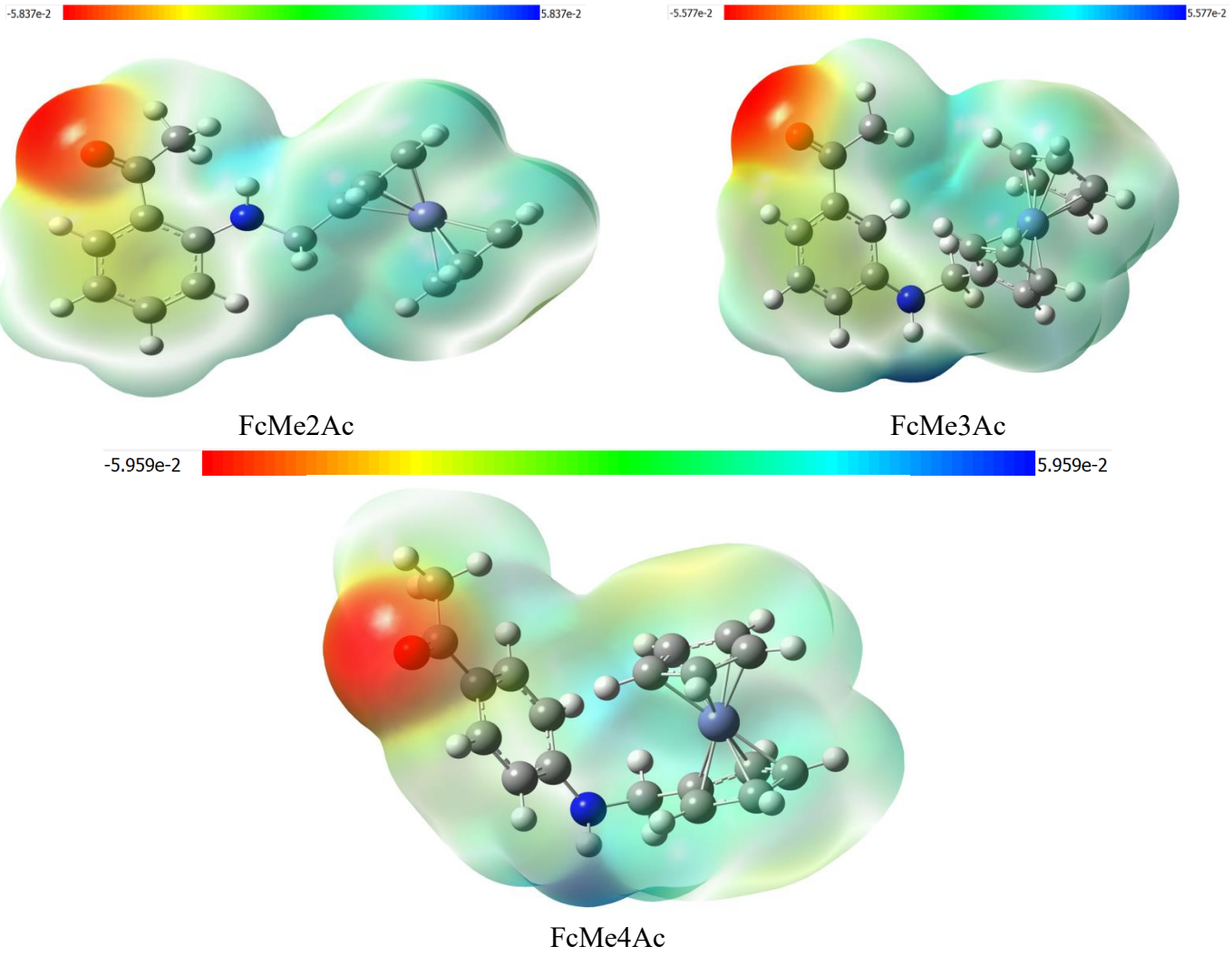

Figure 26. Molecular electrostatic potential (MEP) maps of ferrocenyl acetylaniline derivatives showing charge distribution.

The MEP analysis reveals that regions of highest negative potential are localised around the carbonyl oxygen atoms, indicating areas of high electron density and strong nucleophilic character. These regions are therefore likely to serve as preferential sites for intermolecular interactions, including hydrogen bonding and electrostatic interactions.

In contrast, positive electrostatic potential regions are primarily located around hydrogen atoms and partially over the ferrocenyl unit, corresponding to electron-deficient zones (Lanez et al., 2024c)

Although the overall electrostatic distribution remains similar across the three derivatives, subtle differences are observed, particularly in the para-substituted compound (FcMe4Ac), which exhibits a more delocalised charge distribution. This enhanced delocalisation may contribute to improved interaction capabilities with biological targets (Nadjiba et al., 2018).

7.4. Electron Localisation and Non-Covalent Interaction Analysis

To further investigate electronic behaviour, ELF, LOL and RDG analyses were performed. Representative maps are presented in Figure 27 and 28.

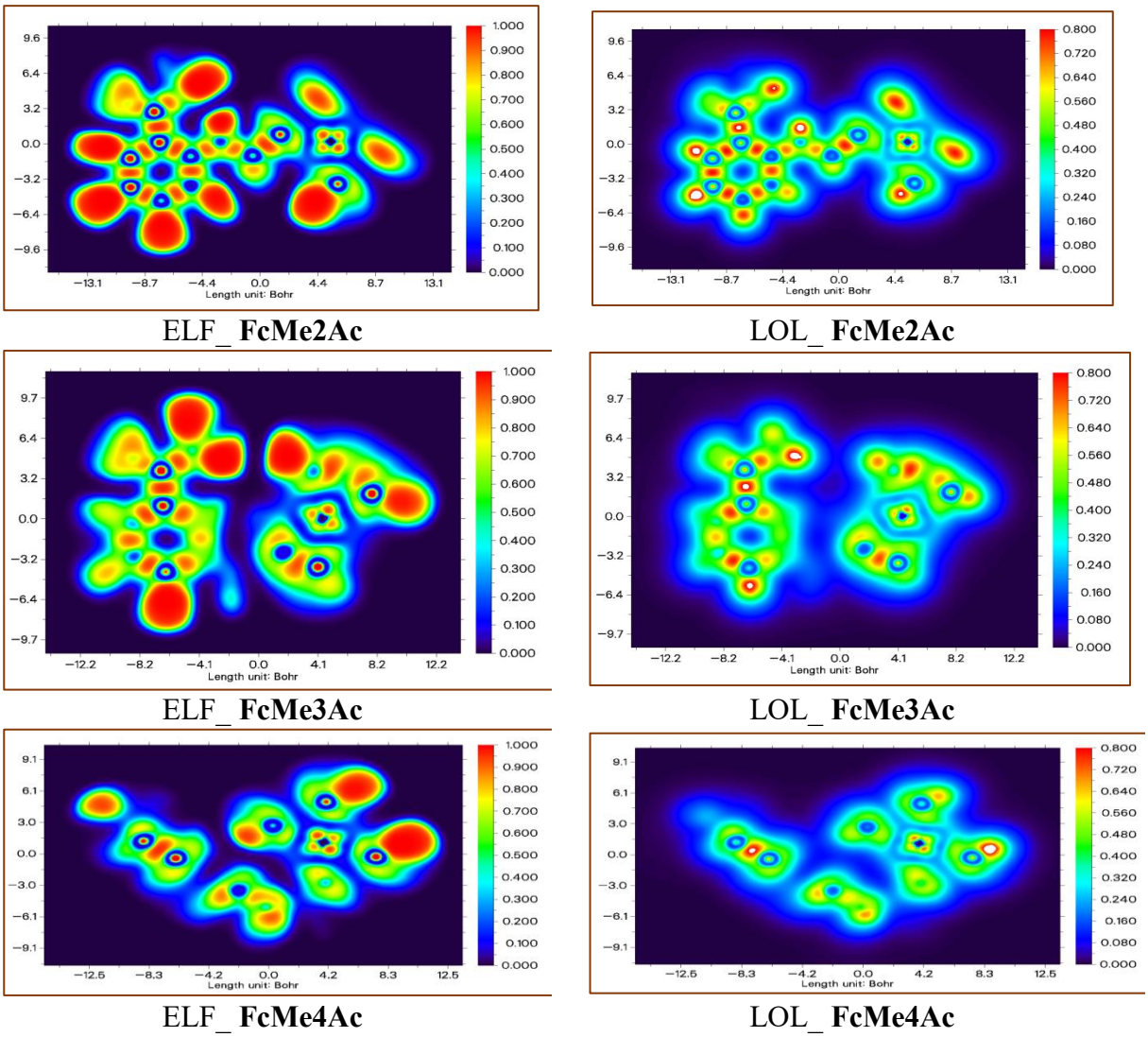

Figure 27. Electron localisation (ELF and LOL) analyses of FcMeAc.

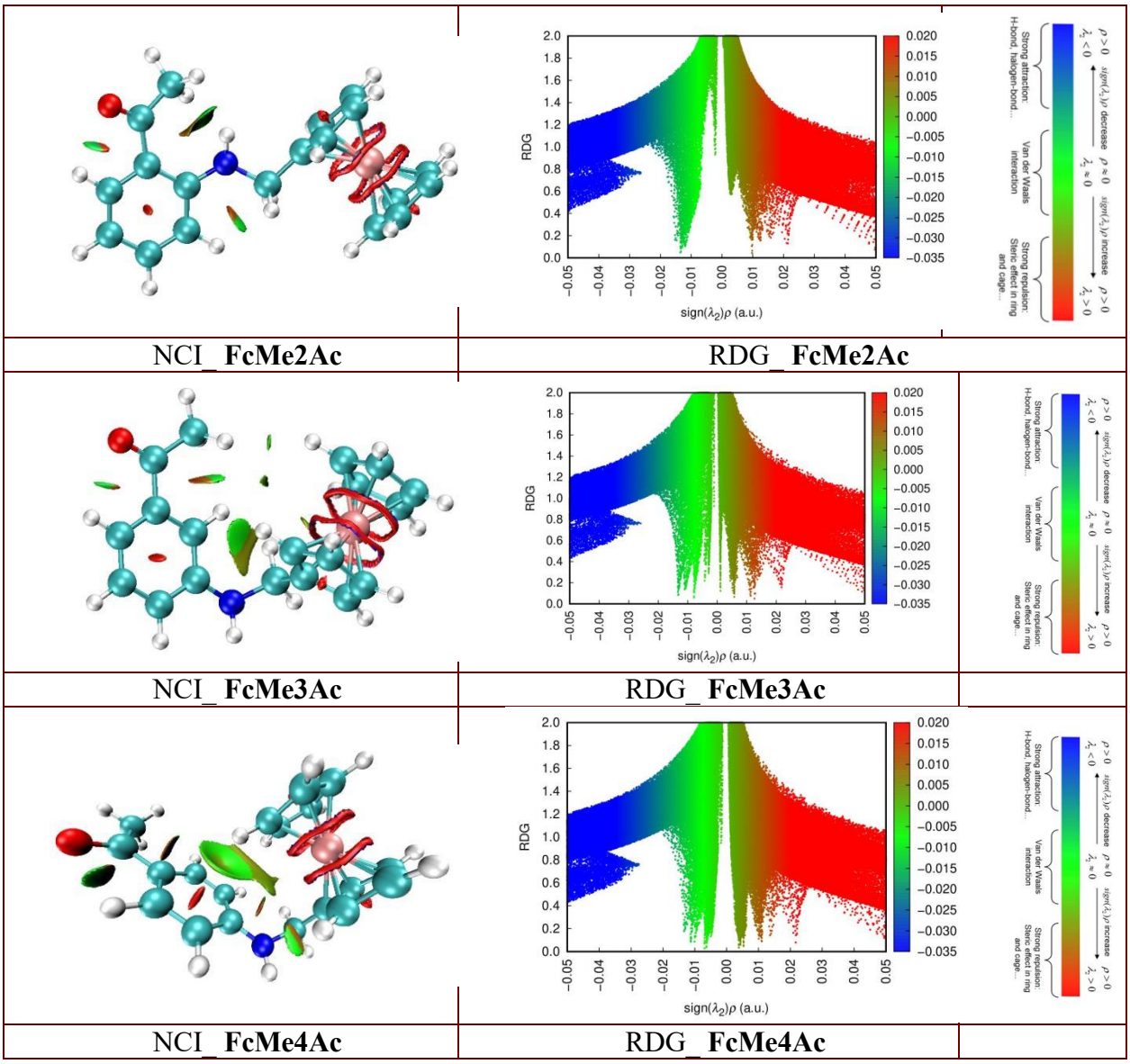

NCI_ **FcMe2Ac**	RDG_ **FcMe2Ac**
NCI_ **FcMe3Ac**	RDG_ **FcMe3Ac**
NCI_ **FcMe4Ac**	RDG_ **FcMe4Ac**

Figure 28. Non-covalent interaction (RDG/NCI) analyses of FcMeAc.

The ELF and LOL maps clearly show strong electron localisation within the cyclopentadienyl rings and the aromatic system, reflecting extensive π-electron delocalisation. Localised electron density around nitrogen and oxygen atoms corresponds to lone-pair regions, which are important for intermolecular interactions.

The RDG analysis highlights weak non-covalent interactions, including van der Waals contacts and steric repulsion zones. These interactions contribute to the overall stability and conformational behaviour of the molecules.

The consistency of these features across the series indicates that the fundamental electronic structure of the ferrocenyl core is preserved, while substitution mainly modulates peripheral electronic properties (Zerrouk et al., 2024) (Adaika et al., 2019)

8. Molecular Docking Study

Molecular docking simulations were conducted to elucidate the binding behaviour and molecular recognition properties of the synthesised ferrocenyl acetylaniline derivatives toward Topoisomerase IIα, a key enzymatic target involved in DNA topology regulation and widely recognised in anticancer drug design. The objective of this analysis was to characterise the binding affinity, preferred conformations and interaction profiles of the ligands within the catalytic domain of the enzyme, thereby providing mechanistic insight into their potential inhibitory activity.

8.1. Docking Protocol Validation

Prior to the evaluation of ligand–protein interactions, the reliability and predictive accuracy of the docking protocol were rigorously assessed through a redocking procedure. The native co-crystallised ligand was extracted from the active site of Topoisomerase IIα and re-docked under identical computational conditions. The resulting pose was subsequently superimposed onto the experimental crystallographic conformation, as illustrated in Figure 29.

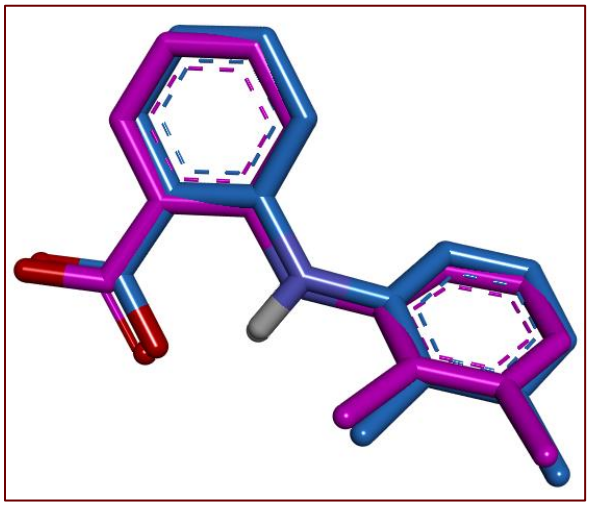

Figure 29. Superposition of the co-crystallised ligand and the redocked pose within the active site (validation of docking protocol).

The calculated root-mean-square deviation (RMSD) between the experimental and predicted poses was **0.339 Å**, which is substantially lower than the commonly accepted validation threshold

of 2.0 Å. This very low deviation indicates an excellent overlap between the two conformations, confirming that the docking protocol accurately reproduces the native binding mode of the reference ligand.

Such a high level of agreement demonstrates the robustness of the adopted computational setup, including the grid definition, search algorithm and scoring function. Moreover, it confirms that the structural features of the Topoisomerase IIα active site are properly captured, allowing reliable prediction of ligand positioning and interaction patterns.

Consequently, the validated protocol can be confidently applied to the ferrocenyl acetylaniline derivatives, ensuring that the subsequent docking results provide meaningful and reproducible insights into their binding behaviour within the enzyme active site (Lanez et al., 2018)

8.2. Binding Affinity and Energetic Analysis

The calculated docking scores and associated energetic components for the ferrocenyl acetylaniline derivatives are presented in Table 16.

Table 16. Molecular docking results of ferrocenyl acetylaniline derivatives.

Compound	Intermolecular Energy (kcal·mol^{-1})	Internal Energy (kcal·mol^{-1})	Torsional Energy (kcal·mol^{-1})	Binding Energy (kcal·mol^{-1})
FcMe2Ac	−7.52	−0.55	+0.72	−6.95
FcMe3Ac	−8.67	−0.69	+0.85	−7.91
FcMe4Ac	−9.48	−0.81	+0.96	−8.72
Reference ligand	—	—	—	−7.58

All compounds exhibit **negative binding free energies**, confirming that their association with the Topoisomerase IIα active site is thermodynamically favourable. However, significant differences in binding strength are observed among the regioisomers.

FcMe4Ac displays the most favourable binding energy (**−8.72 kcal·mol^{-1}**), exceeding that of the reference ligand and indicating a strong interaction with the enzyme. FcMe3Ac shows intermediate affinity, while FcMe2Ac presents the weakest interaction profile.

The ranking of binding affinity follows the order: **FcMe4Ac > FcMe3Ac > FcMe2Ac**. This trend suggests that the substitution pattern directly influences the ability of the ligand to effectively engage with the enzyme binding pocket.

From an energetic perspective, the intermolecular energy term constitutes the dominant contribution to binding stabilisation, indicating that ligand–protein interactions govern complex formation. The relatively low internal energy values confirm that the ligands undergo minimal structural strain upon binding, while moderate torsional contributions reflect limited conformational adjustments required for optimal accommodation within the active site.

These observations collectively indicate that FcMe4Ac achieves an optimal balance between interaction strength and conformational adaptability, which is essential for efficient enzyme binding (Zegheb et al., 2020)

8.3. Binding Mode and Interaction Analysis

The binding conformation of the most active compound (FcMe4Ac) within the Topoisomerase IIα active site is illustrated in Figure 30.

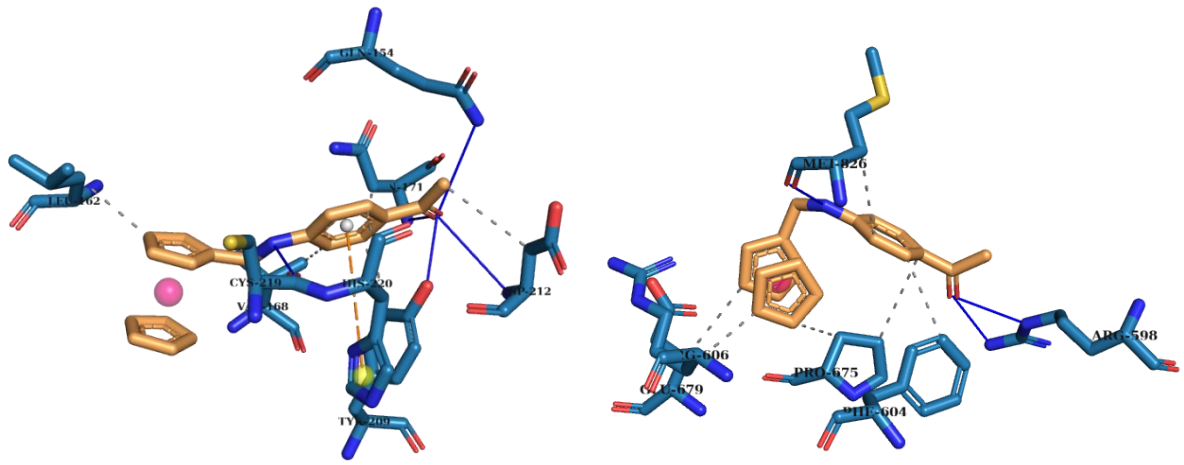

Figure 30. Three-dimensional binding conformation of FcMe4Ac within the catalytic site of Topoisomerase IIα.

The docking analysis reveals that all ferrocenyl derivatives occupy a well-defined region within the enzyme cavity, characterised by a predominantly hydrophobic environment adjacent to key catalytic residues. The ferrocenyl core is deeply embedded within this pocket, where it establishes stabilising contacts with non-polar amino acids.

The interaction pattern is governed by a combination of non-covalent forces, including:

- **Hydrophobic interactions** between the cyclopentadienyl rings and apolar residues lining the binding cavity
- **π–π stacking interactions** involving the aromatic acetylaniline moiety and nearby aromatic residues
- **Hydrogen bonding interactions**, primarily mediated by the carbonyl oxygen and amine functionalities

Notably, FcMe4Ac exhibits a highly organised and extended interaction network. The para-substituted configuration promotes a more linear molecular geometry, enabling deeper penetration into the binding pocket and facilitating simultaneous interactions with multiple residues.

In contrast, FcMe2Ac shows a less favourable orientation, likely due to steric hindrance imposed by the ortho substitution, which restricts its ability to align efficiently within the active site. FcMe3Ac adopts an intermediate conformation, allowing partial interaction optimisation but lacking the extended contact network observed for FcMe4Ac.

The enhanced binding of FcMe4Ac can therefore be attributed to:

- improved spatial accommodation within the catalytic pocket
- increased interaction surface area
- favourable orientation of functional groups for intermolecular interactions (Lanez et al., 2023c)

8.4. Structure–Interaction Relationship

The differences in binding behaviour among the three derivatives can be rationalised by considering both structural and electronic factors.

The **para-substituted derivative (FcMe4Ac)** benefits from:

- optimal geometric extension allowing deeper insertion into the active site
- enhanced electronic delocalisation promoting stronger intermolecular interactions
- improved steric compatibility with the enzyme cavity

In contrast, the **ortho isomer (FcMe2Ac)** is affected by intramolecular steric constraints, which limit conformational flexibility and reduce binding efficiency. The **meta derivative (FcMe3Ac)** exhibits moderate behaviour, reflecting a compromise between steric accessibility and electronic distribution.

Additionally, the increased dipole moment and polarizability observed for FcMe4Ac (DFT results) contribute to stronger electrostatic and dispersion interactions within the binding pocket, further enhancing its affinity.

Overall, these findings demonstrate that **substitution pattern plays a decisive role in modulating ligand–enzyme interactions**, influencing both binding strength and molecular recognition. The superior performance of FcMe4Ac highlights its potential as a promising scaffold for further optimisation targeting Topoisomerase Iiα (Mouada et al., 2019)

9. Molecular Dynamics Simulation

Molecular dynamics (MD) simulations were performed to investigate the stability and dynamic behaviour of FcMe4Ac in complex with Topoisomerase IIα, using crystallographic structures PDB ID: 4FM9 and 5GWK. These systems represent biologically relevant enzyme–DNA–inhibitor complexes and provide a reliable framework for evaluating ligand binding under dynamic conditions.

9.1. System Stability: RMSD Analysis

The temporal evolution of backbone RMSD for both apo and FcMe4Ac-bound Topoisomerase IIα systems (PDB IDs: 4FM9 and 5GWK) is presented in Figure 31.

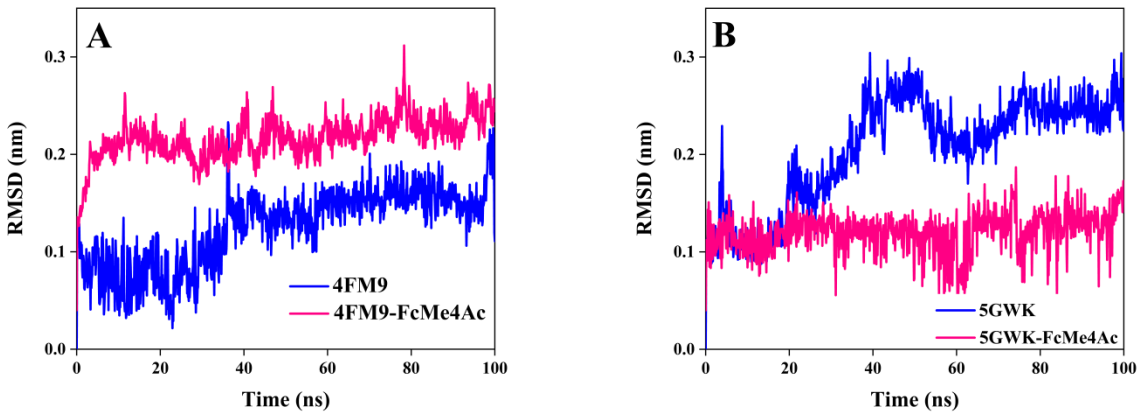

Figure 31. RMSD evolution of Topoisomerase IIα systems: (A) 4FM9 and (B) 5GWK over 100 ns.

As shown in Figure 31A, the apo form of **4FM9** stabilises around ~0.10–0.15 nm after an initial equilibration phase, indicating an intrinsically stable protein conformation. Upon binding of

FcMe4Ac, the RMSD increases moderately and stabilises within the range of ~0.20–0.25 nm. This shift reflects a ligand-induced conformational adaptation associated with accommodation of the ligand within the catalytic domain, while the absence of large fluctuations confirms the stability of the complex throughout the simulation (Lanez et al., 2019c)

In contrast, the **5GWK system** exhibits a different dynamic behaviour. The apo protein shows higher initial fluctuations (~0.20–0.30 nm), suggesting greater intrinsic flexibility of this Topoisomerase IIα conformation. Upon ligand binding, the RMSD is significantly reduced (~0.10–0.15 nm) and remains stable over time. This observation indicates that FcMe4Ac exerts a stabilising effect on the protein structure, reducing conformational mobility (Lanez et al., 2019c)

Overall, the RMSD analysis demonstrates that FcMe4Ac forms stable complexes with both Topoisomerase IIα targets, with a more pronounced stabilising effect observed in the **5GWK system**.

9.2. Residue Flexibility: RMSF Analysis

The root-mean-square fluctuation (RMSF) profiles, presented in Figure 32, provide insight into residue-level flexibility within the Topoisomerase IIα complexes.

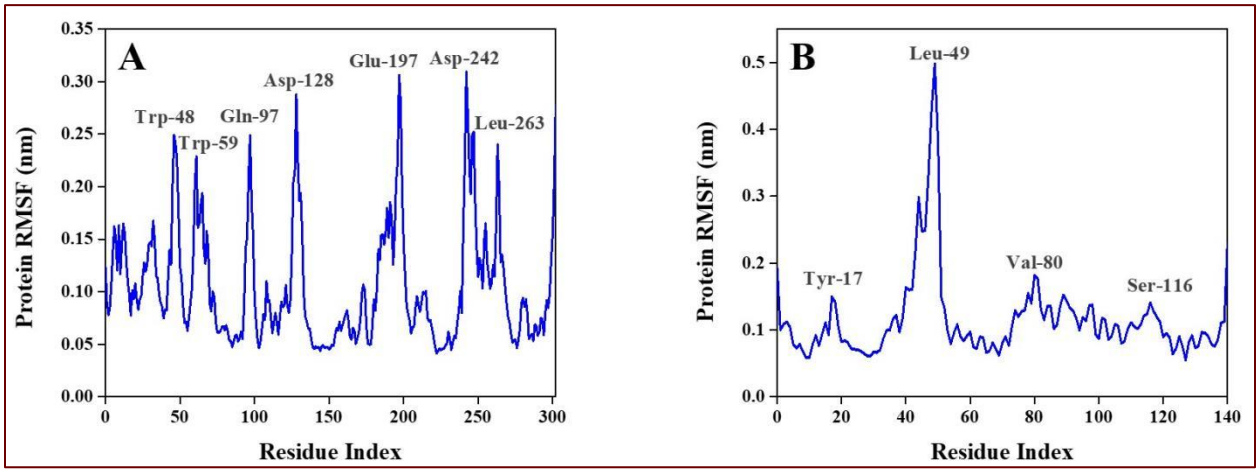

Figure 32. RMSF profiles of protein residues in complex with FcMe4Ac: (A) 4FM9 and (B) 5GWK systems.

For the 4FM9 system (Figure 32A), several fluctuation peaks are observed, notably at residues such as Trp48, Trp59, Gln97, Asp128, Glu197 and Asp242. These regions correspond mainly to loop segments and solvent-exposed residues, which are inherently flexible. Importantly, residues

located within or near the ligand-binding site exhibit relatively low fluctuations, indicating stable ligand–protein interactions.

In the 5GWK system (Figure 32B), the overall fluctuation profile is significantly reduced. Most residues remain below ~0.15 nm, with only limited mobility observed for residues such as Leu49. This reduction in flexibility reflects a more rigid and stabilised protein conformation upon ligand binding.

These results indicate that FcMe4Ac enhances structural rigidity, particularly in the 5GWK complex, where flexibility is markedly suppressed.

9.3. Ligand Stability: Ligand RMSF Analysis

The conformational stability of FcMe4Ac within the binding pocket was evaluated through ligand RMSF analysis (Figure 33).

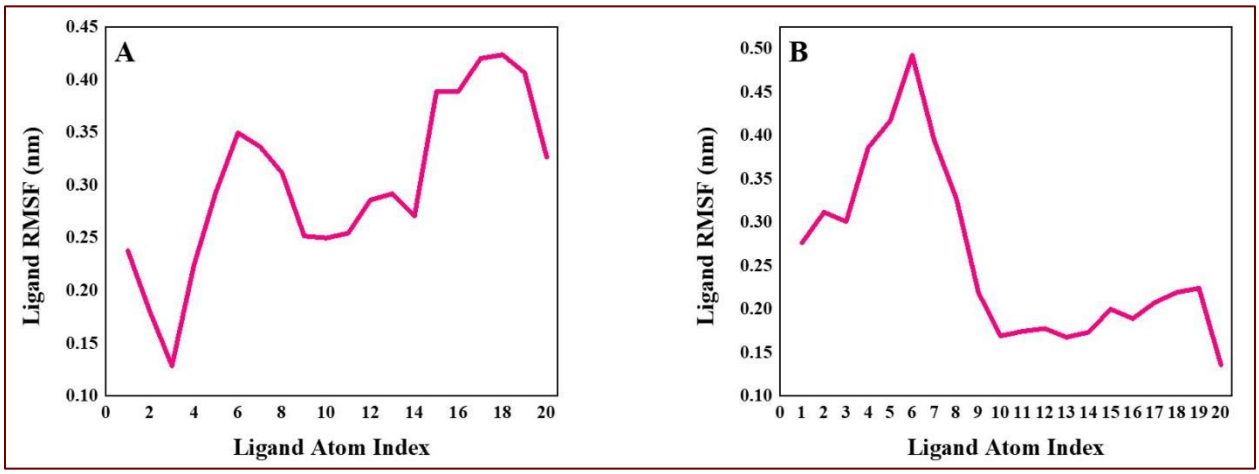

Figure 33. Ligand RMSF profiles of FcMe4Ac: (A) 4FM9 and (B) 5GWK complexes.

In the 4FM9 complex (Figure 33A), FcMe4Ac exhibits moderate fluctuations (~0.25–0.42 nm), particularly in terminal regions. This behaviour suggests that peripheral groups retain some flexibility, while the core of the molecule remains anchored within the binding site.

In contrast, in the 5GWK complex (Figure 33B), the ligand displays significantly lower fluctuations (~0.15–0.22 nm), indicating a more rigid and well-confined conformation. This reduced mobility reflects stronger and more persistent interactions with the surrounding residues.

These findings confirm that FcMe4Ac is more tightly bound and conformationally stabilised in the 5GWK system, consistent with the enhanced stability observed in RMSD analysis.

9.4. Interaction Profile Analysis

The interaction profiles between FcMe4Ac and Topoisomerase IIα residues during the simulation are shown in Figure 34.

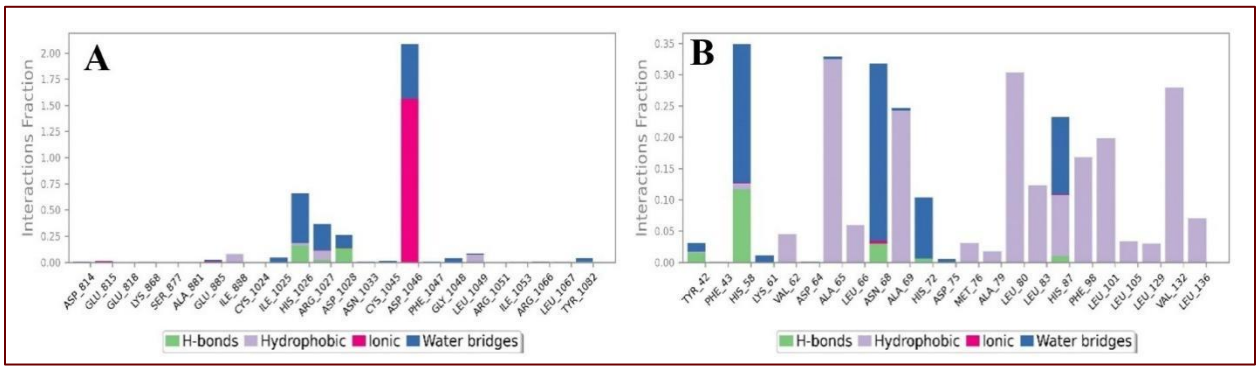

Figure 34. Interaction fraction analysis showing hydrogen bonds, hydrophobic interactions, ionic contacts and water bridges: (A) 4FM9 and (B) 5GWK complexes.

The stabilisation of the complexes is primarily governed by:

- Hydrophobic interactions involving residues such as PHE, LEU and VAL
- Hydrogen bonding interactions contributing to directional stability
- Water-mediated bridges enhancing interaction persistence

In the 4FM9 system, interactions are relatively localised, with significant contributions from residues such as HIS1025 and ARG1027, indicating a moderately stable interaction network.

In contrast, the 5GWK complex exhibits a broader and more consistent interaction pattern involving multiple residues (e.g., TYR42, PHE43, LEU80 and LEU136). This extended interaction network contributes to enhanced stability and stronger ligand retention within the active site.

9.5. Global Structural Properties (Rg, SASA, PSA)

The evolution of global structural parameters is presented in Figure 35.

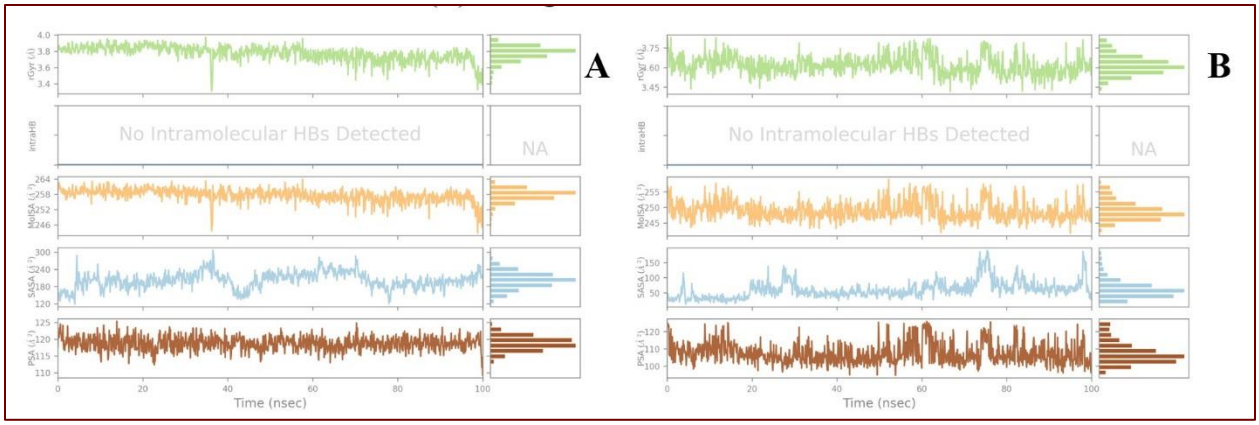

Figure 35. Time evolution of radius of gyration (Rg), molecular surface area (MolSA), solvent-accessible surface area (SASA) and polar surface area (PSA): (A) 4FM9 and (B) 5GWK systems.

The radius of gyration (Rg) remains relatively stable in both systems (~3.6–3.9 Å), indicating that no significant unfolding or structural collapse occurs during the simulation.

The SASA profiles show moderate fluctuations, reflecting normal solvent exposure dynamics without major conformational rearrangements. Similarly, the polar surface area (PSA) remains nearly constant throughout the simulation, suggesting that ligand binding does not significantly alter the global polarity of the protein.

Notably, the **5GWK system** exhibits slightly smoother and more stable profiles across all parameters, further confirming its enhanced structural stability in the presence of FcMe4Ac 65. (Lanez & Lanez, 2016)

10. ADMET Prediction and Pharmacokinetic Evaluation

To complement the structural, electronic and dynamic investigations, the pharmacokinetic behaviour and toxicity profile of the synthesised ferrocenyl acetylaniline derivatives were assessed using in silico ADMET prediction tools. This analysis provides critical insight into the drug-likeness, absorption, distribution, metabolism, excretion and safety characteristics of the compounds, which are essential parameters for evaluating their suitability as potential Topoisomerase IIα-targeting anticancer agents.

10.1. Drug-Likeness and Physicochemical Properties

The fundamental physicochemical parameters governing drug-likeness are summarised in Table 17.

Table 17. Predicted physicochemical properties and drug-likeness parameters of ferrocenyl derivatives.

Parameter	FcMe2Ac	FcMe3Ac	FcMe4Ac
Molecular weight (g·mol⁻¹)	335.2	335.2	335.2
LogP (consensus)	3.12	3.28	3.45
Lipinski violations	0	0	0

All compounds comply with Lipinski's rule of five, indicating favourable characteristics for oral bioavailability. Their molecular weights (~335 g·mol⁻¹) remain well below the upper threshold of 500 g·mol⁻¹, while their LogP values (3.12–3.45) fall within the optimal range for balanced lipophilicity.

A progressive increase in lipophilicity is observed from FcMe2Ac to FcMe4Ac, reflecting the influence of substitution pattern on hydrophobic character. This moderate lipophilicity is advantageous, as it promotes efficient membrane permeability while maintaining adequate solubility.

Importantly, such physicochemical properties are particularly relevant for ligands targeting Topoisomerase IIα, where efficient penetration into cellular environments and interaction with hydrophobic regions of the enzyme are required (Guan et al., 2019)

10.2. Absorption and Distribution Properties

The predicted absorption and distribution profiles are presented in Table 18.

Table 18. Predicted absorption and distribution properties of the studied compounds**.**

Parameter	FcMe2Ac	FcMe3Ac	FcMe4Ac
Gastrointestinal absorption	High	High	High
Blood–brain barrier permeability	No	No	No

All derivatives exhibit **high gastrointestinal absorption**, indicating favourable oral uptake and bioavailability. This behaviour is consistent with their moderate molecular size and optimised lipophilicity.

None of the compounds are predicted to cross the **blood–brain barrier (BBB)**, suggesting limited central nervous system exposure. This characteristic is advantageous for anticancer agents targeting peripheral enzymes such as Topoisomerase IIα, as it minimises the risk of neurological side effects.

Overall, the absorption and distribution profiles indicate that the compounds possess suitable pharmacokinetic properties for systemic administration (Xiong et al., 2021)

10.3. Toxicological Profile

The toxicity predictions are summarised in Table 19.

Table 19. Predicted toxicity profiles of ferrocenyl acetylaniline derivatives.

Parameter	FcMe2Ac	FcMe3Ac	FcMe4Ac
Ames toxicity	No	No	No
Hepatotoxicity	No	No	No
Skin sensitisation	Low risk	Low risk	Low risk

All derivatives are predicted to be non-mutagenic (Ames test negative) and non-hepatotoxic, indicating a favourable safety profile. Additionally, the low risk of skin sensitisation further supports their potential as biologically compatible compounds (Dascalu et al., 2020)

10.4. Structure–Property Relationship and Comparative Analysis

The ADMET results reveal a coherent and favourable pharmacokinetic profile across the three derivatives, with subtle structure-dependent variations:

- FcMe4Ac, which demonstrated superior binding affinity and dynamic stability, also exhibits the highest lipophilicity, potentially enhancing membrane permeability and protein interaction capacity
- Increasing substitution contributes to enhanced polarizability and hydrophobic character, which may improve binding within hydrophobic regions of Topoisomerase IIα
- Despite these variations, all compounds maintain a balanced physicochemical profile, avoiding excessive lipophilicity that could compromise solubility

Importantly, the absence of toxicity alerts and full compliance with drug-likeness criteria indicate that structural modification of the ferrocenyl framework leads to optimised pharmacokinetic properties without compromising safety (Hodgson, 2001).

General Conclusion

General Conclusion

The present work was devoted to the rational design, synthesis, comprehensive characterisation and advanced computational evaluation of a series of ferrocenyl acetylaniline derivatives, with particular emphasis on their potential as modulators of Topoisomerase IIα, a key enzymatic target in anticancer therapy. The adopted multidisciplinary strategy enabled a coherent integration of experimental and theoretical approaches, providing a robust framework for understanding structure–property–activity relationships.

The synthetic methodology successfully yielded three regioisomeric derivatives (FcMe2Ac, FcMe3Ac and FcMe4Ac) under mild and reproducible conditions. Structural elucidation, achieved through FT-IR, UV–Visible spectroscopy and one- and two-dimensional NMR techniques, unequivocally confirmed the formation of the target compounds and validated the substitution patterns on the aromatic ring. The consistency of the spectroscopic data demonstrates the reliability of the synthetic route and the structural integrity of the ferrocenyl framework.

Electrochemical investigations revealed that all derivatives preserve the characteristic redox behaviour of the ferrocenyl core, exhibiting quasi-reversible Fe(II)/Fe(III) transitions. The observed modulation of redox potentials across the series highlights the influence of acetylaniline substitution on the electronic environment of the metal centre. Furthermore, diffusion-controlled electron-transfer processes and variation in kinetic parameters underline the sensitivity of electrochemical behaviour to molecular structure and substitution pattern.

From a theoretical perspective, DFT calculations provided detailed insight into the electronic structure and reactivity of the compounds. The frontier molecular orbital analysis demonstrated a pronounced donor–acceptor character, with electron density predominantly localised on the ferrocenyl unit and transferred towards the aromatic moiety. The calculated global descriptors, together with MEP, ELF and RDG analyses, confirmed the presence of well-defined reactive regions and emphasised the role of substitution in modulating electronic distribution, polarity and intermolecular interaction potential.

Molecular docking investigations against Topoisomerase IIα revealed favourable binding affinities for all derivatives, governed by a combination of hydrophobic interactions, hydrogen bonding and π–π stacking within the enzyme active site. Among the

series, FcMe4Ac consistently exhibited superior binding performance, reflecting optimal steric complementarity, enhanced electronic delocalisation and an extended interaction network within the catalytic pocket.

The dynamic stability of the ligand–protein complexes was further validated through molecular dynamics simulations, which confirmed the persistence and robustness of the interactions under physiological conditions. Notably, FcMe4Ac demonstrated reduced structural fluctuations, increased conformational rigidity and a highly stable interaction profile, particularly in one of the investigated Topoisomerase IIα conformations, indicating a strong and sustained binding mode.

In parallel, in silico ADMET analysis revealed that all compounds possess favourable pharmacokinetic and safety profiles, characterised by compliance with drug-likeness criteria, high predicted gastrointestinal absorption and absence of significant toxicity alerts. These properties reinforce the suitability of the ferrocenyl scaffold for the development of bioactive molecules targeting enzymatic systems.

Collectively, the results obtained in this work demonstrate that structural modulation of ferrocenyl derivatives through acetylaniline substitution has a significant impact on their electronic properties, interaction behaviour and pharmacokinetic profile. The strong agreement between experimental observations and computational predictions further validates the reliability of the integrated methodological approach.

Among the investigated compounds, FcMe4Ac emerges as the most promising candidate, combining optimal electronic characteristics, strong binding affinity, dynamic stability and favourable ADMET properties. This derivative represents a valuable lead structure for future optimisation and development of ferrocenyl-based Topoisomerase IIα inhibitors.

In conclusion, this study provides a comprehensive and scientifically rigorous contribution to the field of organometallic medicinal chemistry, highlighting the potential of ferrocenyl derivatives as versatile scaffolds for anticancer drug design and paving the way for further experimental and biological investigations.

REFERENCES
BIBLIOGRAPHY

References

A. Adaika, A. Adaika, T. Lanez, E. Lanez, in Vitro and in Silico Evaluation of Anticancer Activity of N,N-Dimethylaminomethylferrocene, Journal of Fundamental and Applied Sciences 11 (2019) 748–768. https://jfas.info/index.php/JFAS/article/view/289.

A. Adaika, Y. Bekkar, S. Youmbai, L. Bourougaa, E. Lanez, M.L. Ben Amor, K. Nesba, T. Lanez, L. Bechki, Synthesis, Antioxidant, and Antidiabetic Potential of Ferrocenylmethylnucleobase Compounds: In Vitro, In Silico Molecular Docking, DFT Calculation, and Molecular Dynamic Simulations, Appl. Organomet. Chem. 39 (2025) e7988.

A. Boutarfaia, L. Bechki, T. Lanez, E. Lanez, M. Kadri, Synthesis, Antioxidant Activity, and Determination of Binding Parameters of Meso-Tetra-4-Actophenyl-Porphyrin and its Palladium (II) Complex with Superoxide Anion Radicals, Curr. Bioact. Compd. 16 (2019) 1063–1071. https://doi.org/10.2174/1573407215666191017105239.

A. Kedadra, T. Lanez, E. Lanez, H. Hemmami, M. Henni, Synthesis and antioxidant activity of six novel N-ferrocenylmethyl-N-(nitrophenyl)and-N-(cyanophenyl)-acetamides: Cyclic voltammetry and molecular docking studies, Journal of Electrochemical Science and Engineering 12 (2022) 293–304. https://doi.org/10.5599/jese.1162.

A. Khelef, T. Lanez, In vitro assays of the antioxidant activities of ferrocene derivatives bearing amine, amide or hydrazine groups, . 7 (2015) 318–323.

A. Khennoufa, L. Bechki, T. Lanez, E. Lanez, N. Zegheb, Spectrophotometric, voltammetric and molecular docking studies of binding interaction of N-ferrocenylmethylnitroanilines with bovine serum albumin, J. Mol. Struct. 1224 (2021) 129052. https://doi.org/10.1016/j.molstruc.2020.129052.

A. Rebiai, T. Lanez, M.L. Belfar, Total polyphenol contents, radical scavenging and cyclic voltammetry of algerian propolis, Int. J. Pharm. Pharm. Sci. 6 (2014) 395–400.

A. Yahiaoui, N. Benyza, A. Messai, T. Lanez, E. Lanez, Voltametric and molecular docking investigations of ferrocenylmethylaniline and its N-acetylated derivative

interacting with DNA, Journal of Electrochemical Science and Engineering (2023). https://doi.org/10.5599/jese.2061.

Allen, M. P., & Tildesley, D. J. (1987). Computer simulation of liquids. Clarendon Press.

Anderson, A. C. (2003). The process of structure-based drug design. Chemistry & Biology, 10(9), 787–797. https://doi.org/10.1016/j.chembiol.2003.09.002

Bildstein, B. (2000). Ferrocene-based dendrimers. Coordination Chemistry Reviews, 200–202, 369–394. https://doi.org/10.1016/S0010-8545(00)00289-X

Biot, C., & Chibale, K. (2006). Novel approaches to antimalarial drug discovery. Infectious Disorders–Drug Targets, 6(2), 173–204. https://doi.org/10.2174/187152606776056706

Biot, C., Glorian, G., Maciejewski, L. A., & Brocard, J. S. (1997). Synthesis and antimalarial activity in vitro and in vivo of a new ferrocene–chloroquine analogue. Journal of Medicinal Chemistry, 40(23), 3715–3718. https://doi.org/10.1021/jm970401y

Biot, C., Ndiaye, E. H. A., Wintjens, R., Dive, D., & Melnyk, P. (2012). Ferroquine: An ingenious antimalarial drug—thinking outside the box. Future Medicinal Chemistry, 4(10), 1285–1292. https://doi.org/10.4155/fmc.12.65

C. Benine, D.A. Boutlelis, L.A. Touhami, E. Lanez, D.G. Amara, G. Rim, N. Hanen, W. Zahnit, M. Messaoudi, Green synthesis, characterization, antioxidant, interaction with DNA/BSA, and investigation of cytotoxicity against MCF-7 cancer cells of zinc oxide nanoparticles using Hammada scoparia (Pomel) Iljin extract, Int. J. Biol. Macromol. 295 (2025) 139709.

C. Filote, E. Lanez, V.I. Popa, T. Lanez, I. Volf, Characterization and Bioactivity of Polysaccharides Separated through a (Sequential) Biorefinery Process from Fucus spiralis Brown Macroalgae, Polymers (Basel). 14 (2022) 4106. https://doi.org/10.3390/polym14194106.

C. Steffen, K. Thomas, U. Huniar, A. Hellweg, O. Rubner, A. Schroer, AutoDock4 and AutoDockTools4: Automated Docking with Selective Receptor Flexibility, J. Comput. Chem. 31 (2010) 2967–2970.

Case, D. A., Cheatham, T. E., Darden, T., Gohlke, H., Luo, R., Merz, K. M., Onufriev, A., Simmerling, C., Wang, B., & Woods, R. J. (2005). The Amber biomolecular simulation programs. Journal of Computational Chemistry, 26(16), 1668–1688. https://doi.org/10.1002/jcc.20290

Clark, T., Chandrasekhar, J., Spitznagel, G. W., & Schleyer, P. V. R. (1983). Efficient diffuse function-augmented basis sets for anion calculations. Journal of Computational Chemistry, 4(3), 294–301. https://doi.org/10.1002/jcc.540040303

Corbeil, C. R., Williams, C. I., & Labute, P. (2012). Variability in docking success rates due to dataset preparation. Journal of Computer-Aided Molecular Design, 26(6), 775–786. https://doi.org/10.1007/s10822-012-9570-1

Corminboeuf, C., Heine, T., Seifert, G., Schleyer, P. V. R., & Weber, J. (2006). Induced magnetic fields in aromatic [n]-annulenes—Interpretation of NICS tensor components. Physical Chemistry Chemical Physics, 8(18), 2927–2934. https://doi.org/10.1039/b601402e

D. Dascalu, D. Larisa Roman, M. Filip, A. Ciorsac, V. Ostafe, A. Isvoran, Solubility and Admet Profiles of Short Oligomers of Lactic Acid, ADMET DMPK 8 (2020) 425–436. https://doi.org/10.5599/admet.801.

Daina, A., Michielin, O., & Zoete, V. (2017). SwissADME: A free web tool to evaluate pharmacokinetics, drug-likeness and medicinal chemistry friendliness of small molecules. Scientific Reports, 7, 42717. https://doi.org/10.1038/srep42717

Darden, T., York, D., & Pedersen, L. (1993). Particle mesh Ewald: An N-log(N) method for Ewald sums in large systems. The Journal of Chemical Physics, 98(12), 10089–10092. https://doi.org/10.1063/1.464397

Degani, Y., & Heller, A. (1987). Direct electrical communication between chemically modified enzymes and metal electrodes. Journal of Physical Chemistry, 91(6), 1285–1289. https://doi.org/10.1021/j100289a045

Desbois, N., Brande, M., Montembault, V., Boissier, J., Dobrzeniek, A., & Gross, M. (2008). Organometallic complexes for topoisomerase inhibition. Bioorganic & Medicinal Chemistry Letters, 18(12), 3509–3513.

Diedrich, C., & Grimme, S. (2003). Systematic investigation of modern quantum chemical methods to predict electronic circular dichroism spectra. Journal of Physical Chemistry A, 107(14), 2524–2539. https://doi.org/10.1021/jp0275802

Dive, D., & Biot, C. (2008). Ferroquine, an aminoquinoline bearing a ferrocenyl group: A new generation of antimalarials. ChemMedChem, 3(3), 383–391. https://doi.org/10.1002/cmdc.200700231

Doak, B. C., Over, B., Giordanetto, F., & Kihlberg, J. (2014). Oral druggable space beyond the rule of 5: Insights from drugs and clinical candidates. Chemistry & Biology, 21(9), 1115–1142. https://doi.org/10.1016/j.chembiol.2014.08.013

Dolg, M., Wedig, U., Stoll, H., & Preuss, H. (1987). Energy-adjusted ab initio pseudopotentials for the first row transition elements. The Journal of Chemical Physics, 86(2), 866–872. https://doi.org/10.1063/1.452288

Dunitz, J. D., Orgel, L. E., & Rich, A. (1956). The crystal structure of ferrocene. Acta Crystallographica, 9(4), 373–375. https://doi.org/10.1107/S0365110X56001091

Durrant, J. D., & McCammon, J. A. (2011). Molecular dynamics simulations and drug discovery. BMC Biology, 9, 71. https://doi.org/10.1186/1741-7007-9-71

E. Lanez, A. Kedadra, T. Lanez, A. Adaika, N. Zegheb, In vitro antioxidant activity, QSAR, in silico toxicity prediction, molecular docking studies, and molecular dynamics of a series of N-ferrocenylmethylanilines as potent antioxidant agents, J. Organomet. Chem. (2024) 123284.

E. LANEZ, D. BENKHELIFA, F.Z. CHERIET, K. GORI, C. SLIMANI, S. KEBACHE, R. OUAKOUAK, O. ABDELLAOUI, Y. DJOUGHI, M.L. BENAMOR, Theoretical Investigation of Mitomycin Derivatives as Dual Inhibitors of HER2 and ER-α: Prospects for Novel Breast Cancer Treatment Strategies, Algerian Journal of Biosciences 6 (2025) 1–20.

E. Lanez, L. Bechki, T. Lanez, Antioxidant Activities, Binding Parameters, and Electrochemical Behavior of Superoxide Anion Radicals Twords 1-Ferrocenylmethylthymine and 1-Ferrocenylmethylcytosine, Curr. Phys. Chem. 10 (2020) 10–22.

E. Lanez, L. Bechki, T. Lanez, Antioxidant Activities, Binding Parameters, and Electrochemical Behavior of Superoxide Anion Radicals Twords 1-Ferrocenylmethylthymine and 1-Ferrocenylmethylcytosine, Curr. Phys. Chem. 10 (2019) 10–22. https://doi.org/10.2174/1877946809666190424143752.

E. Lanez, L. Bechki, T. Lanez, Computational molecular docking, voltammetric and spectroscopic DNA interaction studies of 9N-(Ferrocenylmethyl)adenine, Chemistry and Chemical Technology 13 (2019) 11–17. https://doi.org/10.23939/chcht13.01.011.

E. Lanez, L. Bechki, T. Lanez, Ferrocenylmethylnucleobases: Synthesis, dft calculations, electrochemical and spectroscopic characterisation, Chemistry (Easton). 14 (2020) 146–153.

E. Lanez, L. Bechki, T. Lanez, Ferrocenylmethylnucleobases: Synthesis, dft calculations, electrochemical and spectroscopic characterisation, Chemistry and Chemical Technology 14 (2020) 146–153. https://doi.org/10.23939/chcht14.02.146.

E. Lanez, L. Bechki, T. Lanez, N6, 9-bis (ferrocenylmethyl) adenine: synthesis, cyclic voltammetric, spectroscopic characterization, and DFT calculations, Scientific Study & Research. Chemistry & Chemical Engineering, Biotechnology, Food Industry 20 (2019) 509–519.

E. Lanez, L. Zerrouk, L. Bechki, T. Lanez, A. Adaika, N. Zegheb, K. Nesba, Synthesis, molecular docking, drug-likeness analysis, and ADMET prediction of nickel and zinc tetraphenyl-porphyrin complexes as possible antioxidant agents, Journal of the Chinese Chemical Society (n.d.).

E. Lanez, M. Saidi, T. Lanez, Assessment of antioxidant and DPPH free radical scavenging activity of 1,2-dithiole-3-thione derivatives by using cyclic voltammetry, spectroscopic, and molecular docking studies, Journal of Sulfur Chemistry 44 (2023) 542–558. https://doi.org/10.1080/17415993.2023.2200142.

E. Lanez, N. Zegheb, T. Lanez, In silico ADME, toxicological analysis, molecular docking studies and Molecular dynamics simulation of Afzelin with potential antibacterial effects against Staphylococcus aureus, Turkish Computational and Theoretical Chemistry 7 (2023) 10–16. https://doi.org/10.33435/TCANDTC.1196422.

E. Lanez, T. Lanez, N. Zegheb, In silico ADMET, toxicological analysis, molecular docking studies and Molecular dynamics simulation of Afzelin with potential antibacterial effects against Staphylococcus aureus, Turkish Computational and Theoretical Chemistry 7 (2023) 10–16.

E. Lanez, Y. Bekkar, L. Bourougaa, M.L. Benamor, R. Bouraoui, O. Boudebia, A. Adaika, K. Nesba, H. Chaoua, L. Bechki, Antidiabetic potential of mentha piperita essential oil: GC-MS profiling, in vitro, in vivo and in silico analyses, J. Mol. Struct. (2025) 144239.

Fleming, I. (1976). Frontier orbitals and organic chemical reactions. Wiley.

Fouda, M. F. R., Abd-El-Wahab, M., Abu-Elnasr, A. M., & Morsy, M. A. (2015). Synthesis, characterization and biological activity of ferrocenyl quinolone derivatives. Spectrochimica Acta Part A: Molecular and Biomolecular Spectroscopy, 135, 900–909. https://doi.org/10.1016/j.saa.2014.07.071

Friesner, R. A., Banks, J. L., Murphy, R. B., Halgren, T. A., Klicic, J. J., Mainz, D. T., Repasky, M. P., Knoll, E. H., Shelley, M., Perry, J. K., Shaw, D. E., Francis, P., & Shenkin, P. S. (2004). Glide: A new approach for rapid, accurate docking and scoring. 1. Method and assessment of docking accuracy. Journal of Medicinal Chemistry, 47(7), 1739–1749. https://doi.org/10.1021/jm0306430

Furche, F., & Perdew, J. P. (2006). The performance of semilocal and hybrid density functionals in 3d transition-metal chemistry. The Journal of Chemical Physics, 124(4), 044103. https://doi.org/10.1063/1.2162161

G. Xiong, Z. Wu, J. Yi, L. Fu, Z. Yang, C. Hsieh, M. Yin, X. Zeng, C. Wu, A. Lu, ADMETlab 2.0: an integrated online platform for accurate and comprehensive predictions of ADMET properties, Nucleic Acids Res. 49 (2021) W5–W14.

Gázquez, J. L., Cedillo, A., & Vela, A. (2007). Electrodonating and electroaccepting powers. Journal of Physical Chemistry A, 111(10), 1966–1970. https://doi.org/10.1021/jp065459f

Gottlied, H. B., & Neufeld, L. (1965). Electrophilic aromatic substitution rates of ferrocene. Journal of the American Chemical Society, 87(18), 4041.

Gritzner, G., & Kůta, J. (1984). Recommendations on reporting electrode potentials in nonaqueous solvents. Pure and Applied Chemistry, 56(4), 461–466. https://doi.org/10.1351/pac198456040461

Guengerich, F. P. (2008). Cytochrome P450 and chemical toxicology. Chemical Research in Toxicology, 21(1), 70–83. https://doi.org/10.1021/tx700079z

H. Benamara, T. Lanez, E. Lanez, Bsa-binding studies of 2-and 4-ferrocenylbenzonitrile: Voltammetric, spectroscopic and molecular docking investigations, Journal of Electrochemical Science and Engineering 10 (2020) 335–346. https://doi.org/10.5599/jese.861.

H. Laraoui, E. Lanez, N. Zegheb, A. Adaika, T. Lanez, M. Benkhaled, Anti-Diabetic Activity of Flavonol Glucosides From Fumana montana Pomel: In vitro Analysis, In Silico Docking, ADMET Prediction, and Molecular Dynamics Simulations, ChemistrySelect 8 (2023) e202204512. https://doi.org/10.1002/slct.202204512.

H. Mouada, T. Lanez, E. Lanez, Investigations of the binding parametres of the interaction of N'-ferrocenylmethyl-N'-phenylaceto-and propionohydrazide with DNA, Journal of Fundamental and Applied Sciences 11 (2019) 875–882.

H. Mouada, T. Lanez, I. Zafar, ROS scavenging, DNA binding and NADPH oxidase inhibition potential of N'-Ferrocenylmethyl-N'-phenylpropionohydrazide using cyclic voltammetry and molecular docking, J. Organomet. Chem. 1007 (2024) 123026.

Haaland, A., & Nilsson, J. E. (1968). The determination of barriers to internal rotation by means of electron diffraction: Ferrocene and ruthenocene. Acta Chemica Scandinavica, 22, 2653–2670. https://doi.org/10.3891/acta.chem.scand.22-2653

Hillard, E. A., Aguiar, F. C., Ferber, C. M., Le Bideau, F., Mothes-Martin, E., Courty, J., Miginiac-Maslow, M., Pierson, A., & Jaouen, G. (2007). Iron and the redox potential: The key to ferrocifen activity. Organometallics, 26(17), 4393–4402. https://doi.org/10.1021/om700275t

Hohenberg, P., & Kohn, W. (1964). Inhomogeneous electron gas. Physical Review, 136(3B), B864–B871. https://doi.org/10.1103/PhysRev.136.B864

Hou, T., Wang, J., Li, Y., & Wang, W. (2011). Assessing the performance of the MM/PBSA and MM/GBSA methods. Journal of Chemical Information and Modeling, 51(1), 69–82. https://doi.org/10.1021/ci100275a

Huang, S. Y., Grinter, S. Z., & Zou, X. (2010). Scoring functions and their evaluation methods for protein–ligand docking: recent advances and future directions. Physical Chemistry Chemical Physics, 12(40), 12899–12908. https://doi.org/10.1039/c0cp00151a

I.U. Khand, T. Lanez, P.L. Pauson, Ferrocene derivatives. Part 24. Synthesis of dihydro-2-pyrindines and dihydro-3 H-2-cyclopent [c] azepines by photolysis of their cyclopentadienyliron derivatives, J. Chem. Soc. Perkin 1 (1989) 2075–2078.

J. Dong, N.N. Wang, Z.J. Yao, L. Zhang, Y. Cheng, D. Ouyang, A.P. Lu, D.S. Cao, Admetlab: A platform for systematic ADMET evaluation based on a comprehensively collected ADMET database, J. Cheminform. 10 (2018) 1–11. https://doi.org/10.1186/s13321-018-0283-x.

J. Hodgson, ADMET—turning chemicals into drugs, Nat. Biotechnol. 19 (2001) 722–726.

J. Huang, A.D. Mackerell, CHARMM36 all-atom additive protein force field: Validation based on comparison to NMR data, J. Comput. Chem. 34 (2013) 2135–2145. https://doi.org/10.1002/jcc.23354.

Jaouen, G., Vessieres, A., & Top, S. (2010). Ferrocifen type anti cancer drugs. Chemical Society Reviews, 39(8), 2534–2544. https://doi.org/10.1039/b920146c

Jolly, W. L. (1976). The synthesis and characterization of inorganic compounds. Prentice-Hall.

Jones, G., Willett, P., Glen, R. C., Leach, A. R., & Taylor, R. (1997). Development and validation of a genetic algorithm for flexible docking. Journal of Molecular Biology, 267(3), 727–748. https://doi.org/10.1006/jmbi.1996.0897

Jørgensen, C. K. (1962). Absorption spectra and chemical bonding in complexes. Pergamon.

Jorgensen, W. L., Maxwell, D. S., & Tirado-Rives, J. (1996). Development and testing of the OPLS all-atom force field on conformational energetics and properties of organic

liquids. Journal of the American Chemical Society, 118(45), 11225–11236. https://doi.org/10.1021/ja9621760

K. Vanommeslaeghe, A.D. MacKerell, Automation of the CHARMM general force field (CGenFF) I: Bond perception and atom typing, J. Chem. Inf. Model. 52 (2012) 3144–3154. https://doi.org/10.1021/ci300363c.

Kealy, T. J., & Pauson, P. L. (1951). A new type of organo-iron compound. Nature, 168(4285), 1039–1040. https://doi.org/10.1038/1681039b0

Knox, G. R., & Pauson, P. L. (1961). Ferrocenyl ketones. Journal of the Chemical Society, 4610–4615. https://doi.org/10.1039/jr9610004610

Koch, W., & Holthausen, M. C. (2001). A chemist's guide to density functional theory (2nd ed.). Wiley-VCH.

Kohn, W., & Sham, L. J. (1965). Self-consistent equations including exchange and correlation effects. Physical Review, 140(4A), A1133–A1138. https://doi.org/10.1103/PhysRev.140.A1133

Kola, I., & Landis, J. (2004). Can the pharmaceutical industry reduce attrition rates? Nature Reviews Drug Discovery, 3(8), 711–716. https://doi.org/10.1038/nrd1470

Kollman, P. A., Massova, I., Reyes, C., Kuhn, B., Huo, S., Chong, L., Lee, M., Lee, T., Duan, Y., Wang, W., Donini, O., Cieplak, P., Srinivasan, J., Case, D. A., & Cheatham, T. E. (2000). Calculating structures and free energies of complex molecules. Accounts of Chemical Research, 33(12), 889–897. https://doi.org/10.1021/ar000033j

Koopmans, T. (1934). Über die Zuordnung von Wellenfunktionen und Eigenwerten zu den einzelnen Elektronen eines Atoms. Physica, 1(1–6), 104–113. https://doi.org/10.1016/S0031-8914(34)90011-2

Köpf-Maier, P., & Köpf, H. (1987). Non-platinum group metal antitumor agents. History, current status, and perspectives. Chemical Reviews, 87(5), 1137–1152. https://doi.org/10.1021/cr00081a012

Kuwana, T., Bublitz, D. E., & Hoh, G. (1960). Chronopotentiometric studies on the oxidation of ferrocene, ruthenocene, osmocene and some of their derivatives. Journal

of the American Chemical Society, 82(22), 5811–5817. https://doi.org/10.1021/ja01507a024

L. Guan, H. Yang, Y. Cai, L. Sun, P. Di, W. Li, G. Liu, Y. Tang, ADMET-score-a comprehensive scoring function for evaluation of chemical drug-likeness, Medchemcomm 10 (2019) 148–157. https://doi.org/10.1039/C8MD00472B.

L. ZERROUK, L. BECHKI, E. LANEZ, T. LANEZ, Synthesis, characterization, cyclic voltammetry, and molecular docking studies of the antioxidant activities of superoxide anion radicals towards meso-tetramethophenyl-porphyrin and meso-tetrabiphenyl-porphyrin, Not. Sci. Biol. 16 (2024) 11823. https://doi.org/10.55779/nsb16211823.

Leach, A. R. (2001). Molecular modelling: Principles and applications (2nd ed.). Prentice Hall.

Leach, A. R., & Gillet, V. J. (2007). An introduction to chemoinformatics (Rev. ed.). Springer.

Lengauer, T., & Rarey, M. (1996). Computational methods for biomolecular docking. Current Opinion in Structural Biology, 6(3), 402–406. https://doi.org/10.1016/S0959-440X(96)80061-3

Lipinski, C. A., Lombardo, F., Dominy, B. W., & Feeney, P. J. (1997). Experimental and computational approaches to estimate solubility and permeability in drug discovery and development settings. Advanced Drug Delivery Reviews, 23(1–3), 3–25. https://doi.org/10.1016/S0169-409X(96)00423-1

Long, N. J. (1998). Metallocenes: An introduction to sandwich complexes. Blackwell.

M. Chebbah, E. Lanez, S. Bouacida, H. Athmani, M.L. Ben Amor, R. Hafidi, A. Bouchemma, Synthesis, Characterization, Structural Analysis, Hirshfeld Surface Studies, and Molecular Docking of 1, 3, 5-Tris (P-Bromophenyl)-1, 3, 5-Triazacyclohexane, Hirshfeld Surface Studies, and Molecular Docking Of 1 (n.d.).

M. Hanane, T. Lanez, I. Zafar, M.S. Afghan, N. Zegheb, N'-Ferrocenylmethyl-N'-phenylbenzohydrazide as a potential DNA binding compound: a combined experimental and computational study, J. Coord. Chem. 76 (2023) 1984–1998. https://doi.org/10.1080/00958972.2023.2275247.

M. Meraghni, T. Lanez, E. Lanez, L. Bechki, A. Kennoufa, Experimental and theoretical study on corrosion inhibition of mild steel by meso-tetraphenyl-porphyrin derivatives in acid solution, Journal of Electrochemical Science and Engineering 13 (2023) 217–229. https://doi.org/10.5599/jese.1400.

M.J. Frisch, G.W. Trucks, H.B. Schlegel, G.E. Scuseria, M.A. Robb, J.R. Cheeseman, G. Scalmani, V. Barone, B. Mennucci, G.A. Petersson, Gaussian 09. Wallingford, CT: Gaussian, 2009.

M.L. Ben Amor, E. Lanez, Y. Bekkar, A. Adaika, T. Lanez, K. Nesba, L. Bechki, EVALUATION OF FERROCENYLMETHYLNUCLEOBASES DERIVATIVES INTERACTING WITH DNA: INSIGHTS FROM ELECTROCHEMICAL, SPECTROSCOPIC, DFT CALCULATION, MOLECULAR DOCKING AND MOLECULAR DYNAMIC SIMULATIONS., Studia Universitatis Babes-Bolyai, Chemia 70 (2025).

M.L. Tlili, F. Alia, E. Bahri, T. Beyat, K. Redouan, E. Lanez, In vivo evaluations of the antidiabetic and antioxidant effects of Olea europaea L.(Chemlali variety) leaves, Acta Periodica Technologica (2025) 3.

M.L. Tlili, I. Laib, K. Salemi, I. Chetehouna, I. BenMoussa, E. Lanez, Phytochemical Analysis and Evaluation of the Antioxidant, Anti-Inflammatory, Hemolytic, and Antibacterial Effects of Astragalus gombo (L.) Leaves., Acta Chim. Slov. 71 (2024).

M.L.B.E.N. AMOR, E. LANEZ, Y. Bekkar, A. ADAIKA, T. LANEZ, K. NESBA, L. BECHKI, Exploring the Interactions of Ferrocenylmethylnucleobase Derivatives With BSA and HHb: Insights From Electrochemical, Spectroscopic, ADMET, in Silico Docking, and MD Simulations, ChemistrySelect 10 (2025) e202404678.

M.P. Andersson, P. Uvdal, New scale factors for harmonic vibrational frequencies using the B3LYP density functional method with the triple-ζ basis set 6-311+ G (d, p), J. Phys. Chem. A 109 (2005) 2937–2941.

MacKerell, A. D., Bashford, D., Bellott, M., Dunbrack, R. L., Evanseck, J. D., Field, M. J., Fischer, S., Gao, J., Guo, H., Ha, S., Joseph-McCarthy, D., Kuchnir, L., Kuczera, K., Lau, F. T. K., Mattos, C., Michnick, S., Ngo, T., Nguyen, D. T., Prodhom, B., … Karplus, M. (1998). All-atom empirical potential for molecular modeling and

dynamics studies of proteins. Journal of Physical Chemistry B, 102(18), 3586–3616. https://doi.org/10.1021/jp973084f

Miller, S. A., Tebboth, J. A., & Tremaine, J. F. (1952). Dicyclopentadienyliron. Journal of the Chemical Society, 632–635. https://doi.org/10.1039/jr9520000632

Mohajeri, A., & Shakerin, N. (2004). The gas-phase acidity and intramolecular hydrogen bonding in acetylferrocene and hydroxyferrocene. Journal of Molecular Structure: THEOCHEM, 711(1–3), 167–172. https://doi.org/10.1016/j.theochem.2004.10.001

Morris, G. M., & Lim-Wilby, M. (2008). Molecular docking. In A. Kukol (Ed.), Molecular modeling of proteins (pp. 365–382). Humana Press.

Morris, G. M., Goodsell, D. S., Halliday, R. S., Huey, R., Hart, W. E., Belew, R. K., & Olson, A. J. (1998). Automated docking using a Lamarckian genetic algorithm and an empirical binding free energy function. Journal of Computational Chemistry, 19(14), 1639–1662. https://doi.org/10.1002/(SICI)1096-987X(19981115)19:14<1639::AID-JCC10>3.0.CO;2-B

Murray, J. S., & Politzer, P. (1998). Electrostatic potentials: Chemical applications. Wiley.

N. Benyza, F. Allouche, S.W. Dammak, E. Lanez, T. Lanez, Chemical Reactivity, Topological Analysis, and Second-Order Nonlinear Optical Responses of M3O@ Al12N12: A Quantum Chemical Study, Russian Journal of Physical Chemistry A 96 (2022) 2909–2920.

N. Zegheb, C. Boubekri, T. Lanez, E. Lanez, T.T. Küçükkılınç, E. Öz, A. Khennoufa, S. Khamouli, S. Belaidi, In Vitro and In Silico Determination of Some N-ferrocenylmethylaniline Derivatives as Anti-Proliferative Agents Against MCF-7 Human Breast Cancer Cell Lines, Anticancer Agents Med. Chem. 22 (2021) 1426–1437. https://doi.org/10.2174/1871520621666210624141712.

N. ZEGHEB, L. Elhafnaoui, T. Lanez, N-ferrocenylmethyl-derivatives as spike glycoprotein inhibitors of sars-cov-2 using in silico approaches, (2020).

N. Zouaghi, E. Lanez, M.L. Benamor, S.N. Nacer, T. Lanez, Y. Bekkar, H. Haddad, K. Al-Abdallat, M. Zihlif, Y. Al-Abdallat, Targeting Alzheimer's Disease via Phytochemicals from Artemisia campestris L.: GC/MS Analysis with an Integrated Computational Approach, Food Biosci. (2025) 108128.

Nitiss, J. L. (2009). Targeting DNA topoisomerase II in cancer chemotherapy. Nature Reviews Cancer, 9(5), 338–350. https://doi.org/10.1038/nrc2607

Ornelas, C. (2011). Application of ferrocene and its derivatives in cancer research. New Journal of Chemistry, 35(10), 1973–1985. https://doi.org/10.1039/c1nj20172g

Ortega-Arizmendi, A. I., Aldeco-Pérez, E., & Cuevas-Yáñez, E. (2014). Organometallics in computer-aided drug design: The docking problem. The Scientific World Journal, 2014, 907686. https://doi.org/10.1155/2014/907686

P. Banerjee, A.O. Eckert, A.K. Schrey, R. Preissner, ProTox-II: A webserver for the prediction of toxicity of chemicals, Nucleic Acids Res. 46 (2018) W257–W263. https://doi.org/10.1093/nar/gky318.

P.W. Rose, A. Prlić, A. Altunkaya, C. Bi, A.R. Bradley, C.H. Christie, L. Di Costanzo, J.M. Duarte, S. Dutta, Z. Feng, R.K. Green, D.S. Goodsell, B. Hudson, T. Kalro, R. Lowe, E. Peisach, C. Randle, A.S. Rose, C. Shao, Y.P. Tao, Y. Valasatava, M. Voigt, J.D. Westbrook, J. Woo, H. Yang, J.Y. Young, C. Zardecki, H.M. Berman, S.K. Burley, The RCSB protein data bank: Integrative view of protein, gene and 3D structural information, Nucleic Acids Res. 45 (2017) D271–D281.

Parr, R. G., & Yang, W. (1989). Density-functional theory of atoms and molecules. Oxford University Press.

Pavlishchuk, V. V., & Addison, A. W. (2000). Conversion constants for redox potentials measured versus different reference electrodes in acetonitrile solutions at 25°C. Inorganica Chimica Acta, 298(1), 97–102. https://doi.org/10.1016/S0020-1693(99)00407-7

Pavlov, M., Siegbahn, P. E. M., Sandström, M., & Blomberg, M. R. A. (2001). Charge dependence of water exchange reactions. A theoretical study. Journal of Physical Chemistry A, 102(1), 219–228.

Perdew, J. P., Ruzsinszky, A., Tao, J., Staroverov, V. N., Scuseria, G. E., & Csonka, G. I. (2005). Prescription for the design and selection of density functional approximations. Journal of Chemical Physics, 123(6), 062201. https://doi.org/10.1063/1.1904565

Pires, D. E. V., Blundell, T. L., & Ascher, D. B. (2015). pkCSM: Predicting small-molecule pharmacokinetic and toxicity properties using graph-based signatures. Journal of Medicinal Chemistry, 58(9), 4066–4072. https://doi.org/10.1021/acs.jmedchem.5b00104

R. Kumari, R. Kumar, A. Lynn, G-mmpbsa -A GROMACS tool for high-throughput MM-PBSA calculations, J. Chem. Inf. Model. 54 (2014) 1951–1962. https://doi.org/10.1021/ci500020m.

Reed, A. E., Curtiss, L. A., & Weinhold, F. (1988). Intermolecular interactions from a natural bond orbital, donor-acceptor viewpoint. Chemical Reviews, 88(6), 899–926. https://doi.org/10.1021/cr00088a005

Richards, C. J., Mulvaney, A. W., & Sparke, M. A. (2006). Planar chiral ferrocene chemistry. Coordination Chemistry Reviews, 250(15–16), 1786–1797.

Rinehart, K. L., & Curby, R. J. (1957). Ferrocenylcarboxaldehyde via Vilsmeier–Haack formylation. Journal of the American Chemical Society, 79(13), 3420. https://doi.org/10.1021/ja01570a048

Rösch, N., & Streitwieser, A. (1983). On the bonding in metallocenes. Journal of the American Chemical Society, 105(24), 7237–7240. https://doi.org/10.1021/ja00362a030

Rosenberg, B., Van Camp, L., Trosko, J. E., & Mansour, V. H. (1969). Platinum compounds: A new class of potent antitumour agents. Nature, 222(5191), 385–386. https://doi.org/10.1038/222385a0

S. Khamouli, S. Belaidi, M. Ouassaf, T. Lanez, S. Belaaouad, S. Chtita, Multi-combined 3D-QSAR, docking molecular and ADMET prediction of 5-azaindazole derivatives as LRRK2 tyrosine kinase inhibitors, J. Biomol. Struct. Dyn. 40 (2022) 1285–1298.

S. Khamouli, S. Belaidi, T. Lanez, Molecular doking and ADMET studies of amino-pyrimidine derivaties as mycobacterium tuberculosis Ser/Thr protein kinases B inhibitors, Journal of Fundamental and Applied Sciences 11 (2019) 914–939.

S.N. Nacer, T. Lanez, Electrochemical properties of N'-ferrocenylmethyl-N'-phenylbenzohydrazide in aqueous and organic mediums, International Letters of Chemistry, Physics and Astronomy 5 (2013) 76–85.

Schleyer, P. V. R., Manoharan, M., Wang, Z. X., Kiran, B., Jiao, H., Puchta, R., & van Eikema Hommes, N. J. R. (2001). Dissected nucleus-independent chemical shift analysis of π-aromaticity and antiaromaticity. Organic Letters, 3(16), 2465–2468. https://doi.org/10.1021/ol016217v

Schmid, N., Eichenberger, A. P., Choutko, A., Riniker, S., Winger, M., Mark, A. E., & van Gunsteren, W. F. (2011). Definition and testing of the GROMOS force-field versions 54A7 and 54B7. European Biophysics Journal, 40(7), 843–856. https://doi.org/10.1007/s00249-011-0700-9

Seiler, P., & Dunitz, J. D. (1979). A new interpretation of the disordered crystal structure of ferrocene. Acta Crystallographica B, 35(5), 1068–1074. https://doi.org/10.1107/S0567740879005598

Shriver, D. F., & Atkins, P. W. (2010). Inorganic chemistry (5th ed.). Oxford University Press.

Snieckus, V. (1990). Directed ortho metalation. Chemical Reviews, 90(6), 879–933. https://doi.org/10.1021/cr00104a001

Štěpnička, P. (Ed.). (2008). Ferrocenes: Ligands, materials and biomolecules. Wiley.

T. Lanez, E. Lanez, A molecular docking study of N-ferrocenylmethylnitroanilines as potential anticancer drugs, International Journal of Pharmacology, Phytochemistry and Ethnomedicine 2 (2016) 5–12.

T. Lanez, H. Benaicha, E. Lanez, M. Saidi, Electrochemical, spectroscopic and molecular docking studies of 4-methyl-5-((phenylimino)methyl)-3H- and 5-(4-fluorophenyl)-3H-1,2-dithiole-3-thione interacting with DNA, Journal of Sulfur Chemistry 39 (2018) 76–88. https://doi.org/10.1080/17415993.2017.1391811.

T. Lanez, H. Hemmami, Antioxidant Activities of N-ferrocenylmethyl-2- and -3-nitroaniline and Determination of their Binding Parameters with Superoxide Anion Radicals, Curr. Pharm. Anal. 13 (2016) 110–116. https://doi.org/10.2174/1573412912666160831145524.

T. Lanez, M. Feizi-Dehnayebi, E. Lanez, Assessment of the electrostatic binding of ferrocenylmethyl-nitroaniline derivatives to DNA: A combined experimental and theoretical study, J. Mol. Struct. (2024) 138386.

T. Lanez, M. Henni, Dual Anti-Inflammatory and Antidiabetic Potential of Ferrocenylmethylcyanophenyl Derivatives: Integrated In Vitro and In Silico Evaluation, J. Organomet. Chem. (2025) 123956.

T. Lanez, M. Henni, H. Hemmami, Development of cyclic voltammetric method for the study of the interaction of antioxidant standards with superoxide anion radicals case of α-tocopherol, Scientific Study and Research: Chemistry and Chemical Engineering, Biotechnology, Food Industry 16 (2015) 161–168.

T. Lanez, M. Lanez, R. Lanez, E. Lanez, B. Talbi-Lanez, Computational Screening of Novel Nitroimidazole Candidates: Targeting Key Enzymes of Oral Anaerobes for Anti-Parasitic Potential, Curr. Drug Discov. Technol. (2024).

T. Lu, F. Chen, Multiwfn: A multifunctional wavefunction analyzer, J. Comput. Chem. 33 (2012) 580–592.

T. Zaiz, T. Lanez, Corrosion inhibition of carbon steel XC70 in H_2SO_4 solution by ferrocene derivative 3-(ferrocenylmethylamine)benzonitrile, Journal of Fundamental and Applied Sciences 4 (2015) 182. https://doi.org/10.4314/jfas.v4i2.8.

Togni, A., & Hayashi, T. (Eds.). (1995). Ferrocenes: Homogeneous catalysis, organic synthesis, materials science. VCH.

Top, S., Vessieres, A., Pigeon, P., & Jaouen, G. (1994). Novel ferrocene-containing anti-estrogen compounds. Journal of the Chemical Society, Chemical Communications, 8, 955–956. https://doi.org/10.1039/c39940000955

Trott, O., & Olson, A. J. (2010). AutoDock Vina: Improving the speed and accuracy of docking with a new scoring function, efficient optimization, and multithreading. Journal of Computational Chemistry, 31(2), 455–461. https://doi.org/10.1002/jcc.21334

van de Waterbeemd, H., & Gifford, E. (2003). ADMET in silico modelling: Towards prediction paradise? Nature Reviews Drug Discovery, 2(3), 192–204. https://doi.org/10.1038/nrd1032

van Staveren, D. R., & Metzler-Nolte, N. (2004). Bioorganometallic chemistry of ferrocene. Chemical Reviews, 104(12), 5931–5986. https://doi.org/10.1021/cr0101510

Veber, D. F., Johnson, S. R., Cheng, H. Y., Smith, B. R., Ward, K. W., & Kopple, K. D. (2002). Molecular properties that influence the oral bioavailability of drug candidates. Journal of Medicinal Chemistry, 45(12), 2615–2623. https://doi.org/10.1021/jm020017n

Wang, J. C. (2002). Cellular roles of DNA topoisomerases: A molecular perspective. Nature Reviews Molecular Cell Biology, 3(6), 430–440. https://doi.org/10.1038/nrm831

Wang, J., Wolf, R. M., Caldwell, J. W., Kollman, P. A., & Case, D. A. (2004). Development and testing of a general amber force field. Journal of Computational Chemistry, 25(9), 1157–1174. https://doi.org/10.1002/jcc.20035

Wei, H., Ruthenburg, A. J., Bechis, S. K., & Verdine, G. L. (2005). Nucleotide-dependent domain movement in the ATPase domain of a human type IIA DNA topoisomerase. Journal of Biological Chemistry, 280(44), 37041–37047. https://doi.org/10.1074/jbc.M506520200

Wilkinson, G., Rosenblum, M., Whiting, M. C., & Woodward, R. B. (1952). The structure of iron bis-cyclopentadienyl. Journal of the American Chemical Society, 74(8), 2125–2126. https://doi.org/10.1021/ja01128a527

Wu, C. C., Li, T. K., Farh, L., Lin, L. Y., Lin, T. S., Yu, Y. J., Yen, T. J., Chiang, C. W., & Chan, N. L. (2011). Structural basis of type II topoisomerase inhibition by the anticancer drug etoposide. Science, 333(6041), 459–462. https://doi.org/10.1126/science.1204117

Xiong, G., Wu, Z., Yi, J., Fu, L., Yang, Z., Hsieh, C., Yin, M., Zeng, X., Wu, C., Lu, A., Chen, X., Hou, T., & Cao, D. (2021). ADMETlab 2.0: An integrated online platform for accurate and comprehensive predictions of ADMET properties. Nucleic Acids Research, 49(W1), W5–W14. https://doi.org/10.1093/nar/gkab255

Y. Bekkar, E. Lanez, T. Lanez, L. Bourougaa, A. Adaika, A. Benine, Z. Saada, Combined In Vitro and In Silico analysis of ferrocenylmethylaniline derivatives: Antibacterial potential, DFT calculations, and molecular dynamics insights, J. Organomet. Chem. (2025) 123618.

Y. Bekkar, E. Lanez, T. Lanez, L. Bourougaa, A. Adaika, Z. Saada, A. Benine, Antidiabetic Potential of Synthesized Ferrocenylmethylaniline Derivatives: Insights From In Vitro Studies, Molecular Docking, ADMET, DFT Calculations, and Molecular Dynamics Simulation, Biotechnol. Appl. Biochem. (2025).

Y. Ouennoughi, H.E. Karce, D. Aggoun, T. Lanez, R. Ruiz-Rosas, B. Bouzerafa, A. Ourari, E. Morallon, A novel ferrocenic copper (II) complex Salen-like, derived from 5-chloromethyl-2-hydroxyacetophenone and N-ferrocenmethylaniline: Design, spectral approach and solvent effect towards electrochemical behavior of Fc+/Fc redox couple, J. Organomet. Chem. 848 (2017) 344–351.

Z. Nadjiba, B. Chérifa, T. Lanez, E. Lanez, In Silico Study on N-ferrocenylmethyl-N-phenylpropionohydrazide and N-ferrocenylmethyl-N-pheylbenzohydrazide as anticancer drugs for breast and prostate cancer, International Journal of Pharmacology, Phytochemistry and Ethnomedicine 11 (2018) 17–25.

Zhao, Y., & Truhlar, D. G. (2008). The M06 suite of density functionals for main group thermochemistry, thermochemical kinetics, noncovalent interactions, excited states, and transition elements. Theoretical Chemistry Accounts, 120(1–3), 215–241. https://doi.org/10.1007/s00214-007-0310-x